Accepted Manuscript

Ion traps in nuclear physics — recent results and achievements

Tommi Eronen, Anu Kankainen, Juha Äystö

PII: S0146-6410(16)30043-6
DOI: http://dx.doi.org/10.1016/j.ppnp.2016.08.001
Reference: JPPNP 3619

To appear in: *Progress in Particle and Nuclear Physics*

Please cite this article as: T. Eronen, A. Kankainen, J. Äystö, Ion traps in nuclear physics — recent results and achievements, *Progress in Particle and Nuclear Physics* (2016), http://dx.doi.org/10.1016/j.ppnp.2016.08.001

Ion Traps in Nuclear Physics — Recent Results and Achievements

Tommi Eronen, Anu Kankainen and Juha Äystö

University of Jyvaskyla, P.O. Box 35 (YFL), FI-40014 University of Jyvaskyla, Finland

Abstract

Ion traps offer a way to determine nuclear binding energies through atomic mass measurements with a high accuracy and they are routinely used to provide isotopically or even isomerically pure beams of short-living ions for post-trap decay spectroscopy experiments. In this review, different ion-trapping techniques and progresses in recent nuclear physics experiments employing low-energy ion traps are discussed. The main focus in this review is on the benefit of recent high accuracy mass measurements to solve some key problems in physics related to nuclear structure, nuclear astrophysics as well as neutrinos. Also, several cases of decay spectroscopy experiments utilizing trap-purified ion samples are summarized.

Keywords: ion traps, atomic masses, trap-assisted spectroscopy

1. Introduction

Progress of ion manipulation technologies in ion traps has opened exciting opportunities for solving fundamental questions in atomic and nuclear physics. Calculation of electron binding energies in atoms using the well-known theory of QED (Quantum Electrodynamics) can be performed with accuracies of the order of a few eV for almost any atom. To be sensitive in this level in atomic mass itself, a relative mass uncertainty of the order of 10^{-10} or better is required. Experimentally this precision is already reached for stable isotope masses [1–3].

The calculation of the nuclear binding, however, has to rely on less accurately quantifiable strong interaction derived from the theory of QCD (Quantum Chromodynamics). The mass M of a neutral atom can be expressed as

$$M = N \times m_{\mathrm{n}} + Z \times m_{\mathrm{p}} + Z \times m_{\mathrm{e}} - \left(B_{\mathrm{atom}} + B_{\mathrm{nucleus}}\right)/c^2, \quad (1)$$

where N and Z are the neutron and proton number and m_{p}, m_{n} and m_{e} are free proton, neutron and electron masses, respectively. B_{atom} and B_{nucleus} are the total electron and nuclear binding energies, respectively. At best, the total mass (or binding energy, see Chapter 3.1) of an atom can presently be calculated to an accuracy of the order of a few 100 keV which corresponds to a relative mass uncertainty $\Delta m/m$ of the order of 10^{-6} only, which is several orders of magnitude less precise than for atomic binding energies. Therefore in nuclear physics, in general, the required experimental accuracies are currently less stringent than in atomic physics. This is particularly true when comparing experimental data with theoretical model predictions for absolute masses and the effects of global correlations on masses.

However, the first- and second-order differentials of masses can serve as sensitive indicators of local behavior of collective or single particle structures with changing proton and/or neutron numbers. In fact, the measurement accuracy required for those observables is of the order of 10 keV or better, and is comparable to that routinely available in spectroscopy of nuclear excited states. This opens up interesting perspectives for studying the binding energy systematics for the excited states as well. The observables, for example, include nucleon or nucleon pair binding energies, Q-values for radioactive decays, isomer masses, pairing gaps and shell gaps. Some examples of differentials and their typically required accuracies are given in Table 1 together with related key physics topics.

In this review, we wish to introduce the newest developments in ion trapping techniques for nuclear physics. The emphasis in the review is in the use of Penning-

Table 1: Required accuracies for different nuclear physics motivations.

Physics motivation	Accuracy
Nuclear structure	
Global correlations	a few 100 keV
Local correlations	$\leq$ 10 keV
Evolution of shell structure, pairing and collectivity	$\leq$ 10 keV
Drip-line phenomena, halos, isomers	$\approx$ 1 keV
Nuclear astrophysics	$\geq$ 1 keV
Charge symmetry in nuclei	$\leq$ 1 keV
Fundamental symmetries	
Tests of the Standard Model	$\leq$ 100 eV
β decay and electroweak interaction	$\leq$ 100 eV
CVC theory and the unitarity of the CKM matrix	$\leq$ 100 eV
Double β decay	10 – 1000 eV
Neutrino mass and mass hierarchy problem	$\ll$ 100 eV

trap technique for high-precision mass measurements as well as in their use as high-resolution mass separators to produce high-purity isotopic or isomeric sources for decay spectroscopy of exotic nuclei. It will be shown that these techniques have opened up unique possibilities for high-precision measurements of rare isotopes of practically all chemical elements down to half-lives of few ms and production rates on the order of few ions per hour.

Then, we move on to present an update of recent progresses of direct mass measurements of neutron-rich nuclei covering a wide range of the chart of nuclei between mass numbers $A = 10$ and $A = 250$. The mass data will mainly be discussed in the framework of mass differentials, such as nucleon and nucleon-pair binding energies, pairing gaps and shell gaps. A comparison with some selected theoretical models will be discussed. In addition, a special class of high-precision measurements of isobaric mass doublets and isotopic mass multiplets will be presented. Finally, a novel technique of trap-assisted decay spectroscopy is introduced with applications on beta, gamma, conversion electron and β delayed neutron studies.

2. Ion trap techniques

Every major radioactive ion beam facility in the world utilizes ion traps. Their role is not just in mass measurement and separation but also as ion beam preparatory devices like ion bunchers, which convert continuous ion beam into a sequence of ion packages (bunches) [4].

The traps can be categorized to electrostatic traps, electric radiofrequency (RF) traps and Penning traps that employ a combination of homogenous magnetic field and electrostatic potential [5]. This section gives an overview of different trap types and their uses in nuclear physics studies.

2.1. Radiofrequency cooler-bunchers

It is quite common that radioactive ion beams after their production and extraction from the source have rather poor ion optical properties and commonly are continuous in nature. Both of these properties are rather unsuitable for ion traps that require ions almost at rest.

To meet the ever-increasing requirements of ion traps, gas-filled radiofrequency cooler-bunchers (RFQCBs) have been developed for this task. The ions from the source are first decelerated to ~100 eV and then injected to an RF-multipole (most commonly a quadrupole) structure that keeps the ions confined between the rods. The space between the rods is filled with dilute gas (usually helium at pressure of about 0.1 mbar) to allow for the reduction of the width of the ions' kinetic energy distribution (ion cooling). The ions collide with gas atoms and consequently lose energy and are centered to the RF electric field axis. Finally, using additional fine (on the order of 0.1 V/cm) DC-gradients, the cooled ions are collected to a potential well, from where they are swiftly released by switching the trap potentials. This is illustrated in Fig. 1.

These devices allow ions to be released downstream to trap experiments as short, well cooled, bunches. These devices have existed for a while now (see for example Refs. [7–9]) and are still in active use. The new devices built after the first-generation experiments have been concentrating on improving throughput of ions like CARIBU buncher [10] at Argonne National laboratory or preparations for DESIR at SPIRAL2 [11].

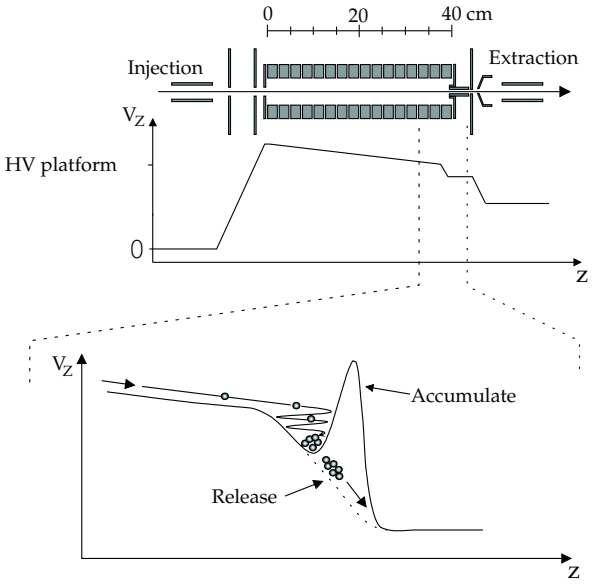

Figure 1: Schematic principle of an RFQCB (used at JYFLTRAP). The ions having 30…60q keV of energy are electrostatically slowed down by setting the RFQ at a high voltage (HV) platform and injected into the gas-filled RF structure with about ~ 100 eV of energy. Ion-atom collisions cool the ions. Finally the ions are collected into an axial potential well, from where they are released as a short bunch downstream. This figure is from Ref. [6].

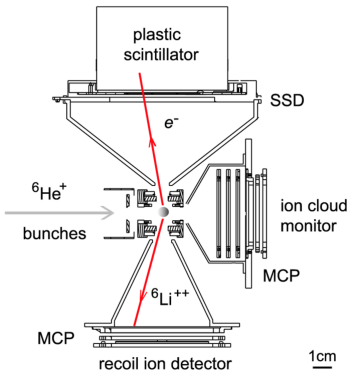

Figure 2: Schematic overview of the LPCTRAP. The ions under study are captured to a small volume of the trap, where the RF field keeps the ions confined. When a β decay occurs, the emitted electron or positron is detected with a position sensitive silicon strip detector (SSD) combined with a plastic scintillator. The recoiling ion is detected with a micro channel plate (MCP) detector. From the position of the β particle and the time-of-flight of the recoil the neutrino energy spectrum can be reconstructed. This figure is from Ref. [19].

RFQ cooler-bunchers are used in two rather distinctive modes of operation. One is preparation of ion bunches that, upon extraction, have extremely small small energy spread (below 1 eV) but have rather long bunch size (typically few μs). Low energy spread is ideal for *e.g.* collinear laser spectroscopy [12, 13] and also is suitable even with long temporal length for Penning traps. The other RFQ operating mode is to provide temporally short (typically 10-100 ns) bunches but this comes with the expense of increased energy spread. This type of bunchers are needed for multi-reflection time-of-flight separators [14–16].

2.2. *Paul traps*

Paul trap is a very simple type of ion trap, which utilizes radiofrequency (RF) electric fields to form a confining potential [17]. These type of traps are ideal for studying properties that require ions to be nearly ”free floating”. Such conditions are needed, e.g. for studying kinematics of radioactive decay. These type of studies require rather elaborate trap geometry designs to allow access for various types of detectors. A pioneering LPCTRAP serves as a good example, see Refs. [18, 19]. Schematic of the experiment is shown in Fig. 2.

The LPCTRAP at GANIL [18] and BPT at Argonne National Laboratory [20] are Paul traps that have been developed to determine β-ν angular correlations in β decays and to study β-delayed neutron emission [21]. The decays will occur in a very small volume (~1 mm^3) and since the decay occurs nearly at rest and in free space, the kinematics can be reconstructed rather accurately. In a β decay, the neutrino will go undetected but the momenta it carried away can be reconstructed from the detection of the emitted electron and the recoil daughter ion. Similarly, in case of a neutron emission, there is no need to detect the neutron but the energy carried away by the neutron can be reconstructed from the kinetic energy of the recoiling ion.

2.3. *Penning traps*

The best mass measurement accuracy and also the best mass resolving power is provided by Penning traps [22]. A Penning trap consists of a strong homogenous magnetic field and a weak quadrupolar electrostatic potential. Such a configuration confines a charged particle in all three spatial directions. In the absence of any electric field, ion undergoes cyclotron motion in a homogenous magnetic field with a so-called free-space cyclotron frequency

$$\nu_c = \frac{1}{2\pi}\frac{q}{m}B, \qquad (2)$$

where q and m are the charge and mass of the particle and B the magnetic field. This relation gives a direct link between charge-over-mass and *frequency*. However, a homogenous magnetic field only offers ion confinement

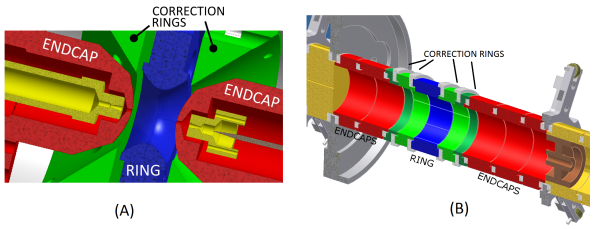

Figure 3: Hyperbolic (A) and cylindrical (B) Penning traps (Tritium-^{3}He trap from Heidelberg, Germany [23] and JYFLTRAP [24], respectively). With both configurations a quadrupolar electric potential can be formed. In both cases additional compensation (correction) electrodes are needed to correct for the truncation of electrodes and unideal geometry. Some components have been stripped for clarity.

in two spatial directions. To achieve full confinement, a quadrupolar electrostatic potential is added in order to restrict ion movement along the magnetic field axis. Commonly hyperbolic or cylindrical electrodes are used as illustrated in Fig. 3.

With an added quadrupolar electrostatic potential, the ion will exhibit *axial motion* with frequency

$$\nu_z = \frac{1}{2\pi}\sqrt{\frac{qV_0}{md^2}} \tag{3}$$

and two *radial motions* with frequencies

$$\nu_\pm = \frac{1}{4\pi}\left(\nu_c \pm \sqrt{\nu_c^2 - 2\nu_z^2}\right). \tag{4}$$

The axial motion with frequency ν_z along the magnetic field lines depends (in addition to ion q/m) on the applied trapping potential V_0 and the geometry described with the characteristic trap dimension d. The two radial motions are called cyclotron motion with frequency ν_+, which is commonly called trap-modified cyclotron frequency, and magnetron motion with frequency ν_- [25]. To get the free-space cyclotron frequency (Eq. (2)) out of these, one can utilize the invariance theorem [26]

$$\nu_c^2 = \nu_-^2 + \nu_z^2 + \nu_+^2 \tag{5}$$

or the radial sideband frequency

$$\nu_c = \nu_+ + \nu_-, \tag{6}$$

which is commonly used in nuclear physics measurements. The former, Eq. (5), is accurate even with small misaligments and inhomogeneity present and is commonly used in the most highest precision mass spectrometry reaching accuracies better than 10^{-11} [1]. The latter, Eq. (6), requiring only the sum of the two radial frequencies to be determined, is commonly used in mass measurements for short-lived nuclei. Recently, mass-over-charge doublets have been measured at 10^{-10} level [27] and non-doublets at 10^{-8} level [28].

To measure an absolute atomic mass through Eq. (2), a well known calibration mass is needed since there is no way to otherwise determine B accurately enough. To this end, a Penning trap provides *frequency ratios* and, with proper treatment of the data, *atomic mass ratios*. Ideally, clusters of ^{12}C ions would be used [29], giving a calibration point every 12 mass units. There are also other suitable reference ions, whose masses have been determined very accurately, such as often used ^{133}Cs or ^{85}Rb.

If the ion of interest and reference ion masses are several mass units away, the frequency ratio is prone to so-called mass-dependent frequency shifts [30, 31]. These are due to imperfections in the electrostatic potential and homogenous magnetic field and depend on the motional amplitudes of the trapped ion.

2.3.1. *Mass doublet technique*

Especially in decay Q-value measurements where both parent and daughter have same mass number A, the aforementioned systematic shifts cancel out in the frequency ratio when both ions have equal starting conditions prior to ion motion excitations. Typically these shifts become small compared to statistical uncertainty [32]. To obtain a Q-value from a frequency ratio, a simple equation (for singly charged ions, omitting electron binding energies) can be used:

$$Q = (r-1)\,(M_d - m_e)\,c^2, \tag{7}$$

where r is the daughter/parent ions' frequency ratio $r = \nu_c^d/\nu_c^p$, M_d the atomic mass of the daughter and m_e the mass of an electron. Typically with Q-values of some MeV, the term $r - 1 < 10^{-3}$. This factor also reflects the cancellation of systematic shifts in the Q-value and the uncertainty contribution from the daughter mass. It is easy to generalize Eq. (7) for other charge states and to take electron binding energies into account.

This doublet technique has been extensively used in measurements of Q-values of superallowed β emitters (see Ref. [33] and references therein), Q-value measurements of double beta decay and double electron capture decays [34].

2.3.2. *The time-of-flight ion-cyclotron resonance technique*

To date, most of the atomic mass determinations for short-living ions with Penning traps are done with the so-called time-of-flight ion-cyclotron resonance technique (TOF-ICR) [35, 36]. Here, a radiofrequency (RF) electric field in quadrupolar configuration around the cyclotron frequency of Eq. (2) is applied for a certain

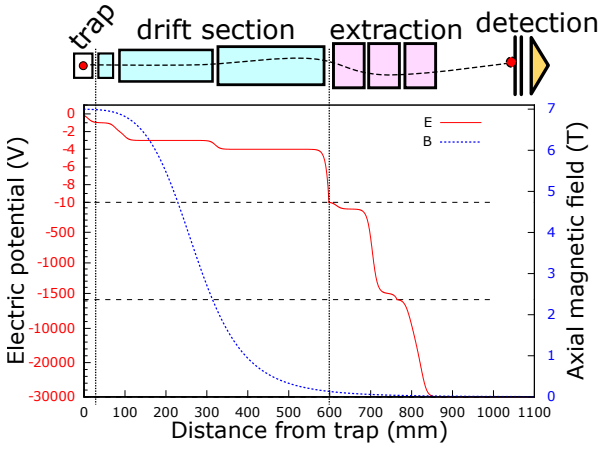

Figure 4: Extraction side of JYFLTRAP showing schematic extraction electrodes, electrostatic potential for extraction mode and the axial magnetic field. When the ions are extracted from the trap, they first pass the so-called drift section that has only few eV lower potential than the trap itself. Since the magnetic field has a rather big gradient there, the ions' radial energy gets converted to axial energy. After this slow drift section the ions are accelerated to 30 $q$keV of energy and finally detected with a microchannel plate detector (MCP).

duration (usually dictated by the half-life of the ion-of-interest or for practical reasons capped to few seconds). With a given amplitude, such a field will periodically convert motion from cyclotron to magnetron and vice versa. The conversion is strongest at the sideband frequency of Eq. (6). Typically the amplitude is chosen so that only one full conversion happens at this frequency. Before this RF excitation, ions are prepared to have some amplitude in magnetron motion, e.g., by applying a dipolar RF electric field or using a Lorenz steerer [37].

After excitation, the ions are released from the trap towards a detector that is outside of the strong magnetic field of the trap (see Fig. 4). The radial energy gets converted to axial in the field gradient, and thus, the ions that have more radial energy (larger cyclotron motion orbit) will reach the detector earlier.

Repeating the measurement for different excitation frequencies, a TOF resonance curve is obtained as shown in Fig. 5. At resonance, the ions possess maximal radial energy, and thus, they are the first to reach the detector. At other frequencies, the conversion is only partial, defined by the excitation amplitude profile. The resonances shown in Fig. 5 is obtained with conventional excitation pulse, *i.e.* the excitation is switched on for a certain duration T_{RF} and off again while keeping the amplitude during the excitation constant.

The width of the resonance is inversely proportional to the excitation time, evident also from Fig. 5. With longer excitation time the resonance becomes narrower and the frequency of the center can be obtained with better precision. In the resonances shown one can also see the motion damping gets worse with longer excitation times. That is, ions collide with rest gas molecules, and consequently, the resonance becomes less pronounced. With measurements of short-living nuclei, also the half-life imposes a limit to the excitation time.

Precision boosting methods

An advanced version of the conventional excitation is the **Ramsey's method of time-separated oscillatory fields.** Instead of applying a constant amplitude for the whole duration of the excitation, the application of the RF is split to two or more excitation pulses interleaved with waiting periods [38]. Usage of two pulses with a waiting period in between boosts the frequency determination precision by a factor of three when same total duration is used for the excitation pattern. The waiting period need to be much longer than the two excitation pulses (e.g. a pattern of 100-700-100 ms on-off-on) in order to get the full benefit of this technique. Ramsey's method has become the norm - nearly all mass measurements utilizing TOF-ICR technique have been performed using Ramsey's method of time-separated oscillatory fields in the recent past [39].

Other precision boosting methods have also been developed. One candidate is **octupolar excitation**. This method has been studied extensively (see e.g. Refs. [40, 41]) and also used in some mass measurements like in Q-value measurement of double-electron capture in ^{164}Er at SHIPTRAP [42]. The experiment would have been impossible with the quadrupole excitation even when Ramsey-type excitation would have been used due to the very low mass difference of the two states.

Octupolar excitation utilizes an 8-pole RF field instead of the quadrupole. The gain factor in mass resolving power between quadrupolar and octupolar excitations is about a factor of ten – much larger than the naively expected factor of two due to doubling of the poles and hence the frequency. It was found out that the lineshape depends strongly on the initial phases and amplitudes of the ion motion and the octupolar field. For this reason, the octupolar excitation has not been used so extensively in experiments as it takes rather long to prepare the experiment for each particular case.

It is worth noting the full width at half maximum of the TOF-resonance is always constant independent of the mass-over-charge of the ion. A way to increase the frequency, and thus to improve the precision of the cyclotron frequency measurement, is to strip more electrons out from the ions. In principle, the precision in-

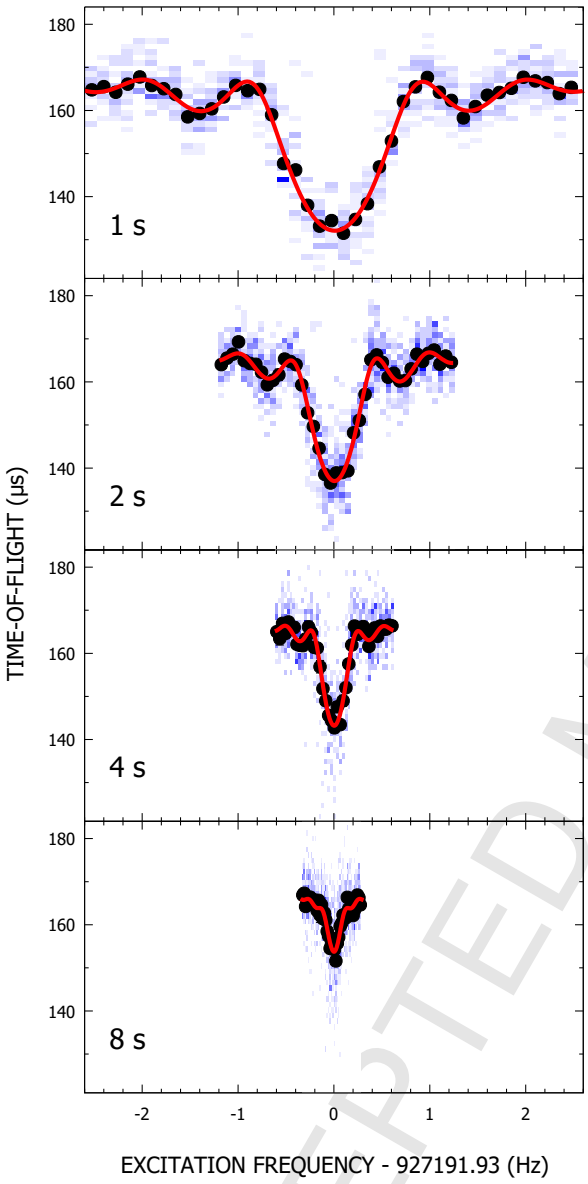

Figure 5: Time-of-flight resonance curves for different excitation (T_{RF}) times as shown in the panels. Black points are the experimental TOF values and red curves are fit to the data. The blue pixels show the scatter of data; darker the pixel, more ions was observed. Each resonance were measured with $^{116}Sn^{1+}$ ions at JYFLTRAP. One can see that the width of the resonance gets narrower when longer excitation times are used. Additionally, motional damping is evident from the decrease of TOF for ions in resonance. See text for more explanation.

creases proportionally to the charge of the ion but in practice charge exchange reactions and difficulties in preparing the ions becomes more and more difficult with increased charge state. **Charge breeding** is currently pursued at TITAN trap [43]. Other limiting factors aside, at some point with high enough charge state the precision of the binding energy of the stripped electrons become the limiting factor in mass determination. Or, put other way around, Penning traps can be used to determine the binding energy.

2.4. Phase-imaging cyclotron resonance technique

The most promising and already demonstrated Penning trap mass measurement technique at the moment is the so-called *phase-imaging cyclotron resonance* (PI-ICR) technique developed at SHIPTRAP [44, 45]. Instead of relying on the energy conversion like in the TOF-ICR method, the new method is based on determination of ion motional phases with a spatially resolving micro channel (MCP) plate detector. This technique is thoroughly explained in Ref. [45].

In practice, the method is used to determine either the magnetron ν_- and modified cyclotron ν_+ frequency separately, or alternatively the cyclotron frequency ν_c (see section 5 of Ref. [45]) by determining the final phase of the motion in question. Axial motion is not measured but cooled to minimal amplitude to minimize frequency shifts and ion scatter due to collisions with rest gas molecules.

Only the magnetron motion phase can be directly projected to the MCP detector since the magnetron period is much longer than the time-of-flight of the ions to the MCP resulting in a well defined spot in the detector. In the case of high-frequency cyclotron motion, direct determination of the cyclotron phase is not possible. Instead of a well defined spot a ring is observed. To get the phase of the fast cyclotron motion a short quadrupole excitation pulse is applied to convert cyclotron motion to slow magnetron motion and consequently its phase can be determined. In addition, to obtain a distortion-free phase image, the ion path from the trap to the MCP detector needs to be electric field free.

Compared with the TOF-ICR technique using Ramsey excitation scheme, this technique is an astonishing factor of 25 faster and provides a 40-fold gain in resolving power. Very recently mass difference of ^{163}Ho and ^{163}Dy was measured at SHIPTRAP with the new method providing a mass ratio at 10^{-10} precision level surpassing any TOF-ICR measurements [27].

This technique is now being implemented in other Penning trap experiments. It is clear that such precision requires the ions in the trap to be prepared extremely

well in order to avoid amplitude-dependent frequency shifts. Although this method boosts the precision or reduces the frequency measurement time, preparation time for the measurement will be considerably longer than for TOF-ICR. Also, in order to utilize the method, the cyclotron frequency needs to be known to some precision so that the measured phase can be correctly assigned to the period preceded by *known* number of full periods. In case of short-lived ions of unknown mass, it is necessary to first obtain a rough frequency with the ordinary TOF-ICR technique. For example $A/q = 100$ ions in 7 T field have about 1 MHz cyclotron frequency. In order to know the number of full periods the ions have circulated after phase accumulation time of 1 second, the mass needs to be known better than 10^{-6} precision (100 keV/c^2).

2.5. Gas-filled Penning trap for beam purification

Perhaps the most used beam purification technique for short-lived rare ions is the sideband cooling technique developed nearly three decades ago at ISOLTRAP [46]. By filling a Penning trap with low-pressure gas (10^{-5} mbar), the amplitudes of the fast modified cyclotron and axial motions gets damped. The amplitude of the magnetron motion, on the other hand, slowly increases.

The recipe for mass-selective cleaning in a buffer-gas filled Penning trap is rather simple (example duration given in parenthesis, case dependent):

1. cooling (50 ms)
2. magnetron excitation (5 ms or simultaneously with quadrupole excitation)
3. mass-selective quadrupolar excitation (100 ms)
4. cooling (30 ms)
5. extract through narrow aperture (10 μs).

The first step simply reduces the axial amplitude of the ions due to ion collisions with buffer gas atoms. The second step increases the magnetron motion diameter of all ions. The magnetron orbit diameter needs to become larger than the diameter of the extraction hole aperture in order for this cleaning technique to work.

The third step is where the mass selectivity comes into play. The excitation frequency is set to be the ion cyclotron frequency (Eq. (2)) and thus the magnetron motion for the ions of interest with some frequency bandwidth gets converted to cyclotron motion. The subsequent cooling period cools the cyclotron motion and thus ions of interest have now both their magnetron and cyclotron motion mostly removed. Once the bunch is extracted through an electrode having a narrow aperture (see Fig. 3 (B), electrode on far left) only the ions of interest can pass and the contaminants hit the electrode.

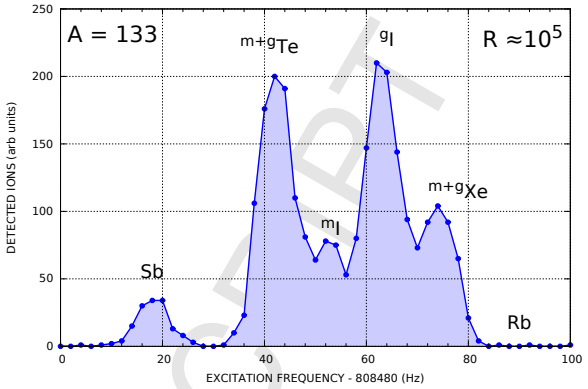

Figure 6: An example frequency scan utilizing sideband cooling method of Ref. [46] using JYFLTRAP's gas filled purification trap [24]. The ions were produced in proton induced fission of uranium. The scan shows the various isotopes and isomers produced. A mass resolving power $M/\Delta M$ of about 10^5 is obtained. Both ^{133}Te and ^{133}Xe have low-lying isomeric states, which can't be fully separated with this method.

The obtained resolving power depends on various factors like gas pressure, excitation times, amplitudes and durations. The resolving power is often tuned to "as low as necessary required" to gain in transmission and to properly cool the ions. The purity of the used gas (typically helium) and the background pressure plays an important role. The background gas molecules like water vapor can cause charge exchange to happen, *i.e.* the ion of interest getting neutralized (and subsequently lost) and the contaminant molecule ionized. An example of a rather high resolving power frequency scan of the quadrupolar electric field is shown in Fig. 6.

2.6. High-resolution Penning trap cleaning techniques

In absence or in addition to the cleaning method described in the previous section, a Penning trap without buffer gas can be utilized for cleaning purposes. Without any cooling method, it is necessary to be very careful to not excite the ion of interest with a too short excitation pulse duration, especially when its mass is being measured, in order to avoid frequency shifts.

Most often the cleaning is accomplished by exciting the contaminant ions' cyclotron motion with dipolar excitation near or at it's ν_+ frequency. This frequency offers the most mass resolving power as it is directly proportional to $\nu_c = \frac{1}{2\pi}\frac{q}{m}B$ with a small offset due to the almost-constant magnetron frequency ν_-. One example of dipolar cleaning is described in Ref. [47], where states of ^{70}Cu were separated using this

method at ISOLTRAP. It has been used in many Penning trap experiments, especially in the ones lacking high-resolution preseparation. It is quite easy to remove known contaminants but with unknown ones it is rather tedious to apply cleaning to every possible contaminant (especially to identify every contaminant) as explained well in Ref. [48], where a cleaning method based on stored waveform inverse fourier transform (SWIFT) is explained. In short, SWIFT excitation scheme is applied that ions beyond a narrow "no excitation gap" are removed with rather large bandwidth.

For extremely high resolution cleaning, the dipolar excitation can be used by scaling the excitation time up. Alternatively, if cooling is available (not necessarily in the trap where the cleaning is applied), also the ion-of-interest can be, to some extent, excited. This shortens the required excitation time considerably, especially if Ramsey-type excitation is used described in Ref. [49]. This so-called Ramsey cleaning method that is frequently used at JYFLTRAP and can provide separation at the ~0.5 Hz level. For singly charged ions with mass of 100 u in 7 T field this corresponds to $M/\Delta M \approx 2 \times 10^6$ ($\approx$ 50 keV/c^2). A glimpse of the available resolving power can be seen in Fig. 7.

The Ramsey cleaning method has enabled contaminant-free mass measurements and decay spectroscopy of various nuclei. It is possible to determine mass when a contaminant is present but in Penning trap mass spectrometry the measured frequencies are prone to shifts, which might result in a reduction of the measurement accuracy [52]. Especially Q_{EC}-values of several superallowed beta emitters could be determined in absence of low-lying isomeric contaminants [33] and masses near ^{132}Sn for nuclear structure studies [53].

Recently, other types of cleaning methods have emerged. One promising is the so-called SIMCO method (simultaneous magnetron and resonant conversion), where simultaneous dipolar magnetron and quadrupolar cyclotron excitation is applied [54]. Also octupolar excitation has been studied for cleaning purposes [55].

2.7. Multi-reflection time-of-flight separators

The long-awaited multi-reflection time-of-flight (MR-TOF) separators [56] have finally entered to the field of nuclear physics [14–16]. These devices can provide similar or even better [57] mass resolving power in much shorter time than a buffer gas filled purification Penning trap.

The principle of an MR-TOF separator is rather simple. A well-focused bunch of ions is injected inside the

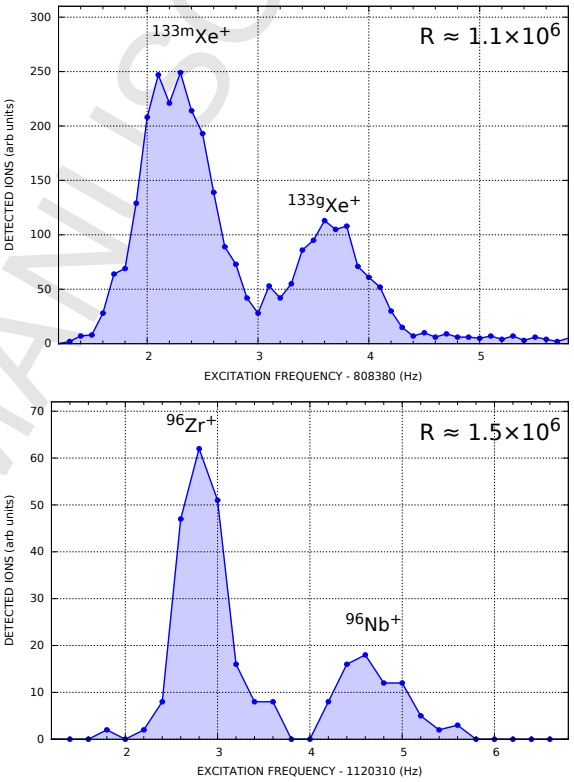

Figure 7: (Top) Separation of the isomeric states of ^{133}Xe having mass difference 233 keV [50]. (Bottom) Separation of ^{96}Nb and ^{96}Zr having mass difference 163.96(13) keV [51].

device and let freely drift between two electrostatic mirrors. The geometry and potential of the mirror electrodes are chosen such that ions retain isochronocity: Ions can have tens of eV of energy spread and this is what the mirrors have to compensate for to keep the "lap time" constant. With each turn there is dispersion in mass. It has been shown that MR-TOFs can obtain and even surpass the mass resolving power of a gas-filled purification trap and reach resolving power beyond 10^5 in as little as 10 ms. This has enabled purification of ion beams with much worse ion-of-interest to contamination ratios and shorter half-lives [58].

Since the interest is to go further out from the valley of stability towards more exotic ions, the relative amount of accompanying contaminating ions is dramatically increasing. Buffer gas filled purification traps and other preseparators can do only that much and this is where MR-TOFs come in need. At the moment MR-TOFs are being built in many facilities, see Table 2.

2.8. Summary of ion-trap facilities in the world

Currently, there are seven operating Penning-trap facilities dedicated to high-precision mass measurements in the world (see Table 2, REXTRAP has not been used for mass measurements). With respect to the number of measured ground or isomeric states in nuclei, ISOLTRAP [59] at the ISOLDE facility at CERN has been the most productive Penning trap in the world. JYFLTRAP [24] holds the second place, thanks to the universal ion-guide technique employed at the IGISOL facility in the JYFL Accelerator Laboratory in Jyväskylä. The CPT Penning trap [60] has performed a massive number of mass measurements of neutron-rich fission fragments at the CARIBU facility in the Argonne National Laboratory. SHIPTRAP [61] at GSI has specialized in measuring masses of superheavy elements (see e.g. [62–64]). TITAN [65] at TRIUMF utilizes highly-charged ions in their experiments, and has measured many light, neutron-rich isotopes. LEBIT [66] employs exotic ions produced via fast beam fragmentation and in-flight separation at the National Superconducting Cyclotron Laboratory (NSCL). TRIGA-TRAP [67] in Mainz is also operating, and has been mainly dedicated to very high-precision Q-value measurements.

3. Overview of recent mass measurements employing ion traps

Over the years, Penning-trap measurements have yielded more than thousand mass or Q-values that have improved our knowledge of *e.g.* evolution of shell closures, onset of deformation, and nucleosynthesis in stars (see Fig. 8). Most of the mass values have been compiled in the Atomic Mass Evaluation 2012 (AME12) [68]. After AME12, around 100 mass values from experiments with ion traps have been published. Twelve nuclei (^{52,53}K [58], ^{53,54}Ca [69], ^{82}Zn [70], ^{100}Rb [71], ^{129,131}Cd [72], ^{141}I [73], ^{198}At[74], ^{232,233}Fr [75]) have been measured for the first time. The new measurements have revealed large deviations from the adopted or extrapolated mass values in the AME12 (see Fig. 9). For example, ^{52,53}K and ^{53,54}Ca are 400-1000 keV lower than the AME12 values. On the other hand, in the ^{132}Sn region, ^{129,130,131}Cd [72] all yield 100-360 keV higher values than in the AME12. The CPT results for ^{130,131}In [73] also differ by more than 100 keV from the AME12. However, the results are for an unknown mixture of isomeric and ground states which can explain the deviations to AME12 and JYFLTRAP [53, 76]. Discrepancies at ^{140}Te [73, 76] and ^{146}Cs [73] are intriguing and call for new measurements.

The recent Penning-trap measurements have focused on a couple of regions on the chart of nuclides. Firstly, several measurements of nuclei in the vicinity of doubly magic ^{132}Sn have been performed [53, 72, 73, 76, 80]. These nuclei are also important not only for studying the evolution of the $Z = 50$ and $N = 82$ shell-gap energies but also for modeling the astrophysical r process [81]. Secondly, the evolution of $N = 28$ and $N = 32$ shell closures in neutron-rich K and Ca nuclei have been studied at ISOLTRAP [82, 83] and TITAN [82, 83]. A third region of recent interest is located around the $Z = 82$ shell closure, which has been explored via measurements of Tl, Pb, Fr, Ra isotopes at ISOLTRAP [74, 75, 84]. In addition, new measurements of neutron-rich Sr and Rb nuclei have probed the nuclear structure changes in the midshell region [71, 85], and extended these studies towards more neutron-rich regions than in previous works [86, 87]. Islands of inversion at $N = 40$ and $N = 20$ have been explored via measurements of neutron-rich Mn and Fe [88] and Mg [89] isotopes. In the neutron-deficient side, several measurements have focused on the isobaric multiplet mass equation at A=9 [90], A=20 and A=21 [91] and A=31 [92]. Studies of mirror nuclei ^{21}Na [93], ^{23}Mg [94], ^{25}Al [95], ^{29}Na [93], ^{45}V [96], and ^{49}Mn [96] have improved the precisions of the Q_{EC} values considerably (see Table 6). Also many stable nuclei have been studied, such as Zr and Mo isotopes at LEBIT [97] and JYFLTRAP [98, 99], or ^{184}Os at TRIGA-TRAP [100], which revealed a 2.9σ deviation to the AME12. The recently published mass-excess values, which have not been included in the AME12, have

Table 2: Table of all ion traps that are currently in use, being commissioned or under planning at the radioactive beam facilities around the world.

Location	Facility	Setup name	Type	Status
North America				
USA	Argonne NL	CPT	PT (+ MR-TOF)	Operational
USA	NSCL/MSU	LEBIT	PT	Operational
Canada	TRIUMF	TITAN	PT (+ MR-TOF)	Operational
USA	Texas A&M	TAMUTRAP	PT	Commissioning
Europe				
Switzerland	ISOLDE	ISOLTRAP	PT+MR-TOF	Operational
Finland	JYFL	JYFLTRAP	PT (+ MR-TOF)	Operational
Germany	GSI	SHIPTRAP	PT	Operational
Germany	Univ. Mainz	TRIGATRAP	PT	Operational
Switzerland	ISOLDE	REXTRAP	PT	Operational
Germany	GSI	HITRAP	PT	Commissioning
Germany	GSI/FAIR	FRS Ion Catcher	MR-TOF	Operational
Germany/France	Univ. Munich/ALTO	MLL-TRAP	PT	Commissioning
Germany	GSI/FAIR	MATS	PT	Planning
France	GANIL	DESIR-TRAP	PT	Planning
France	GANIL	PIPERADE	PT	Planning
France	GANIL	PILGRIM	MR-TOF	Planning
Russia	PNPI	PITRAP	PT	Planning
Asia				
Japan	RIKEN	SLOWRI	MR-TOF	Operational
China	IMP Lanzhou	Lanzhou-trap	PT	Planning
China	CIAE, BRIF	BRIF-TRAP	PT	Planning
China	CIAE, CARIF	CARIF-TRAP	PT	Planning
India	VECC	VECC-TRAP	PT	Planning
Japan	RIKEN	RIKEN-TRAP	PT	Planning
South Korea	RISP	RISP-TRAP	PT	Planning

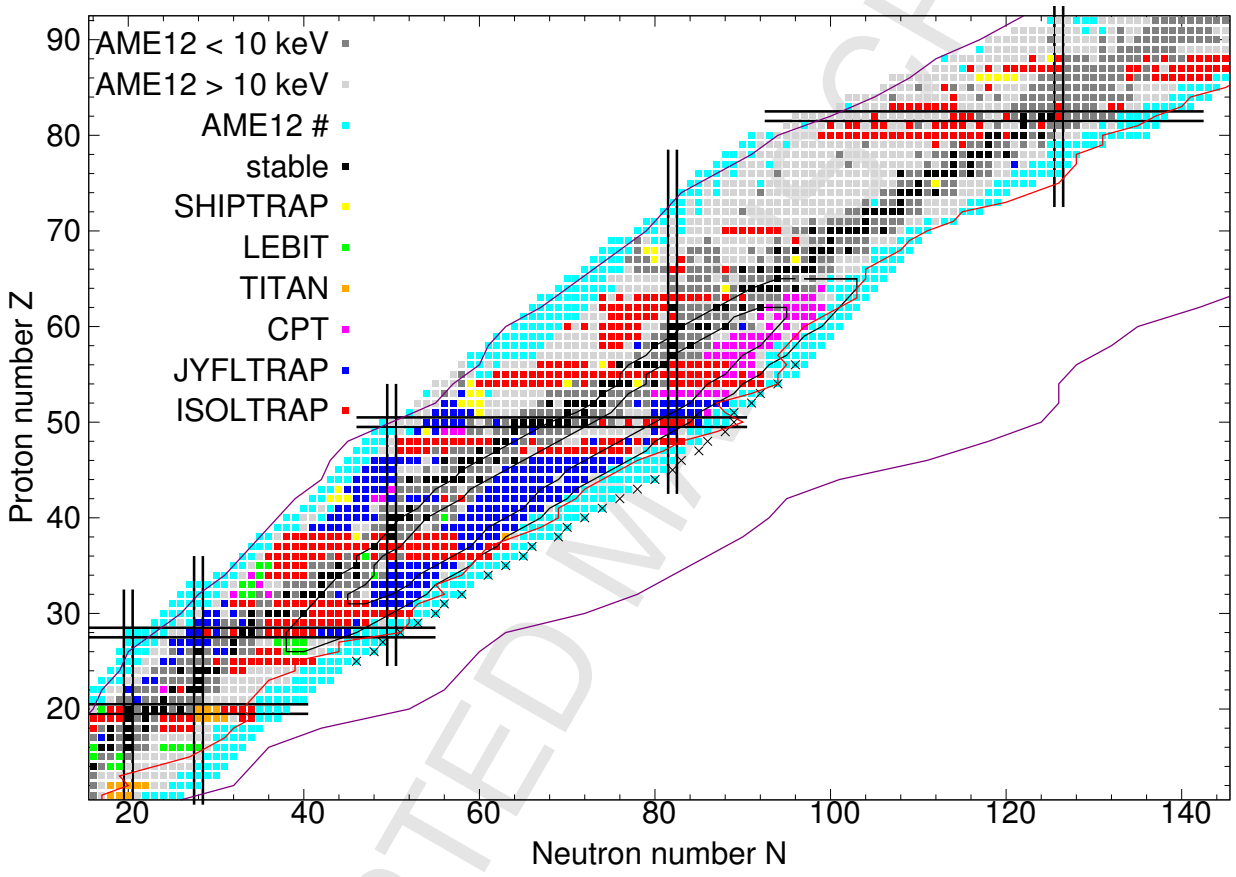

Figure 8: (Color online) Penning-trap measurements performed at ISOLTRAP, JYFLTRAP, SHIPTRAP, LEBIT, CPT and TITAN. Since many nuclei have been measured at several facilities, all data points are not visible in the figure. The nuclei whose mass-excess values in AME2012 [68] are known with a precision better than 10 keV (dark grey), worse than 10 keV (light grey) or have extrapolated mass values (cyan) are also shown. The average two-proton and two-neutron driplines from the energy-density functional calculations are plotted in purple [77]. The crosses highlight the most neutron-rich isotopes whose half-lives have been measured recently at RIKEN [78, 79]. A 100-ms contour for half-lives of neutron-rich isotopes (red line) and contours for calculated 1-μb and 1-mb ^{238}U(p 25 MeV,f) fission cross sections are also shown (black lines).

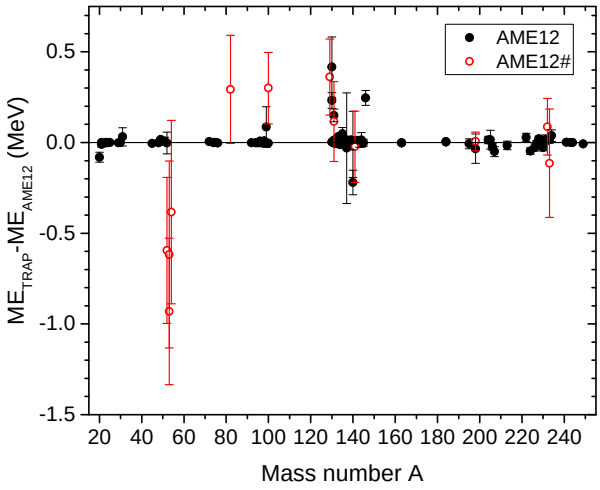

Figure 9: Comparison of recent ion-trap mass measurements to the AME12 [68]. The general agreement with the AME12 is rather good. However, several isotopes deviate significantly. The largest deviations are observed for nuclei around ^{52}Ca and ^{132}Sn.

been summarized in Tables 3, 4, and 5.

3.1. Comparison with theoretical mass models

The Penning-trap measurements provide a data pool for comparisons with different theoretical mass models. We have now compared five different mass models (FRDM2012 [108], Duflo-Zuker [109], WS4 [110], HFB-24 [111], and UNEDF0 [112]) to experimental mass-excess values in three different regions in the chart of nuclides. The regions, $Z = 15 - 25$, $Z = 45 - 55$ and $Z = 80 - 90$, were selected due to their locations close to magic neutron and proton shells at ^{48}Ca, ^{132}Sn, and ^{208}Pb, and since recently mass measurements have been performed in these regions (see Table 3). Most of the theoretical models selected are relatively new [108, 110–112], the only exception is the Duflo-Zuker formula. Three of the models, FRDM2012, Duflo-Zuker, and WS4 are macroscopic-microscopic models where the macroscopic part is based on the liquid drop model. The HFB-24 and UNEDF0 models are based on Hartree-Fock-Bogoliubov mass model with Skyrme forces. Of these, UNEDF0 is purely energy density functional without any additional procedures done to match the experimental data. Below, the different models are shortly described.

FRDM2012 is a macroscopic-microscopic mass model. It is based on finite-range droplet macroscopic and the folded-Yukawa single-particle microscopic nuclear-structure models. FRDM2012 employs the same model as its precursor, FRDM1995 [113], but with considerably improved treatment of deformation and fewer approximations have been made thanks to more computing power available. The root-mean square (rms) error of the FRDM2012 model is 0.5595 MeV for the entire region of nuclei included in the adjustment, and only 0.3549 MeV for the nuclei with $N \geq 65$ (0.669 MeV and 0.448 MeV for the FRDM1995 model, respectively).

Duflo-Zuker is also a macroscopic-microscopic formula. Its six macroscopic monopole terms lead asymptotically to a liquid drop form, three microscopic terms take into account configuration mixing (multipole) corrections to the monopole shell effects, and one term is for deformed nuclei. Duflo-Zuker, originally fitted to AME1995 values, performed outstandingly well compared to other mass models when AME2003 mass evaluation was published [114] with a root-mean square error of about 0.5 MeV.

WS4 (Weizsäcker–Skyrme 4) model [110] is a macroscopic–microscopic mass formula, where the macroscopic part is treated using the liquid drop model, and axially deformed Woods–Saxon potential is adopted to obtain the shell corrections using the Strutinsky method. The latest WS model, WS4, has taken into account the surface diffuseness effect of nuclei near the drip lines for the first time. This resulted in a better prediction of neutron-rich masses, and the root-mean square to AME12 only 0.298 MeV.

The HFB-24 model [111] is based on the Hartree-Fock-Bogoliubov (HFB) mass model supplemented by the Skyrme forces with a microscopic pairing force, phenomenological Wigner terms and correction terms for the spurious collective energy. The model parameters have been fitted to the AME12 [68] experimental mass values, and the Skyrme force has been simultaneously fitted to the zero-temperature equation of state of infinite homogeneous neutron matter as determined by many-body calculations with realistic two- and three-nucleon forces. The HFB-24 model works rather well with about 0.55 MeV root-mean square deviation to the AME2012 [68] evaluation.

UNEDF0 [112] is a pure energy-density functional model relying on the nuclear energy density of Skyrme type in the framework of the Hartree-Fock-Bogoliubov theory. The energy-density functional was calibrated by fitting to a set of 72 nuclei at closed Z=20, 28, 50, and 82 proton shells, from the mid-shell region with $N \approx 100$ and from the heavy region $Z \geq 100$. Only spherical or axially deformed nuclei are considered in UNEDF0. The root-mean square error, 1.45 MeV, is much better than for example for the SLy4 model [115, 116] with an rms error of 4.80 MeV. It has been suggested that the Sly4 model has an overemphasis on doubly-magic

Table 3: Summary of most recent Penning-trap measurements (not included in the AME12). The reference ions are singly-charged unless stated otherwise.

Nuclide	Ref.	ME_{trap} (keV)	ME_{AME12} (keV)	Trap	Ref.
^{21}Na	^{21}Ne	-2184.63(10)	-2184.64(28)	LEBIT	[93]
^{20}Mg	^{23}Na	17477.7(18)	17559(27)	TITAN	[91]
^{21}Mg	^{23}Na	10903.85(74)	10914(16)	TITAN	[91]
^{23}Mg	^{23}Na	-5473.50(16)	-5473.3(7)	TITAN	[94]
^{24}Al	^{23}Na	-48.86(23)	-47.6(11)	TITAN	[101]
^{25}Al	^{25}Mg	-8915.962(63)	-8916.2(5)	JYFLTRAP	[95]
^{29}P	$^{12}C_3$	-16953.15(47)	-16952.5(6)	LEBIT	[93]
^{30}P	^{30}Si	-20200.854(64)	-20200.6(3)	JYFLTRAP	[95]
^{31}Cl	^{31}P	-7034.7(34)	-7070(50)	JYFLTRAP	[92]
^{52}K	^{39}K,^{52}Cr	-17138(33)	-16540(400)#	ISOLTRAP/MR-TOF	[58]
^{53}K	^{39}K,^{52}Cr	-12298(112)	-11680(500)#	ISOLTRAP/MR-TOF	[58]
^{48}Ca	^{14}N^{18}O^{16}O	-44224.45(27)	-44224.76(12)	TITAN	[102]
^{51}Ca	^{39}K	-36332.07(58)	-36339(22)	ISOLTRAP	[69]
^{52}Ca	^{39}K	-34266.02(71)	-342660(60)	ISOLTRAP	[69]
^{53}Ca	^{39}K,^{53}Cr	-29388(43)	-28460(400)#	ISOLTRAP/MR-TOF	[69]
^{54}Ca	^{39}K,^{54}Cr	-25161(49)	-24780(500)#	ISOLTRAP/MR-TOF	[69]
^{48}Ti	^{14}N^{18}O^{16}O	-48492.71(21)	-48491.7(4)	TITAN	[102]
^{45}V	^{45}Ti	-31885.3(9)	-31881(8)	JYFLTRAP	[96]
^{49}Mn	^{49}Cr	-37620.3(24)	-37637(10)	JYFLTRAP	[96]
^{82}Zn	^{85}Rb	-42314(3)	-42610(300)#	ISOLTRAP	[70]
^{74}Ga	^{85}Rb^{9+}	-68049.7(50)	-68050(3)	TITAN	[103]
^{72}Br	^{85}Rb	-59062.2(10)	-59067(7)	LEBIT	[104]
^{74}Rb	^{85}Rb^{9+}	-51916.5(60)	-51916(3)	TITAN	[103]
^{75}Rb	^{85}Rb^{9+}	-57218.7(17)	-57218.7(12)	TITAN	[103]
^{76}Rb	^{85}Rb^{9+}	-60481.0(16)	-60479.1(9)	TITAN	[103]
^{98}Rb	^{85}Rb	-54309.4(40)	-54318(3)	ISOLTRAP	[71]
^{99}Rb	^{85}Rb	-51120.3(45)	-51205(110)	ISOLTRAP	[71]
^{100}Rb	^{85}Rb	-46247(20)	-46550(200)#	ISOLTRAP	[71]
^{96}Zr	^{96}Mo	-85437.5(4)	-85445(2)	JYFLTRAP	[51]
^{96}Nb	^{96}Mo	-85601.5(4)	-85607(3)	JYFLTRAP	[51]
^{92}Mo	^{87}Rb,$^{12}C_8$	-86808.53(17)	-86807.8 0,781	LEBIT	[97]
^{94}Mo	^{87}Rb,$^{12}C_8$	-88413.96(25)	-88412.8(4)	LEBIT	[97]
^{95}Mo	^{87}Rb,$^{12}C_8$	-87711.51(26)	-87710.6(4)	LEBIT	[97]
^{96}Mo	^{87}Rb,$^{12}C_8$	-88794.53(30)	-88793.6(4)	LEBIT	[97]
^{97}Mo	^{87}Rb,$^{12}C_8$	-87544.44(25)	-87543.6(5)	LEBIT	[97]
^{98}Mo	^{87}Rb,$^{12}C_8$	-88115.95(38)	-88114.8(5)	LEBIT	[97]
^{100}Mo	^{87}Rb,$^{12}C_8$	-86193.04(30)	-86189.5(10)	LEBIT	[97]

Table 4: Table 3 continued.

Nuclide	Ref.	ME_{trap} (keV)	ME_{AME12} (keV)	Trap	Ref.
^{129}Cd	^{133}Cs	-63148(74)	-63510(200)#	ISOLTRAP	[72]
^{130}Cd	^{133}Cs	-61118(22)	-61530(160)	ISOLTRAP	[72]
^{131}Cd	^{131}Cs,^{133}Cs	-55215(100)	-55330(200)#	ISOLTRAP/MR-TOF	[72]
^{130}In	^{133}Cs	-69652(20)	-69880(40)	CPT	[73]
^{131}In	^{133}Cs	-67876(35)	-68025.6(27)	CPT	[73]
^{130}Sn	^{133}Cs	-80130.8(36)	-80132.9(21)	CPT	[73]
^{131}Sn	^{133}Cs	-77259.6(43)	-77272(6)	CPT	[73]
^{132}Sn	^{133}Cs	-76549.0(28)	-76543.9(29)	CPT	[73]
^{133}Sn	^{133}Cs	-70869.1(36)	-70874.2(24)	CPT	[73]
^{134}Sn	^{133}Cs	-66444(16)	-66432(3)	CPT	[73]
^{135}Sn	^{133}Cs	-60584(34)	-60632(3)	CPT	[73]
^{131}Sb	^{133}Cs	-81986(10)	-81981.9(21)	CPT	[73]
^{132}Sb	^{133}Cs	-79633.8(61)	-79635.6(27)	CPT	[73]
^{133}Sb	^{133}Cs	-78921.3(76)	-78923(3)	CPT	[73]
^{134}Sb	^{133}Cs	-74012(10)	-74020.5(17)	CPT	[73]
^{135}Sb	^{133}Cs	-69693.9(65)	-69689.6(29)	CPT	[73]
^{136}Sb	^{133}Cs	-64491(15)	-64510(6)	CPT	[73]
^{137}Sb	^{133}Cs	-60061(52)	-60030(300)	CPT	[73]
^{133}Te	^{133}Cs	-82899.8(65)	-82932(4)	CPT	[73]
^{135}Te	^{133}Cs	-77729.6(21)	-77727.9(27)	CPT	[73]
^{136}Te	^{133}Cs	-74423.3(37)	-74425.8(24)	CPT	[73]
^{137}Te	^{133}Cs	-69301.7(37)	-69304.2(25)	CPT	[73]
^{138}Te	^{133}Cs	-65695.3(76)	-65696(4)	CPT	[73]
^{139}Te	^{133}Cs	-60191(17)	-60205(4)	CPT	[73]
^{140}Te	^{133}Cs	-56577(62)	-56357(28)	CPT	[73]
^{133}I	^{133}Cs	-85858.2(64)	-85887(5)	CPT	[73]
^{134}I	^{133}Cs	-84040.8(64)	-84059(6)	CPT	[73]
^{135}I	^{133}Cs	-83778.9(20)	-83789(5)	CPT	[73]
^{139}I	^{133}Cs	-68470.7(40)	-68459(29)	CPT	[73]
^{140}I	^{133}Cs	-63606(13)	-63600(180)	CPT	[73]
^{141}I	^{133}Cs	-59927(16)	-59900(200)#	CPT	[73]
^{142}Cs	^{133}Cs	-70506.9(93)	-70518(7)	CPT	[73]
^{143}Cs	^{133}Cs	-67676.3(79)	-67674(22)	CPT	[73]
^{144}Cs	^{133}Cs	-63256(31)	-63271(25)	CPT	[73]
^{145}Cs	^{133}Cs	-60057(16)	-60056(11)	CPT	[73]
^{146}Cs	^{133}Cs	-55323.2(86)	-55570(40)	CPT	[73]

Table 5: Table 3 continued.

Nuclide	Ref.	ME_{trap} (keV)	ME_{AME12} (keV)	Trap	Ref.
^{163}Dy	$^{12}C_{15}$	-66381.7(8)	-66379.9(19)	TRIGA-TRAP	[105]
^{163}Ho	$^{12}C_{15}$	-66379.3(9)	-66377.3(19)	TRIGA-TRAP	[105]
^{184}W	$^{12}C_{15}$	-45705.40(94)	-45707.6(9)	TRIGA-TRAP	[100]
^{184}Os	$^{12}C_{15}$	-44251.47(113)	-44256.6(13)	TRIGA-TRAP	[100]
^{195}Tl^{g}	^{133}Cs	-28162(25)	-28155(11)	ISOLTRAP	[84]
^{195}Tl^{g,m}	^{133}Cs	-28152(24)		ISOLTRAP	
^{198}Tl^{g}	^{133}Cs	-27528.7(75)	-27490(80)	ISOLTRAP	[84]
^{198}At^{g}	^{133}Cs	-6715(6)	-6721(51)#	ISOLTRAP	[74]
^{204}Rn	^{133}Cs,^{208}Pb	-7969(15)	-7983(15)	SHIPTRAP	[106]
^{205}Rn	^{133}Cs,^{208}Pb	-7698(9)	-7710(50)	SHIPTRAP	[106]
^{206}Rn	^{133}Cs,^{208}Pb	-9139(10)	-9115(15)	SHIPTRAP	[106]
^{207}Rn	^{133}Cs	-8685(26)	-8635(8)	SHIPTRAP	[106]
^{222}Fr	^{133}Cs	16378(7)	16350(21)	ISOLTRAP	[75]
^{224}Fr	^{133}Cs	21748(12)	21795(13)	ISOLTRAP	[75]
^{226}Fr	^{133}Cs	27513(15)	27541(12)	ISOLTRAP	[75]
^{227}Fr	^{133}Cs	29682(7)	29686(13)	ISOLTRAP	[75]
^{228}Fr	^{133}Cs	33389(8)	33369(13)	ISOLTRAP	[75]
^{229}Fr	^{133}Cs,^{238}U	35666(6)	35674(14)	ISOLTRAP	[75]
^{230}Fr	^{133}Cs	39483(8)	39511(16)	ISOLTRAP	[75]
^{231}Fr	^{133}Cs	42080(8)	42064(25)	ISOLTRAP	[75]
^{232}Fr	^{133}Cs	46073(14)	45990(160)#	ISOLTRAP	[75]
^{233}Fr	^{133}Cs	48920(20)	49030(300)#	ISOLTRAP	[75]
^{213}Ra^{2+}	^{133}Cs	342(11)	358(21)	SHIPTRAP	[106]
^{233}Ra	^{133}Cs	44339(12)	44322(16)	ISOLTRAP	[75]
^{234}Ra	^{133}Cs	46931(8)	46890(30)	ISOLTRAP	[75]
^{244}Pu	$^{12}C_{22}$	59806.2(18)	59807(5)	TRIGA-TRAP	[107]
^{241}Am	$^{12}C_{22}$	52936.9(18)	52936.2(18)	TRIGA-TRAP	[107]
^{243}Am	$^{12}C_{22}$	57176.2(14)	57176.3(23)	TRIGA-TRAP	[107]
^{249}Cf	$^{12}C_{22}$	69718.1(13)	69726.0(22)	TRIGA-TRAP	[107]

nuclei during the optimization process which might explain the larger differences.

The mass-excess differences to the FRDM2012 have been plotted for the first region of interest, from P (Z = 15) to Mn (Z = 25), in Fig. 10. Between N = 20 and N = 28, the agreement between the experimental values and theoretical models seems to be rather good with the exception of UNEDF0 for some chains. An interesting feature is observed at N = 32 where FRDM2012 predicts higher mass-excess values, i.e. smaller binding energies, than experimental results. HFB-24 and WS4 follow the experimental trend in a better way. However, when we enter the region where no experimental data exist so far, WS4 model predicts much smaller binding energies than FRDM2012 and the other models. As a result, deviations on the order of several MeV are observed between the models outside the experimentally known region.

For the second region of interest, from Rh (Z = 45) to Cs (Z = 55), the largest deviations to the experimental values are observed at N = 50 and N = 82 (see Fig. 11). The trend in the neutron-rich region, where no experimental data are no available, is the same as for the lower mass region: WS4 predicts much smaller binding energies than FRDM2012, whereas Duflo-Zuker and HFB-24 tend to give higher binding energies than the FRDM2012. The overall deviations are large asking for more refined mass models and systematic studies in order to obtain a better understanding for example on the astrophysical rapid neutron capture process.

In the third region of interest, from Hg (Z=80) to Th (Z=90), the UNEDF0 model seems to have difficulties in producing the binding energies at the closed neutron shell N = 126 (see Fig. 12). The uncertainties in the Skyrme energy-density functional model have been studied e.g. in Refs. [117, 118]. The discrepancy at ^{208}Pb cannot be removed by fit parameters as they are already quite rigidly constrained by other data. This suggests that something is missing in the description of the ^{208}Pb mass (N = 126).This is most probably related to a poor description of the ground-state collective correlations in doubly-magic systems [117]. Otherwise, the trends in the experimentally unknown region are relatively similar as in the lower mass regions, except that the Duflo-Zuker model predicts now smaller binding energies than the FRDM2012 model, and thus, has a similar trend to WS4.

To summarize, most of the mass models are in a reasonable agreement where experimental data exist but the deviations between the models become very large outside the known region. None of the discussed models performs outstandingly well in all three regions dis-

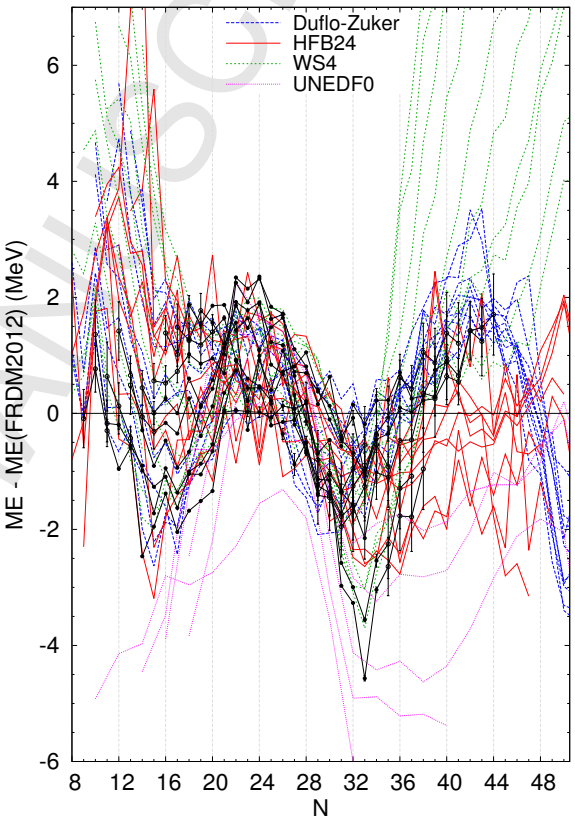

Figure 10: Comparison of experimental mass-excess values to different theoretical models for isotopic chains from P (Z=15) to Mn (Z=25) as a function of neutron number N. FRDM2012 has been used as a baseline. Black solid points are experimental values and hollow points are AME2012 extrapolated values.

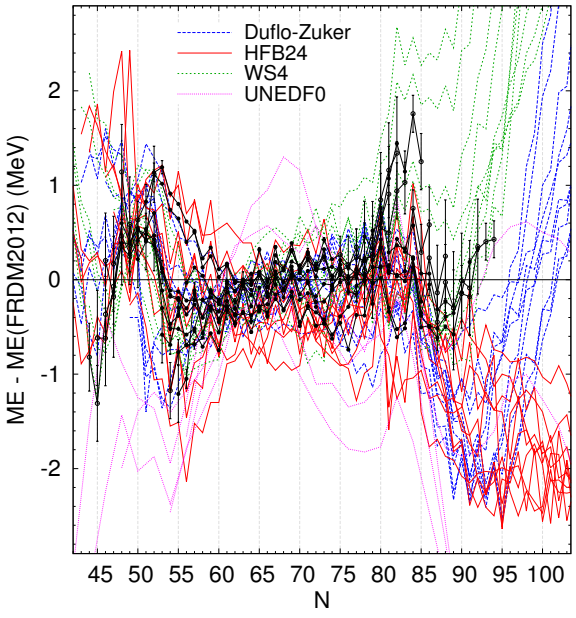

Figure 11: Comparison of experimental mass-excess values to different theoretical models for isotopic chains from Rh (Z=45) to Cs (Z=55) as a function of neutron number N. FRDM2012 has been used as a baseline. Black solid points are experimental values and hollow points are AME2012 extrapolated values.

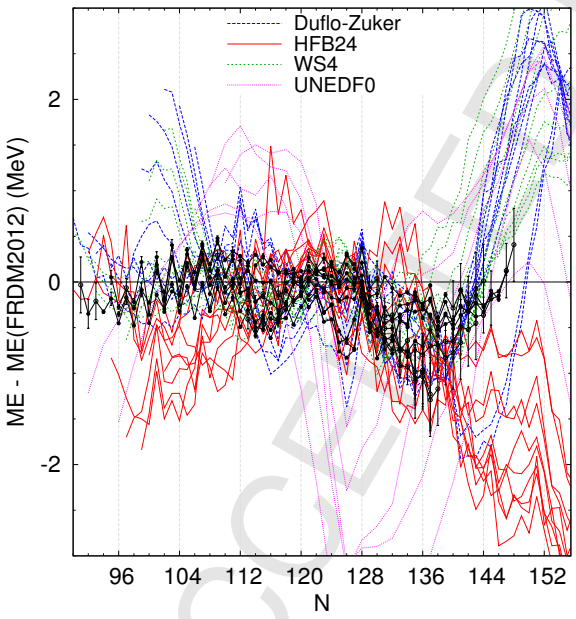

Figure 12: Comparison of experimental mass-excess values to different theoretical models for isotopic chains from Rh (Z=80) to Th (Z=90) as a function of neutron number N. FRDM2012 has been used as a baseline. Black solid points are experimental values and hollow points are AME2012 extrapolated values.

cussed above. It should also be noted that the mass differentials are usually better predicted by the models than the absolute mass values (see e.g. Section 3.2.5 for two-neutron shell gap energies). Thus, scatter e.g. in neutron-separation energies required for the astrophysical r-process modeling may not deviate as much as the mass values shown in Figs. 10, 11 and 12.

3.2. Two-nucleon binding energies and shell gaps

A novel mass measurement technique offered by ion traps provides an accurate microscope to study the fine structure of the nuclear mass surface away from the valley of stability. This is best viewed through the systematic evaluation of various mass differentials as a function of proton and neutron number. Such differentials, as already mentioned in the introductory section of this review are, for example, to the first order the one- and two-nucleon separation energies and decay Q-values and to the second order the shell gap energies and odd-even staggering of masses related to pairing effects. With the ion-trap spectrometry these quantities are now typically available with accuracies of the order of 10 keV or better. This accuracy is comparable to that of excited states spectroscopy far from stability in the outskirts of the known nuclear landscape. Most of the new ion trap mass data since the last five years have been obtained for neutron-rich nuclei. Also, there is a high relevance of this data for nuclear astrophysics, where it is needed in modeling the synthesis of heavy elements via the rapid neutron capture processes occurring in high-temperature and density scenarios (see e.g. reviews [119, 120]). Therefore, in the following sections we will focus on the systematic behavior of two-neutron separation energies in the light of the newest data published since the last atomic mass evaluation in 2012. The two-neutron separation energy S_{2n} is obtained by using the following formula:

$$\begin{aligned} S_{2n} &= B(A,Z) - B(A-2,Z) \\ &= \left(M\left(A-2,Z\right) + 2M_n - M\left(A,Z\right)\right)c^2, \end{aligned} \quad (8)$$

where $B(A,Z)$ and $M(A,Z)$ stand for the binding energy and mass, respectively. This gives the energy required to remove the last two neutrons from the nucleus to continuum. The overall trend for S_{2n} as a function of the increasing neutron number is its nearly monotonic decrease due to the filling of less bound, higher and higher-lying orbitals. As shown in Fig. 13, the above mentioned behavior is clearly seen in the S_{2n} energies as a function of neutron number for neutron-rich isotopes from krypton to tin. For demonstrating the

progress in mass measurements in this region, we show for comparison the knowledge on two-neutron separation energies as in the 2003 atomic mass evaluation [50]. Very recently important new data has been obtained at the ISOLTRAP, TITAN and JYFLTRAP facilities for neutron-rich Kr, Rb, Cd and Sn isotopes. In addition, since the atomic mass evaluation in 2003 over one hundred new masses were measured with the JYFLTRAP setup ranging from nickel to xenon, as reported in our previous review article in 2012 [98].

In addition to a smooth behavior of S_{2n} shown in Fig. 13, there are kinks near $N = 60$ in the isotopic chains from yttrium to molybdenum outside of which a smooth behavior is again observed. This behavior is known to be due to a distinct shape change between $N = 58$ and 60 at which strong prolate ground state deformation sets in. The rapid onset is due to a shape transition and coexistence of shapes around $Z = 40$ and $N = 60$, see Ref. [121] and references therein. While the ground states of these nuclei below $N \approx 60$ appear to be only weakly deformed or nearly spherical, the heavier isotopes display mainly axially symmetric deformed shapes. The shape changes and coexistence picture are well known also from spectroscopic studies. This interpretation has also been confirmed by a series of collinear laser spectroscopy experiments in the form of a sudden increase of the mean-square charge radii around $N = 60$.

A recent theoretical study by Takahara et al. [122] implied that the spin-orbit potential plays a decisive role in the predominance of prolate deformation of ground states. For neutron-rich nuclei above $N = 60$, neutrons start to occupy deformed orbits deriving from the $g_{7/2}$ having considerable overlap with the spin-orbit partner proton levels deriving from the $g_{9/2}$ single-particle level. Interaction between the relevant neutron and proton orbits drives the nucleus to large deformations for nuclides with $Z = 37 - 44$ and $N > 60$. This interpretation is supported by the new data obtained from the mass measurements of neutron-rich Kr isotopes ($Z = 36$). Here, protons are mainly occupying orbitals below the $g_{9/2}$ orbit, and hence this results in a nearly monotonically decreasing trend in two-neutron binding energies.

Concerning the evolution and persistence of the two-neutron shell gap at $N = 82$, it is of interest to note that the new measurement at ISOLTRAP has produced accurate mass values for ^{129,130,131}Cd isotopes. Derived from that data one can observe that the S_{2n} values indicate a smaller drop for Cd from $N = 81$ to $N = 83$ as compared with the neighbouring In and Sn isotope chains. To confirm whether this trend is really happening it would be important to extend the accurate ion-trap measurements to the nearby ^{130,132}In and ^{132}Cd isotopes.

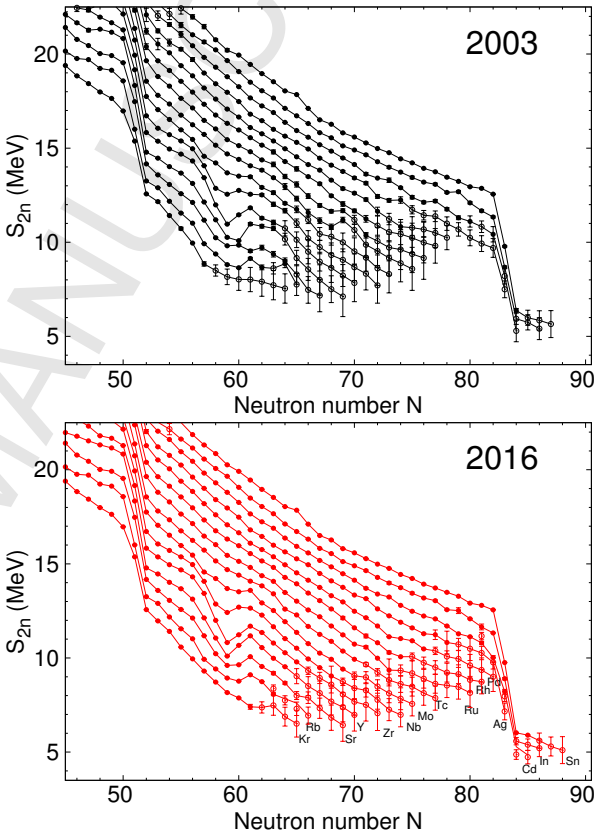

Figure 13: Two-neutron binding energy vs. N from Kr to Sn. Note that the experimental uncertainties, if not shown, are smaller than the data points.

In the following chapters, two-neutron separation energies are presented and discussed in three regions of neutron-rich nuclei; near and above the spherical shell closures at $N = 28, 82, 126$ and the deformed region with $N = 60$. We compare the experimental data with DFT calculations employing two commonly used functionals Sly4 [115, 116] and UNEDF0 [112], see chapter 3.1 for their description.

3.2.1. *Neutron-rich Ca isotopes. A new shell closure?*

Recent experiments employing the ISOLTRAP and TITAN have produced new accurate mass data up to the neutron-rich ^{54}Ca isotope with $N = 34$, see Ref. [69, 83]. The data show a distinct drop of about 5 MeV for S_{2n} between $N = 28$ and $N = 30$ as well as another drop of about 3 MeV from $N = 32$ to 34. A similar trend was observed for the neutron-rich K isotopes in a later study also with the ISOLTRAP mass spectrometer [58].

The drop at $N = 34$ has been interpreted as a prominent new shell closure at $N = 32$. The observation was explained to be due to the influence of three nucleon forces as calculated with a chiral effective field theory. New measurements of the charge radii of the same Ca isotopes up to ^{52}Ca by laser spectroscopy have revealed a somewhat unexpected behavior of the charge radii, see Ref. [123]. Instead of the expected decrease of the charge radius at the shell closure $N = 32$, a significant gradual increase from ^{48}Ca towards heavier Ca isotopes was observed. Adequate theoretical explanation for this is lacking, which sets a challenge for future experiments as well as theories. Figure 14 shows the two-neutron separation energy for neutron-rich Ca isotopes together with the theoretical values derived from the mass values of Ref. [111, 124]. The general agreement is rather satisfactory, although the theoretical calculations seem rather insensitive to experimental shell closures at $N = 28$ and $N = 32$.

3.2.2. *Neutron-rich Kr and Zr isotopes. Deformation around N=60*

As shown in the previous discussion and in Fig. 13 the onset of large deformation is observed between N=58 and 60 for Zr isotopes in the form of a kink in the two-neutron binding energy curve but at the same time this feature seems to completely disappear for krypton isotopes at the corresponding neutron number. Figure 15 shows a comparison between DFT calculations and experimental data for Kr (a) and Zr (b) isotope chains. The Sly4 functional seems to describe the data better, even overemphasizing behavior at the spherical closed shells, whereas the UNEDF0 functional gives clearly a better overall description including the region of deformation (Zr) around $N = 60$.

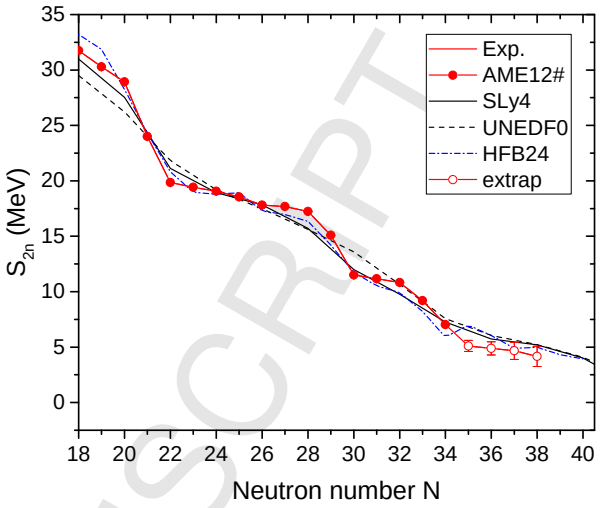

Figure 14: Two-neutron separation energies for neutron-rich calcium isotopes.

3.2.3. *Neutron-rich radium and francium isotopes*

Heavy neutron-rich francium ($Z = 87$) and radium ($Z = 88$) isotopes were studied at ISOLTRAP providing accurate mass data up to N=146, being one of the most neutron-rich data sets far from the valley of beta stability, see Ref. [75]. Both Fr and Ra behave in a similar way for their two-neutron separation energies. Since the DFT calculations are only available for the even-even nuclides we show in Fig. 16 the S_{2n} plots only for the radium isotopes. It seems that the UNEDF0 functional gives a very nice agreement with the experimental data in particular beyond $N = 132$. SLy4 seems to overpredict the values at and below $N = 126$ and underpredict above.

3.2.4. *Evolution of the two-neutron shell closure at N = 50*

For more quantitative insight into the question of the changes in mass values around shell closures, one can investigate the two-nucleon binding energy differences for neutrons or protons. For this purpose, we have plotted two-neutron separation energies in Fig. 17 for $N = 46$, 48, 50, 52 and 54 isotones as a function of the proton number. The energy difference between the $N = 50$ and $N = 52$ isotones corresponds to a two-neutron shell gap across $N = 50$. When moving down in Z from the semi-doubly magic ^{90}Zr, there is an obvious trend for lowering the value having a minimum at Ge ($Z = 32$). This corresponds also to a minimum in

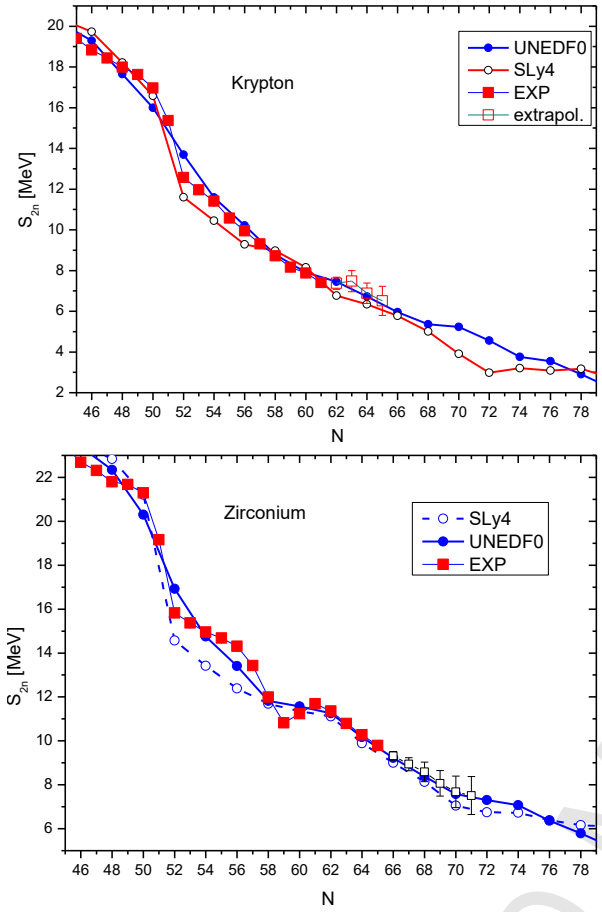

Figure 15: Two-neutron separation energies for neutron-rich krypton and zirconium isotopes.

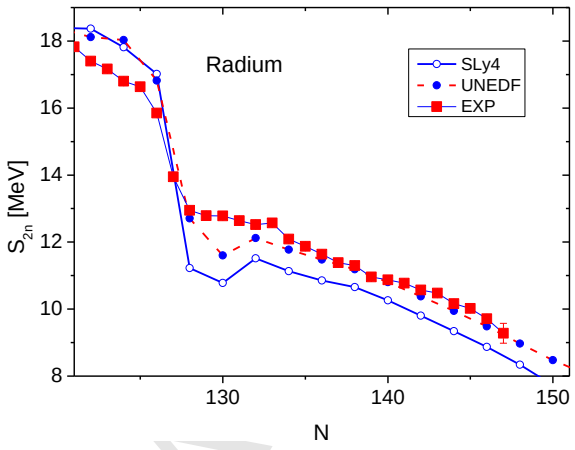

Figure 16: Two-neutron separation energies for neutron-rich radium isotopes.

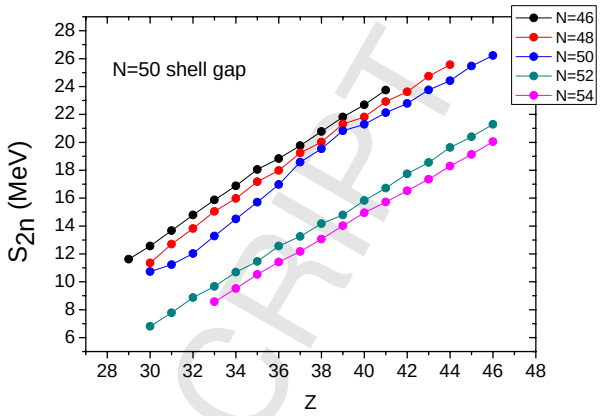

Figure 17: Experimental two-neutron separation energies as a function of proton number for $N = 50$ shell gap. The uncertainties are smaller than the sizes of the data points.

the systematics of the first 2^+ energies of known even-A $N = 50$ isotones suggesting maximum impact from core polarization effects. The isotone curves also indicate that the $N = 50$ gap seems to increase towards the doubly-magic Ni core ($Z = 28$). Since our previous review a new and important additional data point obtained from the measurement of the mass of ^{82}Zn at ISOLTRAP [70] could be included in the plot.

3.2.5. Two-neutron shell gaps and theoretical comparison

The question of how the known spherical shell closures persist when moving far away from the valley of stability is a fundamental and important question for nuclear structure physics. Therefore, the comparisons of the data with various theoretical approaches are needed. Figures 18 and 19 show the comparison of the experimental values with three different types of theoretical models. These models are described and tested against the total mass values in chapter 3.1. It is obvious that all models follow the general trend of the shell gaps for all studied neutron shell closures in a reasonable way. The new finite range droplet model FRDM2012 seems to reproduce the shell gaps in the studied region rather well. Also, the other similar microscopic-macroscopic approach WS-4 follows the FRDM2012 values closely except for the $N = 50$ but with some shifts in the neutron number. The more universal HFB model HFB24 seems to reproduce the trends best, in particular near the $Z = 28, N = 50$ region. However, its prediction below $Z = 28$ shows somewhat odd large drop which is difficult to understand.

The values obtained with two density functionals used in the mean-field calculations, Sly4 and UNEDF0

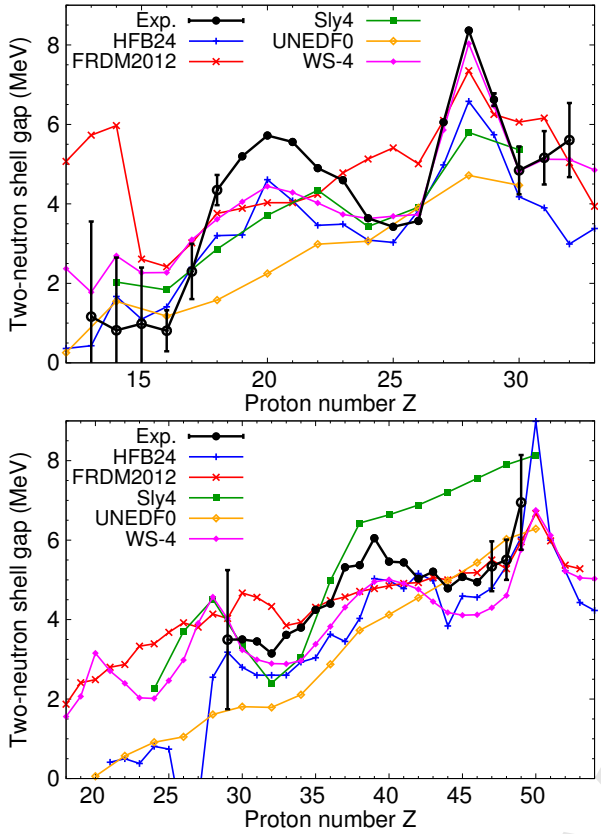

Figure 18: The $N = 28$ (top panel) and $N = 50$ (bottom panel) two-neutron shell gaps as a function of the proton numbers. See text for the explanation of the model calculations.

differ strongly from each other. The former one produces better the doubly-closed shell-gap values, but the UNEDF0 functional is rather insensitive to those, and rather exhibits a gradual reduction in its value outwards from stability. In fact, it even seems to predict a gradual disappearance of the shell gap towards the limits of nuclear binding. This is very interesting in the light of its fairly good agreement with the two-neutron binding energies shown in Figs. 14, 15 and 16 in the neutron-rich wings of the curves.

4. Isobaric mass doublets and isospin multiplets

As described in section 2.3.1, measurements of mass differences of mass doublets (those that have the same A/q) form a special subset of Penning trap mass spectrometry. From experimental point of view, the mass difference can be determined with extremely high precision: even on the order of 10^{-10} in the frequency ratio, allowing eV-level precision for Q-value determination

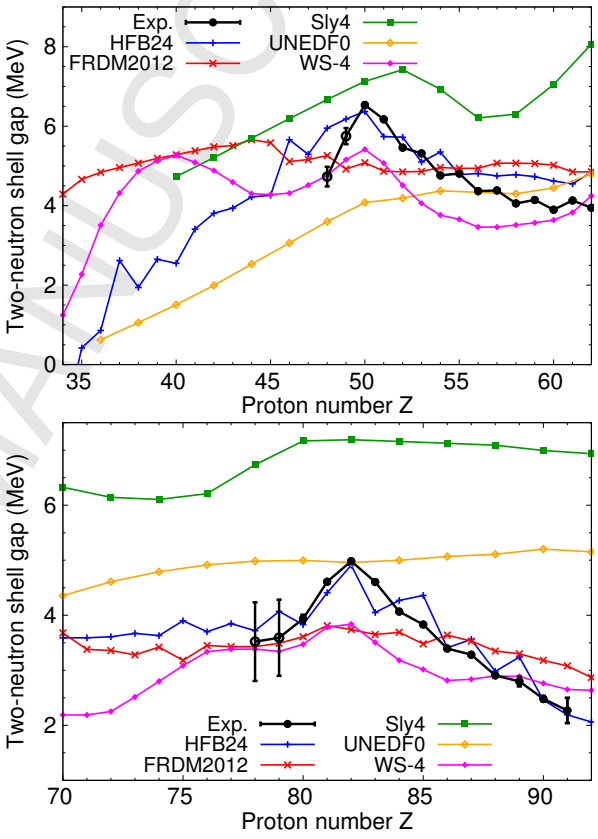

Figure 19: The $N = 82$ (top panel) and $N = 126$ (bottom panel) two-neutron shell gaps as a function of the proton numbers. See text for the explanation of the model calculations.

[27] with the PI-ICR technique or 10^{-9} level with TOF-ICR technique.

4.1. Superallowed and $T = 1/2$ mirror beta decays

The doublet technique has been extensively used for measuring the Q_{EC} values of $T = 1$ superallowed and $T = 1/2$ mirror beta decays. In these cases the parent and daughter have always same mass number. Both mirror β decays and superallowed β decays contribute to the testing of the Standard Model of Particle Physics. Namely, the V_{ud} of the Cabibbo-Kobayashi-Maskawa (CKM) quark mixing matrix can be deduced. Here the superallowed beta decays, due to very simple decay matrix element, produce the most precise V_{ud} value [125]. In addition to half-life, branching ratio and Q-value needed for superallowed β decays, it is necessary to determine $\beta - \nu$ angular correlations for mirror nuclei [126].

4.1.1. Superallowed β decays

As of today, Q-values of all the "well known" Superallowed β emitters spanning in 14 transitions in total, have been measured to a high precision with Penning traps (see Ref. [125] and references therein). JYFLTRAP has been the most contributing trap here and some cases like ^{38}Ca, have been measured with many trap facilities. The Q-value of the final 14th, ^{14}O was measured in 2015 by LEBIT [127].

The most controversial findings of the Q-values was the disagreement of ^{46}V Q-value to the older reaction-based results [128, 129] by CPT and JYFLTRAP groups. Measurements of ^{50}Mn and ^{54}Co revealed similar disagreements prompting for re-evaluation of the isospin-symmetry breaking corrections [130].

4.1.2. Mirror decays

Mirror decays might soon yield the next-best V_{ud} value after superallowed β emitters. Clearly the most challenging quantity to measure is the β-ν angular correlation coefficient, which are currently being pursued at many facilities.

The Q-values are now actively being measured, and several new Q-values have emerged recently, summarized in Table 6. Some mirror nuclei have been already measured earlier at JYFLTRAP, such as ^{23}Mg [131], ^{31}S [132], and heavier mirror nuclei ^{53}Co, ^{55}Ni, ^{57}Cu, and ^{59}Zn [133].

4.2. Isobaric Multiplet Mass Equation

Assuming nuclear force is charge-independent, the masses of the members of an isobaric multiplet should show a quadratic behaviour:

$$M(A,T,T_Z) = a(A,T) + b(A,T)T_Z + c(A,T)T_Z^2 \quad (9)$$

where T is the isospin, T_Z the isospin projection and $M(A,T,T_Z)$ is the mass of the isobaric analogue state (IAS) of the T_Z member in the T isobaric multiplet. The Eq. (9) is known as the Isobaric Multiplet Mass Equation (IMME). The quadratic form works quite well for a majority of isobaric multiplets, see e.g. recent reviews and compilations of the IMME coefficients [134–136]. However, in a couple of cases, it deviates significantly from the quadratic form. Penning-trap measurements have revealed a breakdown of the quadratic IMME for several multiplets. The TITAN mass measurements of ^{8}He [137], ^{9}Li [90], ^{9}Be [90] and ^{21}Mg [91] have revealed breakdowns of the quadratic IMME for the $T = 2$ quintet at $A = 8$ [137, 138], as well as for the $T = 3/2$ quartets at $A = 9$ [90] and $A = 21$ [91], respectively. Recent measurement of ^{31}Cl [92] at JYFLTRAP has shown that the quadratic form cannot describe the $T = 3/2$ quartet at $A = 31$. The $T = 2$ quintet at $A = 32$ has been probed via ^{32}Si and ^{32}S mass measurements at LEBIT [139], ^{32}Ar at ISOLTRAP [140], and indirectly via the mass measurement of ^{31}S [132] at JYFLTRAP combined with the measured proton separation energy of ^{32}Cl, and it has been shown to be significantly deviate from the quadratic form. The ISOLTRAP measurement of ^{35}K for the $T = 3/2$ quartet at $A = 35$ [141] has also revealed a breakdown of the IMME. The breakdown of the IMME has been explained, e.g. by isospin mixing of the states and charge-dependent effects [90, 142].

The precision achieved in Penning-trap measurements today is so high that the the excitation energies of the isobaric analog states of the other members of multiplets than $T_Z = \pm T$, in particular of the $T_Z = 1 - T$ member, have become the limiting factors for probing the validity of the IMME. For example, the TITAN experiment on ^{20}Mg showed a breakdown of the IMME [91], but it was later revalidated by a new measurement

Table 6: Q_{EC}-values of mirror nuclei published recently. Both the reported Q_{EC}-value and comparison from AME2012 derived values are given.

Decay	new Q_{EC} (keV)	AME2012	Ref.
^{21}Na	3547.11(9)	3547.14(28)	[93]
^{23}Mg	4056.35(16)	4056.6(7)	[94]
^{25}Al	4276.805(45)	4276.6(5)	[95]
^{29}P	4942.18(37)	4942.6(6)	[93]
^{45}V	7123.82(22)	7128(8)	[96]
^{49}Mn	7712.42(24)	7695(10)	[96]

of the IAS in ^{20}Na via β^+ decay of ^{20}Mg. The breakdowns for the $T = 3/2$ quartets at $A = 33$ [143] and $A = 53$ [144], have also been revalidated by measurements of the IAS energies in ^{33}Cl [145] and ^{53}Co [146].

5. Trap-assisted spectroscopy

Although ion traps in nuclear physics are mostly used for direct measurements of nuclear masses they can also contribute to providing isotopically and sometimes even isomerically pure sources for measurements of radioactive decays. Routinely, the mass resolving power $M/\Delta M$ of the order of 10^5 can be reached which allows clean separation of neighboring isobaric nuclides and thus decay spectroscopy of sources free from contaminant activities. Recently separation of a heavy ion isomeric beam with a multiple-reflection time-of-flight mass spectrometer has also been demonstrated as a potential device for trap-assisted spectroscopy [147].

With the Ramsey cleaning technique, as described in chapter 2.6 for JYFLTRAP, decay spectroscopy of a nucleus in its pure isomeric state with energy of the order of > 100 keV has become possible [49]. Ions of isotopically or isomerically purified radionuclides can either be extracted out of or stored in the trap for subsequent in-trap decay measurements. In the former case, ions are extracted out of the trap as a beam which is directed and deposited on a catcher foil or a movable tape for subsequent decay measurements using standard detector arrays for beta-, gamma-, neutron or charged particle detection. In the latter case, the ions can also be kept by the trapping potential inside the trap vacuum where their decays are observed. Such massless sources of short half-lived nuclei provide ideal conditions for high-resolution detection of emitted charged particles down to very low energies

5.1. In-trap spectroscopy

Measurement of particles and photons emitted in the decays of radioactive ions stored in a trap offers many interesting applications for fundamental physics as well as for nuclear structure physics. Such experiments can utilize, for example, Paul traps, Penning traps or electron beam ion traps (EBITs) or coupled combinations of them.

5.1.1. Penning trap spectroscopy

Among the first applications of ion traps for in-trap spectroscopy has been discrete-energy conversion electron spectroscopy. As an example, the scheme of the JYFLTRAP setup used in feasibility studies for short-lived isomers is shown in Fig. 20 (from Ref. [148]).

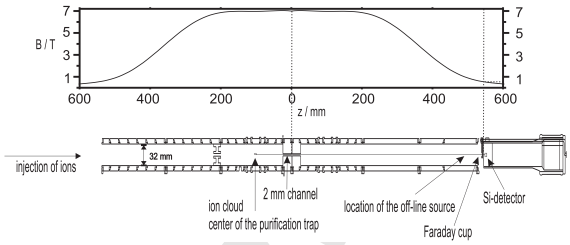

Figure 20: The electrode structure inside the magnetic solenoid of the JYFLTRAP spectrometer. This figure is from Ref. [148].

The studied nuclei in their isomeric states were produced in proton-induced fission of ^{238}U at the IGISOL3 facility followed by their injection into the linear RFQ cooler buncher device. Ions were then extracted in short bunches and injected into a double Penning trap described in chapter 2. Inside the first trapping region the motion of ions was cooled with helium buffer gas and simultaneously applying successive magnetron (ν_-) and cyclotron (ν_c) excitations. As a result of this mass-selective process, only the ions obeying the cyclotron resonance condition were centered in the symmetry axis of the trap. In order to maintain the ions in a cloud of about 1 mm in diameter, successive RF pulses at ν_c were applied for a repeated re-centering [148]. Conversion electrons emitted from the centered ions were transported through a 2 mm diameter channel to the Si-detector while the electrons emitted from the off-centered ions hit the center electrode of the trap. The measurements employed a high-resolution Si-detector having a 10 mm^2 sensitive area and a thickness of 500 μm and with a dead-layer thickness of 250 Å.

A conversion electron spectrum recorded from the decays of short-lived ^{117m}Pd isomer is shown in Fig. 21. The decay of this isomer is featured by electron peaks due to two converted transitions at 34.5 and 168.6 keV. The corresponding K conversion lines at 9 and 143 keV show a resolution of about 2 keV, which consists of the intrinsic resolution of the detector itself and broadening of the lines due to back-scattering effects. The intrinsic line widths of the measured transitions were estimated to be less than eV, due to natural line widths of the transitions as well as thermal effects in the electron emitting ion cloud. The overall detection efficiency for the transitions seen in Fig. 21 were estimated in Ref. [148] to be of the order of 30-40 %.

5.1.2. Paul and Penning trap spectroscopy for beta-neutrino correlation measurements

The early applications of in-trap spectroscopy were devoted to studies of energy and angular correlations

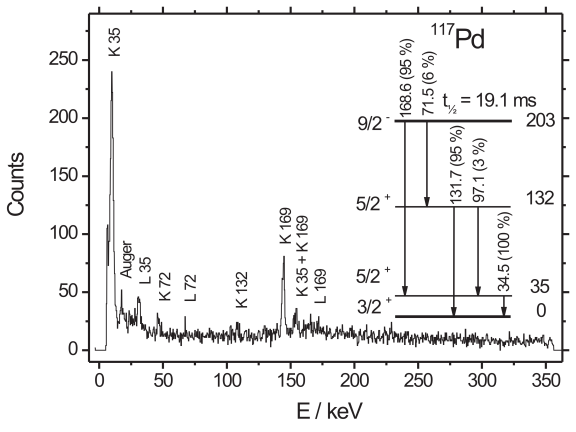

Figure 21: In-trap electron spectrum recorded for ^{117m}Pd. This figure is from Ref. [148].

between beta particles and recoil nuclei with the aim to search for scalar and tensor currents in the weak interaction. Two examples of applying Paul trap in such experiments are described in refs. [149, 150]. The results of both approaches are consistent with a purely V-A interaction, and in the case of couplings, to right-handed neutrinos. The LPC trap is operational at GANIL and has a transparent electrode structure which allows high-efficiency and precise measurements of the $\beta - \nu$ angular correlation parameter in nuclear β decays. The setup is installed at the low energy beam line, LIRAT, of the GANIL/SPIRAL facility. Measurements have been performed for three different nuclei ^{6}He, ^{19}Ne and ^{35}Ar that were ionized in an ECR ion source prior to their injection to the measurement trap. With the precise value of the angular correlation parameter, the experiment on the ^{35}Ar mirror decay will also contribute to the more accurate extraction of the V_{ud} matrix element of the CKM matrix of the standard model.

At Argonne National Laboratory beta-neutrino correlations are studied in the beta decay of ^{8}Li^{+} ions stored in the Beta-Decay Paul Trap (BPT) [151]. This trap is a linear Paul trap constructed with thin planar electrodes that provide an open geometry to allow for large solid-angle detector coverage. Prior to Paul trap the ions produced in ^{7}Li(d,p) reactions were prepared for injection in the CPT Penning trap. The beta-recoil correlation measurement was based on the detection of β decay of ^{8}Li and subsequent breakup of the ^{8}Be daughter to two α-particles.

In the Penning trap side, the WITCH (the Weak Interaction Trap for Charged Particles) trap is dedicated for β–ν angular correlation measurements [152]. There, the angular correlation coefficient is derived from the shape of the recoil energy spectrum by using retardation potential.

5.1.3. Paul trap spectroscopy for beta-delayed neutrons

The Beta-Decay Paul trap configuration as the one described above has also been applied in a feasibility study for beta-delayed neutron spectroscopy. Neutron energy was determined using the beta-recoil-ion coincidence time of flight, see ref. [21]. Neutron emission leads to high-energy recoils having short TOFs, with the lower-energy recoil imparted by the electron and antineutrino being a small perturbation to the measurement. The setup used in this study is shown in Fig. 22. The neutron precursor ^{137}I was produced in fission from a 1 mCi ^{252}Cf source and thermalized as singly charged ions in a large-volume gas catcher [153]. The $A = 137$ singly-charged fission product ions were separated by the Canadian Penning Trap (CPT) prior to their injection into the open Paul trap structure. Recoil-ion TOF spectrum collected with a 30 ions/s ^{137}I^{+} beam is shown in Fig. 22. The TOF spectrum of the ^{136}Xe recoil ions from beta-delayed neutron emission, highlighted by the dotted box, is shown in the inset. The energy range covered extended from about 200 keV threshold energy up to 1.5 MeV. The study showed that this technique has a high potential for delayed-neutron energy measurements with high efficiency of the order of 1 %, neutron-energy thresholds of about 100 keV and a good energy resolution.

5.1.4. Electron Beam Ion Trap for gamma- and X-ray spectroscopy.

A novel concept for in-trap decay spectroscopy has been devised at ISAC of TRIUMF where electron-beam ion trap (EBIT) has been used for long-term storage of highly charged ions [154]. The setup has been developed with a special emphasis on precision spectroscopy of low branching ratios and is being developed in the context of measuring electron-capture branching ratios needed for determining the nuclear ground-state properties of the intermediate odd-odd nuclei in double-beta ($\beta\beta$) decay. The EBIT is a central part of the TITAN ion trap system and can be fed with purified samples from the adjacent linear RFQ trap. Storage of radioactive ions in vacuum in an open-access EBIT allows observing their decay in a backing-free environment. Simultaneously, the high magnetic field of EBIT provided an efficient spatial separation between decay photons and decay positrons removing bremsstrahlung background. This unique feature is especially advantageous in cases of electron-capture (EC) decays, where

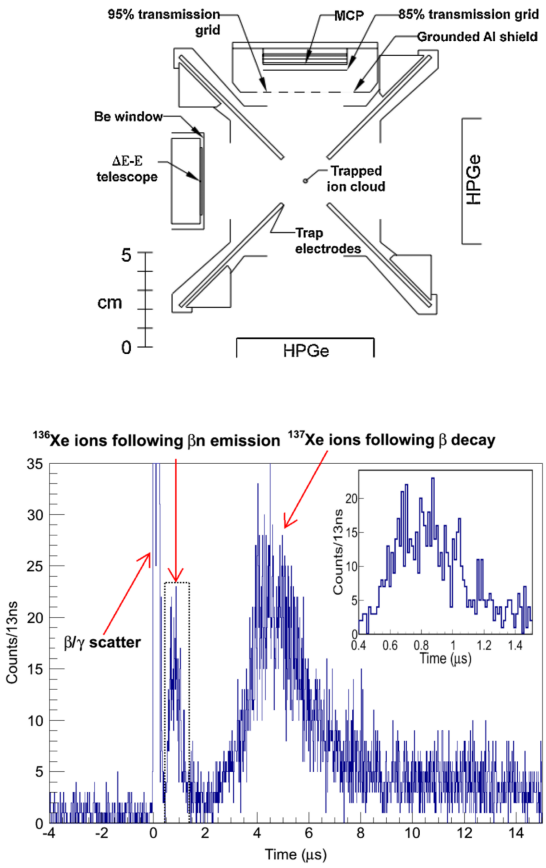

Figure 22: *Above:* A cut view of the Open Paul trap at ANL, *Below:* Time of Flight spectrum of ^{137}Xe ions triggered by the beta detector. These figures are from Ref. [21].

the measurements of low-intensity and low-energy X-rays are required. The approach has been successfully demonstrated by a measurement of the decays of highly charged radioactive ions of ^{124}In and ^{124}Cs [155].

5.2. Post-trap decay spectroscopy

Decay spectroscopy for nuclear structure physics at ISOL facilities has long been a backbone in studies of exotic nuclei far from stability. However, when moving further from the valley of stable nuclei, increasing complexity of decay patterns and low production rates of these nuclei have led to even more stringent requirements for experimental methods. On top of this development there have been many innovations on selective ionization methods applicable to produce initially purified beams. However, with the introduction of novel universal production methods, such as in-flight or IGISOL methods, requirements for fast purification of isomers and isotopes for decay spectroscopy have become necessary. In addition, the ion manipulation by ion traps can significantly improve the emittance, reduce the energy spread and modify the time structure of the ion beams used for decay spectroscopy.

5.2.1. Conventional decay spectroscopy of trap-purified isotope sources

Ion trap systems coupled to ISOL or in-flight gas catcher based production facilities can offer powerful means for spectroscopy applications. In this context we introduce two programs, one at ISOLDE and one at IGISOL, where the method is already in full use. The ISOLTRAP facility at ISOLDE in combination with the recently installed decay-spectroscopy setup [156] will make it possible to combine high-precision mass measurements with nuclear-decay spectroscopy. This combination allows the assignment of masses with the corresponding decaying states, particularly important in cases where isomeric state(s) are involved. A recent experiment utilizing this approach revealed identity (spin/parity/mass) for the ground and isomeric states of even neutron-deficient ^{190,194}Tl isotopes [157].

An active decay spectroscopy program using the JYFLTRAP setup has addressed mainly the nuclear structure studies of neutron-rich nuclei produced in fission. Additionally, a few half-life and branching-ratio measurement campaigns for the superallowed beta decays have been carried out, see e.g. [158–160]. In the next section, we mainly focus on decays of medium-mass neutron-rich nuclei. These nuclides are typically produced in fast proton-induced fission of ^{238}U. Short-lived fission fragments thermalized in helium gas as

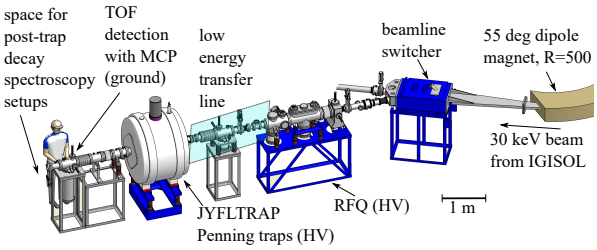

Figure 23: JYFLTRAP setup at IGISOL3. The beam from the IGISOL gas cell is separated with an ordinary dipole magnet (right) before injecting the mass-selected beam to into the RFQ. See text for more explanation.

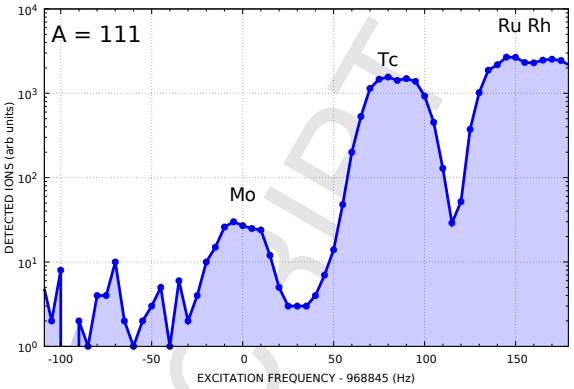

Figure 24: Mass spectrum of $A = 111$ isobars.

ions are reaccelerated and separated by the IGISOL system with a mass resolving power of $M/\Delta M \sim 500$. This resolving power is good enough to separate nuclei of one mass number only from all other nuclear species produced in fission. Thus, separated radioactive beam consist of a complete chain of nuclei within the same isobar produced directly in fission. In the past, these multi-component isobaric beams were successfully used to study many exotic, neutron-rich nuclei of refractory elements unavailable at other ISOL facilities. However, a serious problem with isobaric contaminants made it very difficult to extend these studies weakly produced nuclides further from stability. Therefore, the double Penning trap system JYFLTRAP was developed and constructed to provide high enough mass resolving power for the production of pure isotopic as well as even isomeric beams for nuclear spectroscopy. The layout of the JYFLTRAP at IGISOL3 [24] setup is shown in Fig. 23.

Ions after the mass separation at IGISOL are injected into a buffer-gas filled RFQ trap where they are rapidly (~ms) cooled and subsequently stored in a potential well produced by the combination of the electric RF and DC potential. Ions are then extracted in the form of short, typically a few μs long bunches and transported into the double Penning trap system for purification. The necessary steps for cleaning are described in chapter 2.5. In the simplest approach, mass selective buffer-gas cooling is applied in the first trap, after which the ions are ejected through a narrow channel separating the purification and the precision traps, and out from the trap system to the spectroscopy setup. Another approach, if necessary, would be to use the higher resolution precision trap for additional purification. This technique has been used for example to resolve the ground and isomeric states of ^{100}Nb to study their beta decay schemes to ^{100}Mo [161].

5.2.2. *Nuclear structure studies*

The focus of the decay spectroscopy program at IGISOL has for some years been in studies of the evolution of coexisting shapes in neutron-rich nuclei around A=100-120. This mass region located between the closed doubly magic core nuclei ^{78}Ni and ^{132}Sn is very rich consisting of different structures, including those with prolate, oblate and triaxial shapes. Experimental tracking of the systematics of these structures provides important testing ground for theoretical calculations, which are eventually needed in predicting the properties of even more neutron-rich nuclides involved, for example, in understanding the r-process synthesis of heavy elements. As an example of such a study we describe here the decay spectroscopic study of a neutron-rich isotope ^{111}Mo which employed isotopically purified sources of ^{111}Mo nuclei [162]. The mass spectrum of the $A = 111$ isobars as measured by the purification trap of the JYFLTRAP setup is shown in Fig. 24. As shown in this figure, a monoisotopic beam of ^{111}Mo could be delivered for decay spectroscopy when the filtering frequency of the trap was set to 968845 Hz. A typical rate of about 20 ions/s of ^{111}Mo was observed with the MCP detector positioned after the trap. This rate allowed for a complete X-ray spectroscopy for constructing the low-lying level structure for the daughter nucleus ^{111}Tc. Due to a short half-life of about 200 ms the trap purification cycle of 120 ms was used. The daughter nucleus ^{111}Tc has also a relatively short half-life of about 350 ms. Therefore, its beta-delayed gamma-transitions are also observed as daughter products in the gamma-ray spectrum corresponding to the ^{111}Mo setting of the trap, see Fig. 25.

The level scheme of ^{111}Tc constructed from this experiment revealed excited structures fed in the beta decay up to slightly below 600 keV in excitation energy.

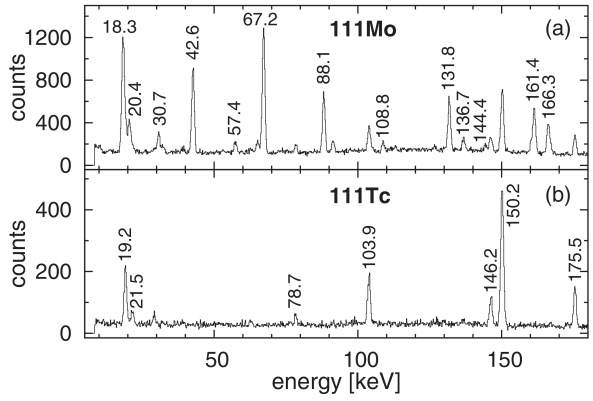

Figure 25: Beta-gated gamma-ray spectra corresponding to the trap cyclotron resonance frequencies for ^{111}Mo and ^{111}Tc.

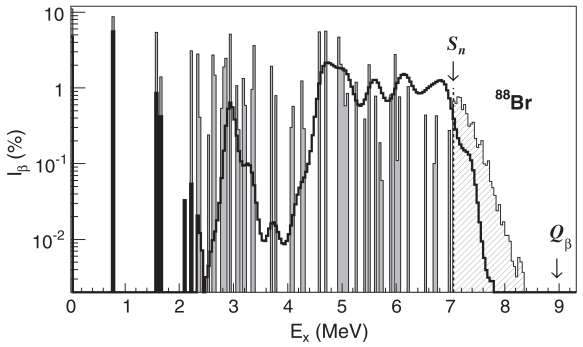

Figure 26: Beta decay strength distribution for ^{88}Br, from Ref. [165].

Earlier unobserved, new excited levels in ^{111}Tc populated in the β-decay of ^{111}Mo provided the first indication for a low-lying oblate deformation in the mass $A \approx 110$ region. This solution coupled to the QPRM calculations offers an explanation for the two lowest-energy states with $I = (1/2, 3/2)^+$ at 30.7 keV and $I = 5/2^+$ at 42.6 keV to present the first clear indication of a triaxial oblate shape in the $A \approx 110$ neutron-rich nuclei. Additionally, a wide range of levels with different spins indicate the existence of at least two β-decaying states in ^{111}Mo which could not be separated with the available resolving power of $M/\Delta M \sim 30,000$. One should note, however, that the beta-decay energy window or the Q-value of ^{111}Mo is considerably larger, e.g. 9085(5) keV as determined by the JYFLTRAP mass measurement. Therefore, although important for producing relevant information on the low-lying level structure of ^{111}Tc the described spectroscopy experiment could cover only marginally gross beta-decay properties of ^{111}Mo.

5.2.3. Total Absorption Gamma-ray Spectroscopy

To correct for the deficit related to observing weak branches to high-lying states, another approach based on the total absorption spectroscopy has to be applied in combination with trap-produced isotopes. So far, in addition to nuclear structure studies, this technique in connection with the trap-purified isotope sources has been applied for the measurements of interest for the decay heat of the nuclear reactors and for the determination of the electron antineutrino spectrum from thermal reactors of relevance for the neutrino oscillation experiments [163]. In the former case, β-feeding probabilities for three important contributors to the decay heat in nuclear reactors, namely ^{102,104,105}Tc, have been measured, resulting significant improvements and solving a large part of the discrepancy in the decay-heat data of ^{239}Pu in the 300–3000 s cooling interval. In the latter case, the decay of ^{92}Rb, which makes the dominant contribution to the reactor antineutrino spectrum in the 5–8 MeV range, was investigated, see ref. [164]. In these experiments, previously unobserved beta feeding was seen in the 4.5–5.5 MeV region and the ground-state to ground-state feeding was found to be 87.5(25) %, which is 7.7 % smaller than the previously used value. The overall impact of the new result from this experiment on the reactor antineutrino spectra is discussed in more detail in Ref. [164]. In another recent study, total absorption spectroscopy was used to investigate the β-decay feeding to states below and above the neutron separation energy followed by γ-ray emission in ^{87,88}Br and ^{94}Rb. An unexpected large γ-emission intensity was observed in all three cases extending well above the excitation energy region where neutron emission is no longer hindered by the angular momentum barrier, see ref. [165]. This is exemplified by the measured beta intensity distribution for ^{88}Br in Fig. 26, where a significant amount of feeding to neutron unbound states can be seen to lead to gamma-emission.

5.2.4. Delayed neutron spectroscopy at JYFLTRAP

Beta-delayed neutron and multi-neutron emission become very important ingredients in the decay processes far away from the valley of stability. They also have a significant impact on the elemental and isotopic abundance distributions of the r-process nuclear synthesis. Thus, the total neutron emission probabilities, often denoted as P_n, are critical for r-process calculations (see, e.g. Ref. [119]). An example of the importance of the role of delayed neutron emission in the beta decay of highly neutron-rich nuclides is demonstrated in Fig. 27 below. Beta-delayed neutron emission probability in the case of niobium isotopes becomes observable already at

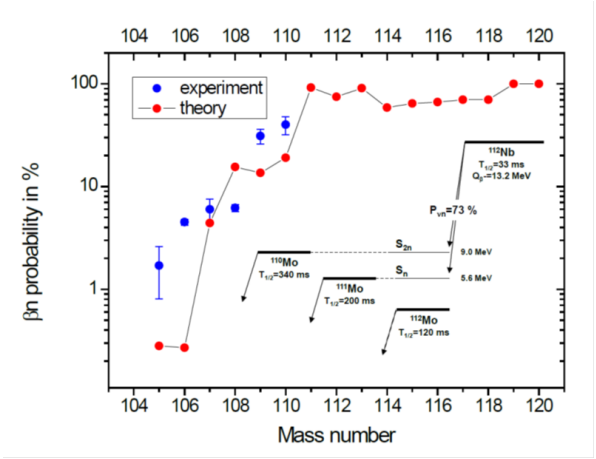

Figure 27: Beta-delayed neutron emission probability for a chain of Nb isotopes. Theoretical values are based on theoretical calculation employing the QRPA calculation and the finite range droplet model, from Ref. [168].

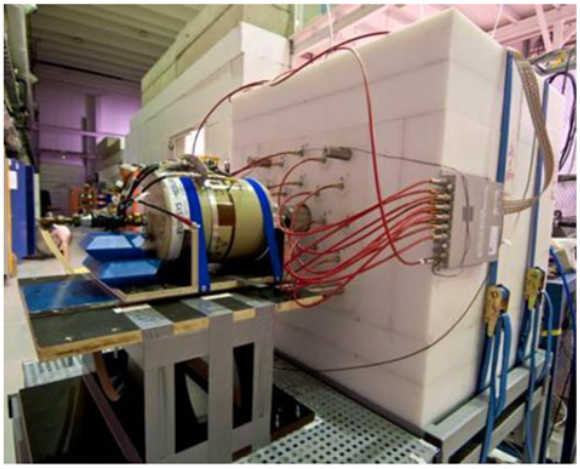

Figure 28: The neutron long counter system behind the JYFLTRAP setup. The setup includes also a HPGe detector for simultaneous gamma-ray spectroscopy.

and beyond $^{106}Nb_{65}$ and reaches rapidly nearly a 100 % probability for more neutron-rich Nb isotopes [166]. As a consequence, beta-decay schemes become highly complex and experimental conditions demanding. One of the key requirements will then be set by the availability of isobarically and isotopically pure sources. One approach to reach such conditions is provided by the Penning-trap purified radioactive sources [167] .

On the other hand, the beta-decay feeding to individual nuclear states and their de-excitation by gamma-ray and (multiple) neutron emission need to be known for nuclear structure studies. This necessitates the measurement of neutron energy, which can be done by using either secondary nuclear reactions or a time-of-flight method. These measurements are challenging due to the high complexity of required detection systems, such as large arrays of either ^{3}He-based counters or scintillator detection systems, respectively. The total number of neutrons can best be measured using a neutron long counter technique where neutrons are first thermalized and then detected, for example, by an array of ^{3}He counters embedded in a thermalisation medium. The P_n value can then be extracted from the ratio of the measured neutrons to the number of β-particles emitted from the source. The experimental uncertainty is highly dependent on the isotopic purity of the source which can be provided by the trap-assisted approach. A detection system under development for the use at the future FAIR facility was recently commissioned with Penning-trap purified delayed neutron activities, see Fig. 28. In this setup, neutrons were detected with the BELEN 4π neutron counter, described in ref. [167]. The employed detector configuration consisted of 20 ^{3}He proportional counter tubes at a pressure of about 20 atm. The tubes were embedded in a high density polyethylene block with overall dimensions 90 cm × 90 cm × 80 cm, which acts as both neutron moderator and neutron background shielding. The detection efficiency ε_n for the setup, as deduced from Monte Carlo (MC) simulations, was close to 50% for neutron energies up to 1 MeV. Well-known neutron-rich neutron emitters ^{88}Br, ^{94,95}Rb and ^{138}I used in the commissioning experiment were produced in fission, separated by the IGISOL facility and prepared as isotopically pure sources with the JYFLTRAP setup. Fig. 29 shows the growth and decay curves for the beta- and neutron-activities for the trap-purified ^{94}Rb activity ($T_{1/2}$ = 2.7 s). The neutron time spectrum could be fitted very nicely using a single half-life component combined with a constant background.

Following this commissioning experiment, some earlier measured delayed neutron emitters east of the N=50 neutron shell were studied by this setup, see Ref. [169]. The measured preliminary P_n values for four isotopes ($^{85}Ge_{53}$, $^{85}As_{52}$, $^{86}As_{53}$ and $^{91}Br_{56}$) agreed perfectly with the earlier measured data whereas the theoretical values based on QRPA- and shell-model based approaches showed remarkable difference between theory and experiment, see Ref. [169] for more detailed information.

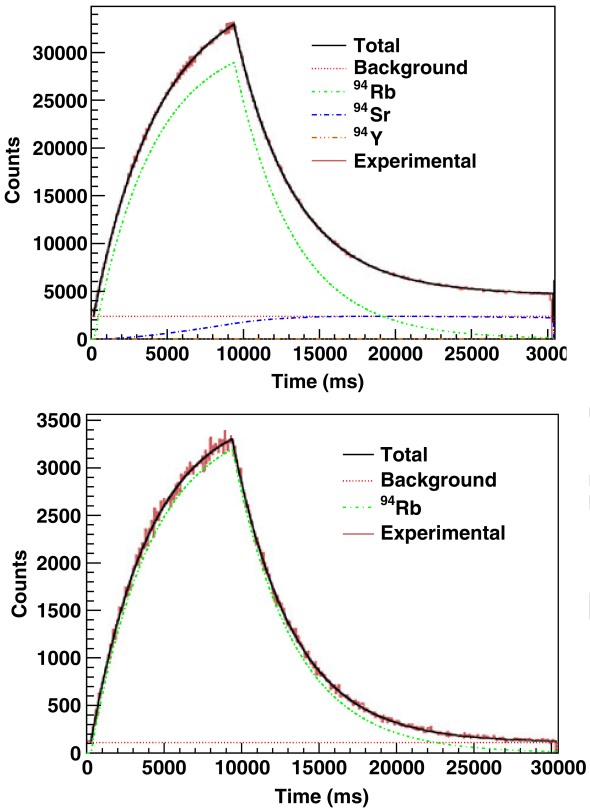

Figure 29: Growth-in and decay curves for trap-purified source of ^{94}Rb as measured with the beta-counter only (top) and beta-gated neutron long counter (bottom). This figure is from Ref. [166].

5.3. *Double Beta decay studies of relevance for neutrino physics*

Neutrinos are one of the least understood fundamental particles. For half a century physicists thought that neutrinos, like photons, had no mass. But recent data from the neutrino oscillation experiments at SuperKamiokande, SNO, and KamLAND overturned this view and confirmed that the neutrinos are massive particles. However, oscillation experiments can yield only the differences in the squares of the neutrino masses, therefore, no absolute mass scale can be determined. In addition, another question remains concerning the fundamental character of neutrinos, whether they are Dirac or Majorana particles. Neutrinoless double beta decay is a process which can address both issues raised above. This decay process is forbidden according to the Standard Model of Particle Physics since it violates the lepton-number conservation and is only allowed if neutrinos are massive Majorana particles. The detection of this mode of double beta decay could result in the missing information on the neutrino mass scale and possibly also its mass hierarchy. In this context, an interesting application for the accurate mass measurements, available by the Penning trap technique, is to measure the decay energy values of all potentially interesting double beta-decaying nuclei. The accurate decay energy measurements are crucial for any experiment by searching for discrete sum energy peak of two emitted electrons (positrons) related to a neutrinoless double beta decay. Penning-trap experiments have recently provided new accurate Q-values for all currently relevant double-beta decay experiments and measured several additional and potentially interesting cases. These included not only $0\nu\beta^-\beta^-$ or $2\nu\beta^-\beta^-$ decaying isotopes but also $0\nu ECEC$ and $2\nu ECEC$ decaying nuclides. A decisive summary of the current experimental status of these Q-value measurements performed using Penning trap mass spectrometry is given in Refs. [22, 34]. In addition to the accurate Q-values needed for searching the signal from the neutrino experiments, also the relevant nuclear matrix elements for the transitions involved in the decay have to be known. This information, needed for the extracting the effective mass of the Majorana neutrino, will have to be obtained from theory. The half-life for $0\nu\beta\beta$, when mediated by the virtual exchange of light but massive Majorana neutrinos (the simplest interpretation), is given by:

$$\frac{1}{T^{0\nu}_{1/2}} = G_{0\nu} g_A^4 \left|M^{0\nu}\right|^2 \left\langle m_{\beta\beta}\right\rangle^2 \qquad (10)$$

where $G_{0\nu}$ is the energy-dependent phase space factor, $M^{0\nu}$ is the nuclear matrix element (NME) and

$m_{\beta\beta}$ is the effective neutrino mass. The NME has to be obtained from theory and has currently significant uncertainties. It can be calculated based on different modern methods of nuclear structure, such as Nuclear Shell Model, Quasi-Random Phase Approximation, Interaction Boson Model or Projected Hartree-Fock-Bogoliubov approach.

The $\beta\beta$ decay process, with neutrinos or without, can proceed via two-step virtual transitions through states in the intermediate nucleus. The $0\nu\beta\beta$ decay would proceed via intermediate states of all spins and parities, whereas the $2\nu\beta\beta$ decay is restricted to Gamow-Teller (GT) transitions through states in the intermediate nucleus with $J^\pi = 1^+$. Therefore, experiments testing different theories for these matrix elements would be important. Three such systems, where linking transitions via the intermediate nucleus are available, have now been studied using the Penning trap setup at the IGISOL facility. These are the mass 96, 100 and 116 multiplets related to possible candidates of ^{96}Zr, ^{100}Mo and ^{116}Cd for the search experiments of the neutrinoless decay, see refs. [51, 170, 171] respectively. In the following we would like to focus on the most recent of these, the cases of ^{116}Cd and ^{96}Mo.

^{116}In case. Fig. 30 shows a simplified energy scheme of relevance for the double-β decay of ^{116}Cd. In this figure, the energy scale for ^{116}In is magnified. The electron-capture decay branch of the ^{116}In 1^+ ground state mediated by the Gamow-Teller decay to the ground state of ^{116}Cd was determined using a Penning-trap purified ^{116}In isotopic source and a high-resolution X-ray detector. Due to a small decay energy 462.81 ± 0.27 keV the corresponding branch is very small and therefore its determination required ultra-pure source of ^{116}In.

In another experiment, the atomic mass difference between ^{116}Cd and ^{116}Sn was determined by a Penning trap technique to be 2813.50(13) keV [172]. This value differed by as much as 4.5 keV from the earlier value and was 30 times more precise. The ratio for the EC branch of $[2.46 \pm 0.44(\text{stat.}) \pm 0.39(\text{syst.})] \times 10^{-4}$ was obtained. This value represents the first measurement of EC on ^{116}In with a statistical significance over five standard deviations in agreement with the previous data, see Ref. [170]. The final value extracted from this experiment for the GT transition strength of ^{116}In to ^{116}Cd ground state turned out as $B(GT) = 0.402 \pm 0.072(\text{stat.}) \pm 0.064(\text{syst.})$. Combining the obtained matrix element with the corresponding one for ^{116}In β^- decay one obtains the $2\nu\beta\beta$-decay matrix element for the virtual transition through the ground state of ^{116}In as $0.168 \pm 0.015(\text{stat.}) \pm 0.13(\text{syst.}) MeV^{-1}$. This value exceed only slightly the total value of 0.129 ± 0.005 MeV^{-1} derived using the directly measured $2\nu\beta\beta$ decay rate of ^{116}Cd. This shows that the intermediate ground state makes a significant contribution to the ^{116}Cd $2\nu\beta\beta$ decay.

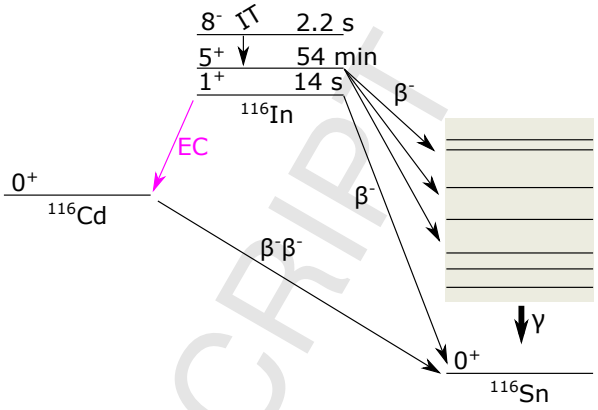

Figure 30: The A=116 system of relevance for the double beta decay of ^{116}Cd.

The ^{96}Zr case. The mass differences of the isobaric multiplet ^{96}Zr-^{96}Nb-^{96}Mo were recently measured with about 100 eV accuracy by the JYFLTRAP mass spectrometer employing a technique where the measurements were performed by switching between the ion species in the pairs (^{96}Zr,^{96}Nb), (^{96}Nb,^{96}Mo), and (^{96}Zr,^{96}Mo) [51]. This eliminated to a high degree any mass-dependent systematic uncertainties. By providing the new highly accurate values for the single- and double-beta decay energies this measurement sheds new light on the corresponding transition strengths, respectively. If the single beta decay of ^{96}Zr to ^{96}Nb were directly observed, a comparison of the measured and theoretical single β-decay rate would allow a direct test of the nuclear-matrix-element calculations for $\beta\beta$ decay, as these follow the same theoretical desscription. However, this case involves four-fold forbidden transitions resulting in additional complications for the calculations. However, the $0\nu\beta\beta$ decay would proceed via intermediate states of all spins and parities, and therefore the case of ^{96}Nb would be particularly interesting case for testing the theory for matrix element calculations.

The $\beta\beta$ decay of ^{96}Zr to ^{96}Mo features a large decay Q-value of 3356.097(86) keV, which makes it an ideal candidate for the search experiments for neutrinoless double-beta decay. The partial half-life for the 2ν variant of the $\beta\beta$ decay to the ^{96}Mo ground state is known from the experiments by the NEMO-3 Collaboration with the value of $T_{1/2} = (2.3 \pm 0.2) \times 10^{19}$ y [51]. On the other hand, a geochemical measurement has resulted in a total half-life of $T_{1/2} = (0.94 \pm 0.32) \times 10^{19}$ y.

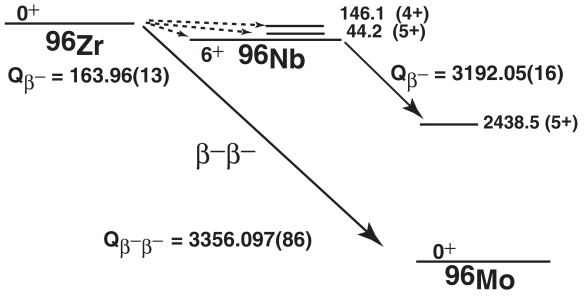

Figure 31: The A=96 system of relevance for the double beta decay of ^{96}Zr. This figure is from Ref. [51].

However, ^{96}Zr is also unstable against single β decay and the corresponding half-life can be derived to be $T_{1/2} = (1.6 \pm 0.9) \times 10^{19}$y. The mass difference, e.g. the Q-value for single beta decay of ^{96}Zr is 163.96(13) keV. The theoretical single β-decay rate has been recalculated using a shell-model approach and assuming a quenched axial-vector coupling constant of $g_A \approx 1$. The resulting half-life, 11×10^{19} y [51], is a factor of two smaller than the value from earlier QRPA calculations, and significantly higher as the experimental value deduced above. However, this indicates that ^{96}Zr single β-decay lifetime is needed and is within reach of an experimental verification.

6. Conclusion and outlook

Ion traps are versatile instruments offering possibilities to explore several interesting physics questions. Precise ground- and isomeric-state ion-trap mass measurements have been important for many aspects of nuclear structure, such as evolution of the shell gaps far from stability, onset of deformation, the role of pairing, three-nucleon forces, and charge symmetry in nuclei. The accuracy of the Penning-trap mass measurements has made it possible to observe subtle changes in nuclear pairing energies and deviations from the quadratic form of the isobaric multiplet mass equation. Precise mass measurements have also provided a fruitful basis to develop theory, for example the role of three-nucleon forces in nuclei.

Modeling of nucleosynthesis in stars requires rather accurate knowledge of nuclear binding energies which play a central role for example in the calculations for the astrophysical r process proceeding along neutron-rich nuclei. Penning-trap measurements have contributed significantly to the mass data needed for nuclear astrophysics modeling. For example, most of the nuclei above ^{56}Ni involved in the rapid proton capture process occurring in type I X-ray bursts [173] were either experimentally unknown or based on beta-decay endpoint energies prone to accumulated uncertainties and missed decay branches to excited states at higher energies in daughter nuclei before Penning-trap measurements. For the astrophysical r process, to answer the question of its astrophysical site(s), more mass measurements in combination with the development of theoretical mass models are needed. New techniques, such as PI-ICR, and MR-TOR devices currently being developed or commissioned at many facilities, will help in this task.

Precise Q-value measurements performed with Penning traps have played a central role in the studies of superallowed beta decays needed to test the CVC hypothesis and the unitarity of the CKM matrix. Many mirror-beta decay Q_{EC} values have also been measured with unprecedented accuracy using Penning traps, and are being actively studied at different facilities. Penning-trap measurements have contributed to neutrino physics studies by determining the Q values for all currently relevant double-beta decay experiments, and finding several additional, potentially interesting cases. The determination of the neutrino mass and solving the neutrino hierarchy problem are one of the biggest open questions in modern physics, setting challenges for future ion-trap experiments.

Ion traps have been exploited in many kinds of decay studies observing decay from trapped ions for example for beta-neutrino angular correlation experiments or for conversion electron spectroscopy. Penning traps and MR-TOF devices have also shown their strength in the beam purification for contaminant-free spectroscopy studies after the trap. The possibility to provide even isomerically pure beams has yielded new possibilities for studies of isomers, but also applications, such as the production of isomerically pure radioxenon ^{133m}Xe and ^{133g}Xe calibration samples for monitoring the nuclear weapon test ban treaty [174].

Ion traps are pivotal for many experiments driven both by fundamental physics questions and by applications. As a consequence, new ion traps are being planned or constructed for present and future radioactive facilities to continue the quest towards measurements of more exotic, unknown nuclei. Novel ion-trapping techniques are being pursued to reach highest accuracies in future ion-trap measurements. To conclude, ion traps have established a firm position in modern nuclear physics experiments.

Acknowledgements

The authors would like to thank prof. Ari Jokinen for fruitful discussions. This work has been supported by the Academy of Finland under the Finnish Centre of Excellence Programme 2012-2017 (Nuclear and Accelerator Based Physics Research at JYFL). AK acknowledges the support from the Academy of Finland under project No. 275389.

[1] S. Rainville, J. K. Thompson, D. E. Pritchard, An Ion Balance for Ultra-High-Precision Atomic Mass Measurements, Science 303 (5656) (2004) 334, doi:10.1126/science.1092320, URL http://www.sciencemag.org/cgi/content/abstract/303/5656/334.

[2] R. S. Van Dyck, Jr., S. L. Zafonte, S. Van Liew, D. B. Pinegar, P. B. Schwinberg, Ultraprecise Atomic Mass Measurement of the alpha Particle and ^{4}He, Phys. Rev. Lett. 92 (22) (2004) 220802, URL http://link.aps.org/doi/10.1103/PhysRevLett.92.220802.

[3] E. G. Myers, A. Wagner, H. Kracke, B. A. Wesson, Atomic Masses of Tritium and Helium-3, Phys. Rev. Lett. 114 (1), doi:10.1103/physrevlett.114.013003, URL http://dx.doi.org/10.1103/PhysRevLett.114.013003.

[4] A. Kellerbauer, T. Kim, R. Moore, P. Varfalvy, Buffer gas cooling of ion beams, Nucl. Instrum. Methods Phys. Res., Sect. A 469 (2) (2001) 276–285, doi:10.1016/s0168-9002(01)00286-8, URL http://dx.doi.org/10.1016/S0168-9002(01)00286-8.

[5] H. Dehmelt, Experiments with an isolated subatomic particle at rest, Rev. Mod. Phys. 62 (3) (1990) 525, URL http://link.aps.org/abstract/RMP/v62/p525.

[6] A. Nieminen, P. Campbell, J. Billowes, D. H. Forest, J. A. R. Griffith, J. Huikari, A. Jokinen, I. D. Moore, R. Moore, G. Tungate, J. Äystö, On-Line Ion Cooling and Bunching for Collinear Laser Spectroscopy, Phys. Rev. Lett. 88 (9) (2002) 094801, URL http://link.aps.org/abstract/PRL/v88/e094801.

[7] T. Sun, S. Schwarz, G. Bollen, D. Lawton, R. Ringle, P. Schury, Commissioning of the ion beam buncher and cooler for LEBIT, Eur. Phys. J. A 25 (S1) (2005) 61–62, doi:10.1140/epjad/i2005-06-126-9, URL http://dx.doi.org/10.1140/epjad/i2005-06-126-9.

[8] A. Nieminen, J. Huikari, A. Jokinen, J. Äystö, P. Campbell, E. C. A. Cochrane, Beam cooler for low-energy radioactive ions, Nucl. Instrum. Methods Phys. Res., Sect. A 469 (2) (2001) 244, URL http://www.sciencedirect.com/science/article/B6TJM-43PGJKX-C/1/93d5587efba5cfe8571b63228952dab8.

[9] F. Herfurth, J. Dilling, A. Kellerbauer, G. Bollen, S. Henry, H. J. Kluge, E. Lamour, D. Lunney, R. B. Moore, C. Scheidenberger, S. Schwarz, G. Sikler, J. Szerypo, A linear radiofrequency ion trap for accumulation, bunching, and emittance improvement of radioactive ion beams, Nucl. Instrum. Methods Phys. Res., Sect. A 469 (2) (2001) 254, ISSN 0168-9002, URL http://www.sciencedirect.com/science/article/B6TJM-43PGJKX-D/2/d5a71a85b9a62763e751fb5a1fcb3716.

[10] G. Savard, S. Baker, C. Davids, A. Levand, E. Moore, R. Pardo, R. Vondrasek, B. Zabransky, G. Zinkann, Radioactive beams from gas catchers: The CARIBU facility, Nucl. Instrum. Methods Phys. Res., Sect. B 266 (19-20) (2008) 4086–4091, doi:10.1016/j.nimb.2008.05.091, URL http://dx.doi.org/10.1016/j.nimb.2008.05.091.

[11] R. Boussaid, G. Ban, J. F. Cam, C. Vandamme, Simulations of high intensity ion beam RFQ cooler for DESIR/SPIRAL 2: SHIRaC, J. Inst. 9 (07) (2014) P07009, doi:10.1088/1748-0221/9/07/p07009, URL http://dx.doi.org/10.1088/1748-0221/9/07/P07009.

[12] S. Kaufman, High-resolution laser spectroscopy in fast beams, Opt. Commun. 17 (3) (1976) 309–312, doi:10.1016/0030-4018(76)90267-4, URL http://dx.doi.org/10.1016/0030-4018(76)90267-4.

[13] K. R. Anton, S. L. Kaufman, W. Klempt, G. Moruzzi, R. Neugart, E. W. Otten, B. Schinzler, Collinear Laser Spectroscopy on Fast Atomic Beams, Phys. Rev. Lett. 40 (10) (1978) 642–645, doi:10.1103/physrevlett.40.642, URL http://dx.doi.org/10.1103/PhysRevLett.40.642.

[14] R. Wolf, F. Wienholtz, D. Atanasov, D. Beck, K. Blaum, C. Borgmann, F. Herfurth, M. Kowalska, S. Kreim, Y. A. Litvinov, D. Lunney, V. Manea, D. Neidherr, M. Rosenbusch, L. Schweikhard, J. Stanja, K. Zuber, ISOLTRAP's multi-reflection time-of-flight mass separator/spectrometer, Int. J. Mass Spectrom. 349-350 (2013) 123–133, doi:10.1016/j.ijms.2013.03.020, URL http://dx.doi.org/10.1016/j.ijms.2013.03.020.

[15] W. R. Plaß, T. Dickel, C. Scheidenberger, Multiple-reflection time-of-flight mass spectrometry, Int. J. Mass Spectrom. doi:10.1016/j.ijms.2013.06.005, URL http://dx.doi.org/10.1016/j.ijms.2013.06.005.

[16] P. Schury, M. Wada, Y. Ito, S. Naimi, T. Sonoda, H. Mita, A. Takamine, K. Okada, H. Wollnik, S. Chon, H. Haba, D. Kaji, H. Koura, H. Miyatake, K. Morimoto, K. Morita, A. Ozawa, A multi-reflection time-of-flight mass spectrograph for short-lived and superheavy nuclei, Nucl. Instrum. Methods Phys. Res., Sect. B 317 (0) (2013) 537–543, ISSN 0168-583X, URL http://www.sciencedirect.com/science/article/pii/S0168583X13006

[17] W. Paul, Electromagnetic traps for charged and neutral particles, Rev. Mod. Phys. 62 (3) (1990) 531–540, doi:10.1103/revmodphys.62.531, URL http://dx.doi.org/10.1103/RevModPhys.62.531.

[18] G. Ban, D. Durand, X. Fléchard, E. Liénard, O. Naviliat-Cuncic, Precision measurements in nuclear β-decay with LPCTrap, Annalen der Physik (2013) DOI: 10.1002/andp.201300043ISSN 1521-3889, doi:10.1002/andp.201300043, URL http://dx.doi.org/10.1002/andp.201300043.

[19] X. Fléchard, E. Liénard, A. Méry, D. Rodríguez, G. Ban, D. Durand, F. Duval, M. Herbane, M. Labalme, F. Mauger, O. Naviliat-Cuncic, J. C. Thomas, P. Velten, Paul Trapping of Radioactive ^{6}He$^+$ Ions and Direct Observation of Their β Decay, Phys. Rev. Lett. 101 (21), doi:10.1103/physrevlett.101.212504, URL http://dx.doi.org/10.1103/PhysRevLett.101.212504.

[20] J. DiSciacca, M. Marshall, K. Marable, G. Gabrielse, Resolving an Individual One-Proton Spin Flip to Determine a Proton Spin State, Phys. Rev. Lett. 110 (14) (2013) 140406–, URL http://link.aps.org/doi/10.1103/PhysRevLett.110.140406.

[21] R. M. Yee, N. D. Scielzo, P. F. Bertone, F. Buchinger, S. Caldwell, J. A. Clark, C. M. Deibel, J. Fallis, J. P. Greene, S. Gulick, D. Lascar, A. F. Levand, G. Li, E. B. Norman, M. Pedretti, G. Savard, R. E. Segel, K. S. Sharma, M. G. Sternberg, J. Van Schelt, B. J. Zabransky, β-Delayed Neutron Spectroscopy Using Trapped Radioactive Ions, Phys. Rev. Lett. 110 (9) (2013) 092501–, URL http://link.aps.org/doi/10.1103/PhysRevLett.110.092501.

[22] K. Blaum, J. Dilling, W. Nörtershäuser, Precision atomic physics techniques for nuclear physics with radioactive beams, Phys. Scr. 2013 (T152) (2013) 014017, ISSN 1402-4896, doi:10.1088/0031-8949/2013/T152/014017, URL http://stacks.iop.org/1402-4896/2013/i=T152/a=014017.

[23] S. Streubel, T. Eronen, M. Höcker, J. Ketter, M. Schuh, J. Van Dyck, R.S., K. Blaum, Toward a more accurate Q value measurement of tritium: status of THe-Trap, Appl. Phys. B 114 (1-2) (2014) 137–145, ISSN 0946-2171, doi:10.1007/s00340-013-5669-x, URL http://dx.doi.org/10.1007/s00340-013-5669-x.

[24] T. Eronen, V. Kolhinen, V. V. Elomaa, D. Gorelov, U. Hager, J. Hakala, A. Jokinen, A. Kankainen, P. Karvonen, S. Kopecky, I. D. Moore, H. Penttilä, S. Rahaman, S. Rinta-Antila, J. Rissanen, A. Saastamoinen, J. Szerypo, C. Weber, J. Äystö, JYFLTRAP: a Penning trap for precision mass spectroscopy and isobaric purification, Eur. Phys. J. A 48 (4) (2012) 46, doi:10.1140/epja/i2012-12046-1.

[25] M. Kretzschmar, Single particle motion in a Penning trap: description in the classical canonical formalism, Phys. Scr. 46 (6) (1992) 544, doi:10.1088/0031-8949/46/6/011, URL http://stacks.iop.org/1402-4896/46/i=6/a=011.

[26] G. Gabrielse, The true cyclotron frequency for particles and ions in a Penning trap, Int. J. Mass Spectrom. 279 (2-3) (2009) 107, ISSN 1387-3806, URL http://www.sciencedirect.com/science/article/B6VND-4TT9GRK-1/2/[illegible]

[27] S. Eliseev, K. Blaum, M. Block, S. Chenmarev, H. Dorrer, C. E. Düllmann, C. Enss, P. E. Filianin, L. Gastaldo, M. Goncharov, et al., Direct Measurement of the Mass Difference of ^{163}Ho ^{163}Dy Solves the Q-Value Puzzle for the Neutrino Mass Determination, Phys. Rev. Lett. 115 (6), ISSN 1079-7114, doi:10.1103/physrevlett.115.062501, URL http://dx.doi.org/10.1103/PhysRevLett.115.062501

[28] K. Gulyuz, J. Ariche, G. Bollen, S. Bustabad, M. Eibach, C. Izzo, S. J. Novario, M. Redshaw, R. Ringle, R. Sandler, S. Schwarz, A. A. Valverde, Determination of the direct double-β-decay Q value of ^{96}Zr and atomic masses of $^{90-92,94,96}$Zr and $^{92,94-98,100}$Mo, Phys. Rev. C 91 (5), doi:10.1103/physrevc.91.055501, URL http://dx.doi.org/10.1103/PhysRevC.91.055501.

[29] K. Blaum, G. Bollen, F. Herfurth, A. Kellerbauer, H.-J. Kluge, M. Kuckein, E. Sauvan, C. Scheidenberger, L. Schweikhard, Carbon clusters for absolute mass measurements at ISOLTRAP, Eur. Phys. J. A 15 (1-2) (2002) 245–248, ISSN 1434-6001, doi:10.1140/epja/i2001-10262-4, URL http://dx.doi.org/10.1140/epja/i2001-10262-4.

[30] G. Bollen, R. B. Moore, G. Savard, H. Stolzenberg, The accuracy of heavy-ion mass measurements using time of flight-ion cyclotron resonance in a Penning trap, J. Appl. Phys. 68 (9) (1990) 4355–4374, doi:10.1063/1.346185, URL http://dx.doi.org/10.1063/1.346185.

[31] J. Ketter, T. Eronen, M. Höcker, S. Streubel, K. Blaum, First-order perturbative calculation of the frequency-shifts caused by static cylindrically-symmetric electric and magnetic imperfections of a Penning trap, Int. J. Mass Spectrom. 358 (2014) 1–16, ISSN 1387-3806, URL http://www.sciencedirect.com/science/article/pii/S1387380613003722

[32] C. Roux, K. Blaum, M. Block, C. Droese, S. Eliseev, M. Goncharov, F. Herfurth, E. M. Ramirez, D. A. Nesterenko, Y. N. Novikov, L. Schweikhard, Data analysis of Q-value measurements for double-electron capture with SHIPTRAP, Eur. Phys. J. D 67 (7) (2013) 1–9, ISSN 1434-6060, doi:10.1140/epjd/e2013-40110-x, URL http://dx.doi.org/10.1140/epjd/e2013-40110-x.

[33] T. Eronen, J. C. Hardy, High-precision Q_{EC}-value measurements for superallowed decays, Eur. Phys. J. A 48 (4) (2012) 48, doi:10.1140/epja/i2012-12048-y, URL http://dx.doi.org/10.1140/epja/i2012-12048-y.

[34] S. A. Eliseev, Y. N. Novikov, K. Blaum, Search for resonant enhancement of neutrinoless double-electron capture by high-precision Penning-trap mass spectrometry, J. Phys. G: Nucl. Part. Phys. 39 (12) (2012) 124003, URL http://stacks.iop.org/0954-3899/39/i=12/a=124003.

[35] G. Gräff, H. Kalinowsky, J. Traut, A direct determination of the proton electron mass ratio, Z. Phys. A 297 (1) (1980) 35–39, doi:10.1007/BF01414243, URL http://dx.doi.org/10.1007/BF01414243.

[36] M. König, G. Bollen, H.-J. Kluge, T. Otto, J. Szerypo, Quadrupole excitation of stored ion motion at the true cyclotron frequency, Int. J. Mass Spectrom. Ion Process. 142 (1–2) (1995) 95, doi:10.1016/0168-1176(95)04146-C, URL http://www.sciencedirect.com/science/article/pii/016811769504

[37] R. Ringle, G. Bollen, A. Prinke, J. Savory, P. Schury, S. Schwarz, T. Sun, A "Lorentz" steerer for ion injection into a Penning trap, Int. J. Mass Spectrom. 263 (1) (2007) 38, URL http://www.sciencedirect.com/science/article/B6VND-4MS3JBM-1/1/

[38] S. George, K. Blaum, F. Herfurth, A. Herlert, M. Kretzschmar, S. Nagy, S. Schwarz, L. Schweikhard, C. Yazidjian, The Ramsey method in high-precision mass spectrometry with Penning traps: Experimental results, Int. J. Mass Spectrom. 264 (2-3) (2007) 110, ISSN 1387-3806, URL http://www.sciencedirect.com/science/article/B6VND-4NF7Y9X-2/2/

[39] H.-J. Kluge, Penning trap mass spectrometry of radionuclides, Int. J. Mass Spectrom. 349–350 (0) (2013) 26–37, ISSN 1387-3806, URL http://www.sciencedirect.com/science/article/pii/S138738061300

[40] R. Ringle, G. Bollen, P. Schury, S. Schwarz, T. Sun, Octupolar excitation of ion motion in a Penning trap–A study performed at LEBIT, Int. J. Mass Spectrom. 262 (1-2) (2007) 33, URL http://www.sciencedirect.com/science/article/B6VND-4MC0TRN-2/1/

[41] S. Eliseev, M. Block, A. Chaudhuri, F. Herfurth, H.-J. Kluge, A. Martin, C. Rauth, G. Vorobjev, Octupolar excitation of ions stored in a Penning trap mass spectrometer–A study performed at SHIPTRAP, Int. J. Mass Spectrom. 262 (1-2) (2007) 45, URL http://www.sciencedirect.com/science/article/B6VND-4M9415X-1/1/

[42] S. Eliseev, C. Roux, K. Blaum, M. Block, C. Droese, F. Herfurth, M. Kretzschmar, M. I. Krivoruchenko, E. Minaya Ramirez, Y. N. Novikov, L. Schweikhard, V. M. Shabaev, F. Simkovic, I. I. Tupitsyn, K. Zuber, N. A. Zubova, Octupolar-Excitation Penning-Trap Mass Spectrometry for Q-Value Measurement of Double-Electron Capture in ^{164}Er, Phys. Rev. Lett. 107 (15) (2011) 152501, URL http://link.aps.org/doi/10.1103/PhysRevLett.107.152501.

[43] A. Lapierre, M. Brodeur, T. Brunner, S. Ettenauer, A. Gallant, V. Simon, M. Good, M. Froese, J. C. López-Urrutia, P. Delheij, S. Epp, R. Ringle, S. Schwarz, J. Ullrich, J. Dilling, The TITAN EBIT charge breeder for mass measurements on highly charged short-lived isotopes—First online operation, Nuclear Instruments and Methods in Physics Research Section A: Accelerators, Spectrometers, Detectors and Associated Equipment 624 (1) (2010) 54–64, doi:10.1016/j.nima.2010.09.030, URL http://dx.doi.org/10.1016/j.nima.2010.09.030.

[44] S. Eliseev, K. Blaum, M. Block, C. Droese, M. Goncharov, E. Minaya Ramirez, D. A. Nesterenko, Y. N. Novikov, L. Schweikhard, Phase-Imaging Ion-Cyclotron-Resonance Measurements for Short-Lived Nuclides, Phys. Rev. Lett. 110 (8) (2013) 082501, URL http://link.aps.org/doi/10.1103/PhysRevLett.110.082501.

[45] S. Eliseev, K. Blaum, M. Block, A. Dörr, C. Droese, T. Eronen, M. Goncharov, M. Höcker, J. Ketter, E. Ramirez, D. Nesterenko, Y. Novikov, L. Schweikhard, A phase-imaging technique for cyclotron-frequency measure-

ments, Appl. Phys. B: Lasers Opt. 114 (1-2) (2014) 107, ISSN 0946-2171, doi:10.1007/s00340-013-5621-0, URL http://dx.doi.org/10.1007/s00340-013-5621-0.

[46] G. Savard, S. Becker, G. Bollen, H. J. Kluge, R. B. Moore, T. Otto, L. Schweikhard, H. Stolzenberg, U. Wiess, A new cooling technique for heavy ions in a Penning trap, Phys. Lett. A 158 (5) (1991) 247, ISSN 0375-9601, URL http://www.sciencedirect.com/science/article/B6TVM-46T4MHS-17Y/2/da0251d2c96981b6b249f2cd4b20f7e0.

[47] J. V. Roosbroeck, C. Guenaut, G. Audi, D. Beck, K. Blaum, G. Bollen, J. Cederkall, P. Delahaye, H. D. Witte, D. Fedorov, V. Fedoseyev, S. Franchoo, H. Fynbo, M. Gorska, F. Herfurth, K. Heyde, M. Huyse, A. Kellerbauer, H.-J. Kluge, U. Köster, K. Kruglov, D. Lunney, A. D. Maesschalck, V. Mishin, W. Müller, S. Nagy, S. Schwarz, L. Schweikhard, N. Smirnova, K. V. de Vel, P. V. Duppen, A. V. Dyck, W. Walters, L. Weissmann, C. Yazidjian, Unambiguous identification of three β-decaying isomers in ^{70}Cu, Phys. Rev. Lett. 92 (2004) 112501.

[48] A. Kwiatkowski, G. Bollen, M. Redshaw, R. Ringle, S. Schwarz, Isobaric beam purification for high precision Penning trap mass spectrometry of radioactive isotope beams with SWIFT, Int. J. Mass Spectrom. 379 (2015) 9–15, doi:10.1016/j.ijms.2014.09.016, URL http://dx.doi.org/10.1016/j.ijms.2014.09.016.

[49] T. Eronen, V.-V. Elomaa, U. Hager, J. Hakala, A. Jokinen, A. Kankainen, S. Rahaman, J. Rissanen, C. Weber, J. Äystö, Preparing isomerically pure beams of short-lived nuclei at JYFLTRAP, Nucl. Instrum. Methods Phys. Res., Sect. B 266 (19-20) (2008) 4527, ISSN 0168-583X, URL http://dx.doi.org/10.1016/j.nimb.2008.05.076.

[50] G. Audi, A. Wapstra, C. Thibault, The Ame2003 atomic mass evaluation: (II). Tables, graphs and references, Nucl. Phys. A 729 (1) (2003) 337 – 676, ISSN 0375-9474, doi:http://dx.doi.org/10.1016/j.nuclphysa.2003.11.003, URL http://www.sciencedirect.com/science/article/pii/S0375947403018098, the 2003 {NUBASE} and Atomic Mass Evaluations.

[51] M. Alanssari, D. Frekers, T. Eronen, L. Canete, J. Dilling, M. Haaranen, J. Hakala, M. Holl, M. Ješkovský, A. Jokinen, A. Kankainen, J. Koponen, A. J. Mayer, I. D. Moore, D. A. Nesterenko, I. Pohjalainen, P. Povinec, J. Reinikainen, S. Rinta-Antila, P. C. Srivastava, J. Suhonen, R. I. Thompson, A. Voss, M. E. Wieser, Single and Double Beta-Decay Q Values among the Triplet ^{96}Zr, ^{96}Nb, and ^{96}Mo, Phys. Rev. Lett. 116 (7), doi:10.1103/physrevlett.116.072501, URL http://dx.doi.org/10.1103/PhysRevLett.116.072501.

[52] G. Bollen, H.-J. Kluge, M. König, T. Otto, G. Savard, H. Stolzenberg, R. B. Moore, G. Rouleau, G. Audi, I. Collaboration, Resolution of nuclear ground and isomeric states by a Penning trap mass spectrometer, Phys. Rev. C 46 (6) (1992) R2140, URL http://link.aps.org/abstract/PRC/v46/pR2140.

[53] A. Kankainen, J. Hakala, T. Eronen, D. Gorelov, A. Jokinen, V. S. Kolhinen, I. D. Moore, H. Penttilä, S. Rinta-Antila, J. Rissanen, A. Saastamoinen, V. Sonnenschein, J. Äystö, Isomeric states close to doubly magic ^{132}Sn studied with the double Penning trap JYFLTRAP, Phys. Rev. C 87 (2013) 024307, doi:10.1103/PhysRevC.87.024307, URL http://link.aps.org/doi/10.1103/PhysRevC.87.024307.

[54] M. Rosenbusch, K. Blaum, C. Borgmann, S. Kreim, M. Kretzschmar, D. Lunney, L. Schweikhard, F. Wienholtz, R. Wolf, Buffer-gas-free mass-selective ion centering in Penning traps by simultaneous dipolar excitation of magnetron motion and quadrupolar excitation for interconversion between magnetron and cyclotron motion, Int. J. Mass Spectrom. 325-327 (2012) 51–57, doi:10.1016/j.ijms.2012.06.008, URL http://dx.doi.org/10.1016/j.ijms.2012.06.008.

[55] M. Rosenbusch, C. Böhm, C. Borgmann, M. Breitenfeldt, A. Herlert, M. Kowalska, S. Kreim, G. Marx, S. Naimi, D. Neidherr, R. Schneider, L. Schweikhard, A study of octupolar excitation for mass-selective centering in Penning traps, Int. J. Mass Spectrom. 314 (2012) 6–12, doi:10.1016/j.ijms.2012.01.002, URL http://dx.doi.org/10.1016/j.ijms.2012.01.002.

[56] H. Wollnik, M. Przewloka, Time-of-flight mass spectrometers with multiply reflected ion trajectories, Int. J. Mass Spectrom. Ion Process. 96 (3) (1990) 267–274, doi:10.1016/0168-1176(90)85127-n, URL http://dx.doi.org/10.1016/0168-1176(90)85127-N.

[57] T. Dickel, W. Plaß, A. Becker, U. Czok, H. Geissel, E. Haettner, C. Jesch, W. Kinsel, M. Petrick, C. Scheidenberger, A. Simon, M. Yavor, A high-performance multiple-reflection time-of-flight mass spectrometer and isobar separator for the research with exotic nuclei, Nucl. Instrum. Methods Phys. Res., Sect. A 777 (2015) 172–188, doi:10.1016/j.nima.2014.12.094, URL http://dx.doi.org/10.1016/j.nima.2014.12.094.

[58] M. Rosenbusch, P. Ascher, D. Atanasov, C. Barbieri, D. Beck, K. Blaum, C. Borgmann, M. Breitenfeldt, R. B. Cakirli, A. Cipollone, S. George, F. Herfurth, M. Kowalska, S. Kreim, D. Lunney, V. Manea, P. Navrátil, D. Neidherr, L. Schweikhard, V. Somà, J. Stanja, F. Wienholtz, R. N. Wolf, K. Zuber, Probing the $N = 32$ Shell Closure below the Magic Proton Number $Z = 20$: Mass Measurements of the Exotic Isotopes ^{52,53}K, Phys. Rev. Lett. 114 (2015) 202501, doi:10.1103/PhysRevLett.114.202501, URL http://link.aps.org/doi/10.1103/PhysRevLett.114.202501.

[59] S. Kreim, M. Hempel, D. Lunney, J. Schaffner-Bielich, Nuclear masses and neutron stars, Int. J. Mass Spectrom. 349–350 (0) (2013) 63–68, ISSN 1387-3806, URL http://www.sciencedirect.com/science/article/pii/S1387380613000

[60] J. Clark, G. Savard, Precision masses for studies of the astrophysical r process, Int. J. Mass Spectrom. 349–350 (0) (2013) 81–86, ISSN 1387-3806, URL http://www.sciencedirect.com/science/article/pii/S1387380613002

[61] M. Block, D. Ackermann, K. Blaum, A. Chaudhuri, Z. Di, S. Eliseev, R. Ferrer, D. Habs, F. Herfurth, F. P. Heßberger, S. Hofmann, H.-J. Kluge, G. Maero, A. Martin, G. Marx, M. Mazzocco, M. Mukherjee, J. B. Neumayr, W. R. Plaß, W. Quint, S. Rahaman, C. Rauth, D. Rodriguez, C. Scheidenberger, L. Schweikhard, P. G. Thirolf, G. Vorobjev, C. Weber, Towards direct mass measurements of nobelium at SHIPTRAP, Eur. Phys. J. D 45 (1) (2007) 39, ISSN 1434-6060, URL http://dx.doi.org/10.1140/epjd/e2007-00189-2.

[62] E. M. Ramirez, D. Ackermann, K. Blaum, M. Block, C. Droese, C. E. Düllmann, M. Dworschak, M. Eibach, S. Eliseev, E. Haettner, F. Herfurth, F. P. Heßberger, S. Hofmann, J. Ketelaer, G. Marx, M. Mazzocco, D. Nesterenko, Y. N. Novikov, W. R. Plaß, D. Rodríguez, C. Scheidenberger, L. Schweikhard, P. G. Thirolf, C. Weber, Direct Mapping of Nuclear Shell Effects in the Heaviest Elements, Science 337 (6099) (2012) 1207–1210, ISSN 0036-8075, doi:10.1126/science.1225636, URL http://science.sciencemag.org/content/337/6099/1207.

[63] M. Block, D. Ackermann, K. Blaum, C. Droese, M. Dworschak, S. Eliseev, T. Fleckenstein, E. Haettner, F. Herfurth, F. P. Heßberger, S. Hofmann, J. Ketelaer, J. Ketter, H.-J. Kluge, G. Marx, M. Mazzocco, Y. N. Novikov, W. R. Plaß, A. Popeko, S. Rahaman, D. Rodríguez, C. Scheidenberger, L. Schweikhard, P. G. Thirolf, G. K. Vorobyev, C. Weber, Direct mass measurements above uranium bridge the gap to the

island of stability, Nature 463 (7282) (2010) 785, ISSN 0028-0836, URL http://dx.doi.org/10.1038/nature08774.

[64] M. Block, Direct mass measurements of the heaviest elements with Penning traps, Int. J. Mass Spectrom. 349–350 (2013) 94 – 101, ISSN 1387-3806, doi:http://dx.doi.org/10.1016/j.ijms.2013.02.013, URL http://www.sciencedirect.com/science/article/pii/S1387380613000742, 100 years of Mass Spectrometry.

[65] A. Kwiatkowski, T. Macdonald, C. Andreoiu, J. Bale, T. Brunner, A. Chaudhuri, U. Chowdhury, S. Ettenauer, A. Gallant, A. Grossheim, A. Lennarz, E. Mane, M. Pearson, B. Schultz, M. Simon, V. Simon, J. Dilling, Precision mass measurements at TITAN with radioactive ions, Nucl. Instrum. Methods Phys. Res., Sect. B 317 (2013) 517, ISSN 0168-583X, URL http://www.sciencedirect.com/science/article/pii/S0168583X13007064.

[66] R. Ringle, S. Schwarz, G. Bollen, Penning trap mass spectrometry of rare isotopes produced via projectile fragmentation at the LEBIT facility, International Journal of Mass Spectrometry 349–350 (0) (2013) 87–93, ISSN 1387-3806, URL http://www.sciencedirect.com/science/article/pii/S1387380613001970.

[67] J. Ketelaer, J. Krämer, D. Beck, K. Blaum, M. Block, K. Eberhardt, G. Eitel, R. Ferrer, C. Geppert, S. George, F. Herfurth, J. Ketter, S. Nagy, D. Neidherr, R. Neugart, W. Nörtershäuser, J. Repp, C. Smorra, N. Trautmann, C. Weber, TRIGA-SPEC: A setup for mass spectrometry and laser spectroscopy at the research reactor {TRIGA} Mainz, Nuclear Instruments and Methods in Physics Research Section A: Accelerators, Spectrometers, Detectors and Associated Equipment 594 (2) (2008) 162 – 177, ISSN 0168-9002, doi:http://dx.doi.org/10.1016/j.nima.2008.06.023, URL http://www.sciencedirect.com/science/article/pii/S0168900208008693.

[68] M. Wang, G. Audi, A. Wapstra, F. Kondev, M. MacCormick, X. Xu, B. Pfeiffer, The Ame2012 atomic mass evaluation, Chinese Physics C 36 (12) (2012) 1603, URL http://stacks.iop.org/1674-1137/36/i=12/a=003.

[69] F. Wienholtz, D. Beck, K. Blaum, C. Borgmann, M. Breitenfeldt, R. B. Cakirli, S. George, F. Herfurth, J. D. Holt, M. Kowalska, S. Kreim, D. Lunney, V. Manea, J. Menendez, D. Neidherr, M. Rosenbusch, L. Schweikhard, A. Schwenk, J. Simonis, J. Stanja, R. N. Wolf, K. Zuber, Masses of exotic calcium isotopes pin down nuclear forces, Nature 498 (2013) 346–349, doi:10.1038/nature12226, URL http://dx.doi.org/10.1038/nature12226.

[70] R. N. Wolf, D. Beck, K. Blaum, C. Böhm, C. Borgmann, M. Breitenfeldt, N. Chamel, S. Goriely, F. Herfurth, M. Kowalska, S. Kreim, D. Lunney, V. Manea, E. Minaya Ramirez, S. Naimi, D. Neidherr, M. Rosenbusch, L. Schweikhard, J. Stanja, F. Wienholtz, K. Zuber, Plumbing Neutron Stars to New Depths with the Binding Energy of the Exotic Nuclide ^{82}Zn, Phys. Rev. Lett. 110 (4) (2013) 041101, doi:10.1103/PhysRevLett.110.041101, URL http://link.aps.org/doi/10.1103/PhysRevLett.110.041101.

[71] V. Manea, D. Atanasov, D. Beck, K. Blaum, C. Borgmann, R. B. Cakirli, T. Eronen, S. George, F. Herfurth, A. Herlert, M. Kowalska, S. Kreim, Y. A. Litvinov, D. Lunney, D. Neidherr, M. Rosenbusch, L. Schweikhard, F. Wienholtz, R. N. Wolf, K. Zuber, Collective degrees of freedom of neutron-rich $A \approx 100$ nuclei and the first mass measurement of the short-lived nuclide ^{100}Rb, Phys. Rev. C 88 (2013) 054322, doi:10.1103/PhysRevC.88.054322, URL http://link.aps.org/doi/10.1103/PhysRevC.88.054322.

[72] D. Atanasov, P. Ascher, K. Blaum, R. B. Cakirli, T. E. Cocolios, S. George, S. Goriely, F. Herfurth, H.-T. Janka, O. Just, M. Kowalska, S. Kreim, D. Kisler, Y. A. Litvinov, D. Lunney, V. Manea, D. Neidherr, M. Rosenbusch, L. Schweikhard, A. Welker, F. Wienholtz, R. N. Wolf, K. Zuber, Precision Mass Measurements of $^{129-131}$Cd and Their Impact on Stellar Nucleosynthesis via the Rapid Neutron Capture Process, Phys. Rev. Lett. 115 (2015) 232501, doi:10.1103/PhysRevLett.115.232501, URL http://link.aps.org/doi/10.1103/PhysRevLett.115.232501.

[73] M. Wehrheim, D. Lascar, G. Savard, J. A. Clark, P. F. Bertone, S. Caldwell, A. Chaudhuri, A. F. Levand, G. Li, G. E. Morgan, R. Orford, R. E. Segel, K. S. Sharma, M. G. Sternberg, First Results from the CARIBU Facility: Mass Measurements on the r-Process Path, Phys. Rev. Lett. 111 (6) (2013) 061102–, URL http://link.aps.org/doi/10.1103/PhysRevLett.111.061102.

[74] J. Stanja, C. Borgmann, J. Agramunt, A. Algora, D. Beck, K. Blaum, C. Böhm, M. Breitenfeldt, T. E. Cocolios, L. M. Fraile, F. Herfurth, A. Herlert, M. Kowalska, S. Kreim, D. Lunney, V. Manea, E. Minaya Ramirez, S. Naimi, D. Neidherr, M. Rosenbusch, L. Schweikhard, G. Simpson, F. Wienholtz, R. N. Wolf, K. Zuber, Mass spectrometry and decay spectroscopy of isomers across the $Z = 82$ shell closure, Phys. Rev. C 88 (2013) 054304, doi:10.1103/PhysRevC.88.054304, URL http://link.aps.org/doi/10.1103/PhysRevC.88.054304.

[75] S. Kreim, D. Beck, K. Blaum, C. Borgmann, M. Breitenfeldt, T. E. Cocolios, A. Gottberg, F. Herfurth, M. Kowalska, Y. A. Litvinov, D. Lunney, V. Manea, T. M. Mendonca, S. Naimi, D. Neidherr, M. Rosenbusch, L. Schweikhard, T. Stora, F. Wienholtz, R. N. Wolf, K. Zuber, Competition between pairing correlations and deformation from the odd-even mass staggering of francium and radium isotopes, Phys. Rev. C 90 (2014) 024301, doi:10.1103/PhysRevC.90.024301, URL http://link.aps.org/doi/10.1103/PhysRevC.90.024301.

[76] J. Hakala, J. Dobaczewski, D. Gorelov, T. Eronen, A. Jokinen, A. Kankainen, V. S. Kolhinen, M. Kortelainen, I. D. Moore, H. Penttilä, S. Rinta-Antila, J. Rissanen, A. Saastamoinen, V. Sonnenschein, J. Äystö, Precision Mass Measurements beyond ^{132}Sn: Anomalous Behavior of Odd-Even Staggering of Binding Energies, Phys. Rev. Lett. 109 (2012) 032501, doi:10.1103/PhysRevLett.109.032501, URL http://link.aps.org/doi/10.1103/PhysRevLett.109.032501.

[77] J. Erler, N. Birge, M. Kortelainen, W. Nazarewicz, E. Olsen, A. M. Perhac, M. Stoitsov, The limits of the nuclear landscape, Nature 486 (2012) 509–512, doi:10.1038/nature11188, URL http://dx.doi.org/10.1038/nature11188.

[78] T. Ohnishi, T. Kubo, . Kusaka, A. Yoshida, K. Yoshida, M. Ohtake, N. Fukuda, H. Takeda, D. Kameda, K. Tanaka, N. Inabe, Y. Yanagisawa, Y. Gono, H. Watanabe, H. Otsu, H. Baba, T. Ichihara, Y. Yamaguchi, M. Takechi, S. Nishimura, H. Ueno, A. Yoshimi, H. Sakurai, T. Motobayashi, T. Nakao, Y. Mizoi, M. Matsushita, K. Ieki, N. Kobayashi, K. Tanaka, Y. Kawada, N. Tanaka, S. Deguchi, Y. Satou, Y. Kondo, T. Nakamura, K. Yoshinaga, C. Ishii, H. Yoshii, Y. Miyashita, N. Uematsu, Y. Shiraki, T. Sumikama, J. Chiba, E. Ideguchi, A. Saito, T. Yamaguchi, I. Hachiuma, T. Suzuki, T. Moriguchi, A. Ozawa, T. Ohtsubo, M. A. Famiano, H. Geissel, A. S. Nettleton, O. B. Tarasov, D. P. Bazin, B. M. Sherrill, S. L. Manikonda, J. A. Nolen, Identification of 45 New Neutron-Rich Isotopes Produced by In-Flight Fission of a ^{238}U Beam at 345 MeV/nucleon, J. Phys. Soc. Jpn 79 (7) (2010) 073201, doi:10.1143/JPSJ.79.073201, URL http://jpsj.ipap.jp/link?JPSJ/79/073201/.

[79] G. Lorusso, S. Nishimura, Z. Y. Xu, A. Jungclaus, Y. Shimizu, G. S. Simpson, P.-A. Söderström, H. Watanabe, F. Browne, P. Doornenbal, G. Gey, H. S. Jung, B. Meyer, T. Sumikama, J. Taprogge, Z. Vajta, J. Wu, H. Baba, G. Benzoni, K. Y. Chae, F. C. L. Crespi, N. Fukuda, R. Gernhäuser, N. Inabe, T. Isobe,

T. Kajino, D. Kameda, G. D. Kim, Y.-K. Kim, I. Kojouharov, F. G. Kondev, T. Kubo, N. Kurz, Y. K. Kwon, G. J. Lane, Z. Li, A. Montaner-Pizá, K. Moschner, F. Naqvi, M. Niikura, H. Nishibata, A. Odahara, R. Orlandi, Z. Patel, Z. Podolyák, H. Sakurai, H. Schaffner, P. Schury, S. Shibagaki, K. Steiger, H. Suzuki, H. Takeda, A. Wendt, A. Yagi, K. Yoshinaga, β-Decay Half-Lives of 110 Neutron-Rich Nuclei across the $N = 82$ Shell Gap: Implications for the Mechanism and Universality of the Astrophysical r Process, Phys. Rev. Lett. 114 (2015) 192501, doi:10.1103/PhysRevLett.114.192501, URL http://link.aps.org/doi/10.1103/PhysRevLett.114.192501.

[80] J. Van Schelt, D. Lascar, G. Savard, J. A. Clark, S. Caldwell, A. Chaudhuri, J. Fallis, J. P. Greene, A. F. Levand, G. Li, K. S. Sharma, M. G. Sternberg, T. Sun, B. J. Zabransky, Mass measurements near the r-process path using the Canadian Penning Trap mass spectrometer, Phys. Rev. C 85 (2012) 045805, doi:10.1103/PhysRevC.85.045805, URL http://link.aps.org/doi/10.1103/PhysRevC.85.045805.

[81] M. Mumpower, R. Surman, G. McLaughlin, A. Aprahamian, The impact of individual nuclear properties on -process nucleosynthesis, Progress in Particle and Nuclear Physics 86 (2016) 86 – 126, ISSN 0146-6410, doi:http://dx.doi.org/10.1016/j.ppnp.2015.09.001, URL http://www.sciencedirect.com/science/article/pii/S0146641015000887.

[82] A. T. Gallant, J. C. Bale, T. Brunner, U. Chowdhury, S. Ettenauer, A. Lennarz, D. Robertson, V. V. Simon, A. Chaudhuri, J. D. Holt, A. A. Kwiatkowski, E. Mané, J. Menéndez, B. E. Schultz, M. C. Simon, C. Andreoiu, P. Delheij, M. R. Pearson, H. Savajols, A. Schwenk, J. Dilling, New Precision Mass Measurements of Neutron-Rich Calcium and Potassium Isotopes and Three-Nucleon Forces, Phys. Rev. Lett. 109 (2012) 032506, doi:10.1103/PhysRevLett.109.032506, URL http://link.aps.org/doi/10.1103/PhysRevLett.109.032506.

[83] A. Lapierre, M. Brodeur, T. Brunner, S. Ettenauer, P. Finlay, A. T. Gallant, V. V. Simon, P. Delheij, D. Lunney, R. Ringle, H. Savajols, J. Dilling, Penning-trap mass measurements of the neutron-rich K and Ca isotopes: Resurgence of the $N = 28$ shell strength, Phys. Rev. C 85 (2012) 024317, doi:10.1103/PhysRevC.85.024317, URL http://link.aps.org/doi/10.1103/PhysRevC.85.024317.

[84] C. Böhm, C. Borgmann, G. Audi, D. Beck, K. Blaum, M. Breitenfeldt, R. B. Cakirli, T. E. Cocolios, S. Eliseev, S. George, F. Herfurth, A. Herlert, M. Kowalska, S. Kreim, D. Lunney, V. Manea, E. Minaya Ramirez, S. Naimi, D. Neidherr, M. Rosenbusch, L. Schweikhard, J. Stanja, M. Wang, R. N. Wolf, K. Zuber, Evolution of nuclear ground-state properties of neutron-deficient isotopes around $Z = 82$ from precision mass measurements, Phys. Rev. C 90 (2014) 044307, doi:10.1103/PhysRevC.90.044307, URL http://link.aps.org/doi/10.1103/PhysRevC.90.044307.

[85] V. V. Simon, T. Brunner, U. Chowdhury, B. Eberhardt, S. Ettenauer, A. T. Gallant, E. Mané, M. C. Simon, P. Delheij, M. R. Pearson, G. Audi, G. Gwinner, D. Lunney, H. Schatz, J. Dilling, Penning-trap mass spectrometry of highly charged, neutron-rich Rb and Sr isotopes in the vicinity of $\mathbf{A} \approx \mathbf{100}$, Phys. Rev. C 85 (2012) 064308, doi:10.1103/PhysRevC.85.064308, URL http://link.aps.org/doi/10.1103/PhysRevC.85.064308.

[86] U. Hager, T. Eronen, J. Hakala, A. Jokinen, V. S. Kolhinen, S. Kopecky, I. Moore, A. Nieminen, M. Oinonen, S. Rinta-Antila, J. Szerypo, J. Äystö, First Precision Mass Measurements of Refractory Fission Fragments, Phys. Rev. Lett. 96 (2006) 042504, doi:10.1103/PhysRevLett.96.042504, URL http://link.aps.org/doi/10.1103/PhysRevLett.96.042504.

[87] S. Rahaman, U. Hager, V. V. Elomaa, T. Eronen, J. Hakala, A. Jokinen, A. Kankainen, P. Karvonen, I. D. Moore, H. Penttilä, S. Rinta-Antila, J. Rissanen, A. Saastamoinen, T. Sonoda, J. Äystö, Precise atomic masses of neutron-rich Br and Rb nuclei close to the r-process path, Eur. Phys. J. A 32 (1) (2007) 87–96, ISSN 1434-601X, doi:10.1140/epja/i2006-10297-y, URL http://dx.doi.org/10.1140/epja/i2006-10297-y.

[88] S. Naimi, G. Audi, D. Beck, K. Blaum, C. Böhm, C. Borgmann, M. Breitenfeldt, S. George, F. Herfurth, A. Herlert, A. Kellerbauer, M. Kowalska, D. Lunney, E. Minaya Ramirez, D. Neidherr, M. Rosenbusch, L. Schweikhard, R. N. Wolf, K. Zuber, Surveying the $N = 40$ island of inversion with new manganese masses, Phys. Rev. C 86 (2012) 014325, doi:10.1103/PhysRevC.86.014325, URL http://link.aps.org/doi/10.1103/PhysRevC.86.014325.

[89] A. Chaudhuri, C. Andreoiu, T. Brunner, U. Chowdhury, S. Ettenauer, A. T. Gallant, G. Gwinner, A. A. Kwiatkowski, A. Lennarz, D. Lunney, T. D. Macdonald, B. E. Schultz, M. C. Simon, V. V. Simon, J. Dilling, Evidence for the extinction of the $N = 20$ neutron-shell closure for ^{32}Mg from direct mass measurements, Phys. Rev. C 88 (2013) 054317, doi:10.1103/PhysRevC.88.054317, URL http://link.aps.org/doi/10.1103/PhysRevC.88.054317.

[90] M. Brodeur, T. Brunner, S. Ettenauer, A. Lapierre, R. Ringle, B. A. Brown, D. Lunney, J. Dilling, Elucidation of the Anomalous $A = 9$ Isospin Quartet Behavior, Phys. Rev. Lett. 108 (2012) 212501, doi:10.1103/PhysRevLett.108.212501, URL http://link.aps.org/doi/10.1103/PhysRevLett.108.212501.

[91] A. T. Gallant, M. Brodeur, C. Andreoiu, A. Bader, A. Chaudhuri, U. Chowdhury, A. Grossheim, R. Klawitter, A. A. Kwiatkowski, K. G. Leach, A. Lennarz, T. D. Macdonald, B. E. Schultz, J. Lassen, H. Heggen, S. Raeder, A. Teigelhöfer, B. A. Brown, A. Magilligan, J. D. Holt, J. Menéndez, J. Simonis, A. Schwenk, J. Dilling, Breakdown of the Isobaric Multiplet Mass Equation for the $A = 20$ and 21 Multiplets, Phys. Rev. Lett. 113 (2014) 082501, doi:10.1103/PhysRevLett.113.082501, URL http://link.aps.org/doi/10.1103/PhysRevLett.113.082501.

[92] A. Kankainen, L. Canete, T. Eronen, D. Gorelov, J. Hakala, A. Jokinen, J. Koponen, I. Moore, D. Nesterenko, J. Reinikainen, S. Rinta-Antila, A. Voss, J. Äystö, Mass of astrophysically relevant ^{31}Cl and the breakdown of the isobaric multiplet mass equation, Phys. Rev. C Rapid. Comm. Accepted for publication.

[93] M. Eibach, G. Bollen, M. Brodeur, K. Cooper, K. Gulyuz, C. Izzo, D. J. Morrissey, M. Redshaw, R. Ringle, R. Sandler, S. Schwarz, C. S. Sumithrarachchi, A. A. Valverde, A. C. C. Villari, Determination of the Q_{EC} values of the $T = 1/2$ mirror nuclei ^{21}Na and ^{29}P at LEBIT, Phys. Rev. C 92 (2015) 045502, doi:10.1103/PhysRevC.92.045502, URL http://link.aps.org/doi/10.1103/PhysRevC.92.045502.

[94] B. E. Schultz, M. Brodeur, C. Andreoiu, A. Bader, A. Chaudhuri, U. Chowdhury, A. T. Gallant, A. Grossheim, R. Klawitter, A. A. Kwiatkowski, K. G. Leach, A. Lennarz, T. D. Macdonald, J. Lassen, H. Heggen, S. Raeder, A. Teigelhöfer, J. Dilling, Precision Q_{EC}-value measurement of ^{23}Mg for testing the Cabibbo-Kobayashi-Maskawa matrix unitarity, Phys. Rev. C 90 (2014) 012501, doi:10.1103/PhysRevC.90.012501, URL http://link.aps.org/doi/10.1103/PhysRevC.90.012501.

[95] L. Canete, A. Kankainen, T. Eronen, D. Gorelov, J. Hakala, A. Jokinen, V. Kolhinen, J. Koponen, I. Moore, J. Reinikainen, S. Rinta-Antila, High-precision mass measurements of ^{25}Al and ^{30}P at JYFLTRAP, Eur. Phys. J. A Accepted for publication.

[96] A. Kankainen, T. Eronen, D. Gorelov, J. Hakala, A. Jokinen,

V. S. Kolhinen, M. Reponen, J. Rissanen, A. Saastamoinen, V. Sonnenschein, J. Äystö, Coulomb displacement energies as a probe for nucleon pairing in the $f_{7/2}$ shell, Phys. Rev. C 89 (2014) 051302, doi:10.1103/PhysRevC.89.051302, URL http://link.aps.org/doi/10.1103/PhysRevC.89.051302.

[97] K. Gulyuz, J. Ariche, G. Bollen, S. Bustabad, M. Eibach, C. Izzo, S. J. Novario, M. Redshaw, R. Ringle, R. Sandler, S. Schwarz, A. A. Valverde, Determination of the direct double-β-decay Q value of ^{96}Zr and atomic masses of $^{90-92,94,96}$Zr and $^{92,94-98,100}$Mo, Phys. Rev. C 91 (2015) 055501, doi:10.1103/PhysRevC.91.055501, URL http://link.aps.org/doi/10.1103/PhysRevC.91.055501.

[98] A. Kankainen, J. Äystö, A. Jokinen, High-accuracy mass spectrometry of fission products with Penning traps, J. Phys. G: Nucl. Part. Phys. 39 (9) (2012) 093101, URL http://stacks.iop.org/0954-3899/39/i=9/a=093101.

[99] M. Alanssari, D. Frekers, T. Eronen, L. Canete, J. Dilling, M. Haaranen, J. Hakala, M. Holl, M. Ješkovský, A. Jokinen, A. Kankainen, J. Koponen, A. J. Mayer, I. D. Moore, D. A. Nesterenko, I. Pohjalainen, P. Povinec, J. Reinikainen, S. Rinta-Antila, P. C. Srivastava, J. Suhonen, R. I. Thompson, A. Voss, M. E. Wieser, Single and Double Beta-Decay Q Values among the Triplet ^{96}Zr, ^{96}Nb, and ^{96}Mo, Phys. Rev. Lett. 116 (2016) 072501, doi:10.1103/PhysRevLett.116.072501, URL http://link.aps.org/doi/10.1103/PhysRevLett.116.072501.

[100] C. Smorra, T. R. Rodríguez, T. Beyer, K. Blaum, M. Block, C. E. Düllmann, K. Eberhardt, M. Eibach, S. Eliseev, K. Langanke, G. Martínez-Pinedo, S. Nagy, W. Nörtershäuser, D. Renisch, V. M. Shabaev, I. I. Tupitsyn, N. A. Zubova, Q value and half-life of double-electron capture in ^{184}Os, Phys. Rev. C 86 (2012) 044604, doi:10.1103/PhysRevC.86.044604, URL http://link.aps.org/doi/10.1103/PhysRevC.86.044604.

[101] U. Chowdhury, K. G. Leach, C. Andreoiu, A. Bader, M. Brodeur, A. Chaudhuri, A. T. Gallant, A. Grossheim, G. Gwinner, R. Klawitter, A. A. Kwiatkowski, A. Lennarz, T. D. Macdonald, J. Pearkes, B. E. Schultz, J. Dilling, First direct mass measurement of the neutron-deficient nucleus ^{24}Al, Phys. Rev. C 92 (2015) 045803, doi:10.1103/PhysRevC.92.045803, URL http://link.aps.org/doi/10.1103/PhysRevC.92.045803.

[102] A. A. Kwiatkowski, T. Brunner, J. D. Holt, A. Chaudhuri, U. Chowdhury, M. Eibach, J. Engel, A. T. Gallant, A. Grossheim, M. Horoi, A. Lennarz, T. D. Macdonald, M. R. Pearson, B. E. Schultz, M. C. Simon, R. A. Senkov, V. V. Simon, K. Zuber, J. Dilling, New determination of double-β-decay properties in ^{48}Ca: High-precision $Q_{\beta\beta}$-value measurement and improved nuclear matrix element calculations, Phys. Rev. C 89 (2014) 045502, doi:10.1103/PhysRevC.89.045502, URL http://link.aps.org/doi/10.1103/PhysRevC.89.045502.

[103] S. Malbrunot-Ettenauer, T. Brunner, U. Chowdhury, A. T. Gallant, V. V. Simon, M. Brodeur, A. Chaudhuri, E. Mané, M. C. Simon, C. Andreoiu, G. Audi, J. R. Crespo López-Urrutia, P. Delheij, G. Gwinner, A. Lapierre, D. Lunney, M. R. Pearson, R. Ringle, J. Ullrich, J. Dilling, Penning trap mass measurements utilizing highly charged ions as a path to benchmark isospin-symmetry breaking corrections in ^{74}Rb, Phys. Rev. C 91 (2015) 045504, doi:10.1103/PhysRevC.91.045504, URL http://link.aps.org/doi/10.1103/PhysRevC.91.045504.

[104] A. A. Valverde, G. Bollen, K. Cooper, M. Eibach, K. Gulyuz, C. Izzo, D. J. Morrissey, R. Ringle, R. Sandler, S. Schwarz, C. S. Sumithrarachchi, A. C. C. Villari, Penning trap mass measurement of ^{72}Br, Phys. Rev. C 91 (2015) 037301, doi:10.1103/PhysRevC.91.037301, URL http://link.aps.org/doi/10.1103/PhysRevC.91.037301.

[105] F. Schneider, T. Beyer, K. Blaum, M. Block, S. Chenmarev, H. Dorrer, C. Düllmann, K. Eberhardt, M. Eibach, S. Eliseev, J. Grund, U. Köster, S. Nagy, Y. Novikov, D. Renisch, A. Türler, K. Wendt, Preparatory studies for a high-precision Penning-trap measurement of the 163Ho electron capture Q-value, Eur. Phys. J. A 51 (7) 89, ISSN 1434-6001, doi:10.1140/epja/i2015-15089-8, URL http://dx.doi.org/10.1140/epja/i2015-15089-8.

[106] C. Droese, D. Ackermann, L.-L. Andersson, K. Blaum, M. Block, M. Dworschak, M. Eibach, S. Eliseev, U. Forsberg, E. Haettner, F. Herfurth, F. Hessberger, S. Hofmann, J. Ketelaer, G. Marx, E. Minaya Ramirez, D. Nesterenko, Y. Novikov, W. Plass, D. Rodriguez, D. Rudolph, C. Scheidenberger, L. Schweikhard, S. Stolze, P. Thirolf, C. Weber, High-precision mass measurements of 203-207Rn and 213Ra with SHIPTRAP, Eur. Phys. J. A 49 (1) 13, ISSN 1434-6001, doi:10.1140/epja/i2013-13013-0, URL http://dx.doi.org/10.1140/epja/i2013-13013-0.

[107] M. Eibach, T. Beyer, K. Blaum, M. Block, C. E. Düllmann, K. Eberhardt, J. Grund, S. Nagy, H. Nitsche, W. Nörtershäuser, D. Renisch, K. P. Rykaczewski, F. Schneider, C. Smorra, J. Vieten, M. Wang, K. Wendt, Direct high-precision mass measurements on ^{241,243}Am, ^{244}Pu, and ^{249}Cf, Phys. Rev. C 89 (2014) 064318, doi:10.1103/PhysRevC.89.064318, URL http://link.aps.org/doi/10.1103/PhysRevC.89.064318.

[108] P. Möller, A. Sierk, T. Ichikawa, H. Sagawa, Nuclear ground-state masses and deformations: FRDM(2012), At. Data and Nucl. Data Tables 109–110 (2016) 1 – 204, ISSN 0092-640X, doi:http://dx.doi.org/10.1016/j.adt.2015.10.002, URL http://www.sciencedirect.com/science/article/pii/S0092640X16000

[109] J. Duflo, A. Zuker, Microscopic mass formulas, Phys. Rev. C 52 (1995) R23–R27, doi:10.1103/PhysRevC.52.R23, URL http://link.aps.org/doi/10.1103/PhysRevC.52.R23.

[110] N. Wang, M. Liu, X. Wu, J. Meng, Surface diffuseness correction in global mass formula, Phys. Lett. B 734 (2014) 215 – 219, ISSN 0370-2693, doi:http://dx.doi.org/10.1016/j.physletb.2014.05.049, URL http://www.sciencedirect.com/science/article/pii/S037026931400

[111] S. Goriely, N. Chamel, J. M. Pearson, Further explorations of Skyrme-Hartree-Fock-Bogoliubov mass formulas. XIII. The 2012 atomic mass evaluation and the symmetry coefficient, Phys. Rev. C 88 (2013) 024308, doi:10.1103/PhysRevC.88.024308, URL http://link.aps.org/doi/10.1103/PhysRevC.88.024308.

[112] M. Kortelainen, T. Lesinski, J. Moré, W. Nazarewicz, J. Sarich, N. Schunck, M. V. Stoitsov, S. Wild, Nuclear energy density optimization, Phys. Rev. C 82 (2010) 024313, doi:10.1103/PhysRevC.82.024313, URL http://link.aps.org/doi/10.1103/PhysRevC.82.024313.

[113] P. Möller, J. Nix, W. Myers, W. Swiatecki, Nuclear Ground-State Masses and Deformations, At. Data Nucl. Data Tables 59 (2) (1995) 185 – 381, ISSN 0092-640X, doi:10.1006/adnd.1995.1002, URL http://www.sciencedirect.com/science/article/pii/S0092640X8571

[114] J. Mendoza-Temis, J. G. Hirsch, A. P. Zuker, The anatomy of the simplest Duflo–Zuker mass formula, Nucle. Phys. A 843 (1–4) (2010) 14 – 36, ISSN 0375-9474, doi:http://dx.doi.org/10.1016/j.nuclphysa.2010.05.055, URL http://www.sciencedirect.com/science/article/pii/S0375947410005

[115] M. V. Stoitsov, J. Dobaczewski, W. Nazarewicz, S. Pittel, D. J. Dean, Systematic study of deformed nuclei at the drip lines and beyond, Phys. Rev. C 68 (2003) 054312, doi:10.1103/PhysRevC.68.054312, URL

http://link.aps.org/doi/10.1103/PhysRevC.68.054312.

[116] M. Stoitsov, J. Dobaczewski, W. Nazarewicz, P. Borycki, Large-scale self-consistent nuclear mass calculations, Int. J. Mass Spectrom. 251 (2 - 3) (2006) 243 – 251, ISSN 1387-3806, doi:10.1016/j.ijms.2006.01.040, URL http://www.sciencedirect.com/science/article/pii/S1387380606000944.

[117] Y. Gao, J. Dobaczewski, M. Kortelainen, J. Toivanen, D. Tarpanov, Propagation of uncertainties in the Skyrme energy-density-functional model, Phys. Rev. C 87 (2013) 034324, doi:10.1103/PhysRevC.87.034324, URL http://link.aps.org/doi/10.1103/PhysRevC.87.034324.

[118] M. Kortelainen, Propagation of uncertainties in the nuclear DFT models, Journal of Physics G: Nuclear and Particle Physics 42 (3) (2015) 034021, URL http://stacks.iop.org/0954-3899/42/i=3/a=034021.

[119] M. Mumpower, R. Surman, G. McLaughlin, A. Aprahamian, The impact of individual nuclear properties on -process nucleosynthesis, Progress in Particle and Nuclear Physics 86 (2016) 86 – 126, ISSN 0146-6410, doi:http://dx.doi.org/10.1016/j.ppnp.2015.09.001, URL http://www.sciencedirect.com/science/article/pii/S0146641015000897.

[120] B. H. Sun, Y. A. Litvinov, I. Tanihata, Y. H. Zhang, Toward precision mass measurements of neutron-rich nuclei relevant to r-process nucleosynthesis, Frontiers of Physics 10 (4) (2015) 1–25, ISSN 2095-0470, doi:10.1007/s11467-015-0503-z, URL http://dx.doi.org/10.1007/s11467-015-0503-z.

[121] K. Heyde, J. L. Wood, Shape coexistence in atomic nuclei, Rev. Mod. Phys. 83 (4) (2011) 1467–1521, doi:10.1103/revmodphys.83.1467, URL http://dx.doi.org/10.1103/RevModPhys.83.1467.

[122] S. Takahara, N. Onishi, Y. R. Shimizu, N. Tajima, The role of spin–orbit potential in nuclear prolate-shape dominance, Phys. Lett. B 702 (5) (2011) 429–432, doi:10.1016/j.physletb.2011.07.030, URL http://dx.doi.org/10.1016/j.physletb.2011.07.030.

[123] R. F. G. Ruiz, M. L. Bissell, K. Blaum, A. Ekström, N. Frömmgen, G. Hagen, M. Hammen, K. Hebeler, J. D. Holt, G. R. Jansen, M. Kowalska, K. Kreim, W. Nazarewicz, R. Neugart, G. Neyens, W. Nörtershäuser, T. Papenbrock, J. Papuga, A. Schwenk, J. Simonis, K. A. Wendt, D. T. Yordanov, Unexpectedly large charge radii of neutron-rich calcium isotopes, Nat Phys doi:10.1038/nphys3645, URL http://dx.doi.org/10.1038/nphys3645.

[124] URL http://massexplorer.frib.msu.edu/, ????

[125] J. C. Hardy, I. S. Towner, Superallowed $0^+ \rightarrow 0^+$ nuclear β decays: 2014 critical survey, with precise results for V_{ud} and CKM unitarity, Phys. Rev. C 91 (2), doi:10.1103/physrevc.91.025501, URL http://dx.doi.org/10.1103/PhysRevC.91.025501.

[126] N. Severijns, O. Naviliat-Cuncic, Structure and symmetries of the weak interaction in nuclear beta decay, Phys. Scr. T152 (T152) (2013) 014018, URL http://stacks.iop.org/1402-4896/2013/i=T152/a=014018.

[127] A. A. Valverde, G. Bollen, M. Brodeur, R. A. Bryce, K. Cooper, M. Eibach, K. Gulyuz, C. Izzo, D. J. Morrissey, M. Redshaw, R. Ringle, R. Sandler, S. Schwarz, C. S. Sumithrarachchi, A. C. C. Villari, First Direct Determination of the Superallowed β-Decay Q_{EC} Value for ^{14}O, Phys. Rev. Lett. 114 (2015) 232502, doi:10.1103/PhysRevLett.114.232502, URL http://link.aps.org/doi/10.1103/PhysRevLett.114.232502.

[128] G. Savard, F. Buchinger, J. A. Clark, J. E. Crawford, S. Gulick, J. C. Hardy, A. A. Hecht, J. K. P. Lee, A. F. Levand, N. D. Scielzo, H. Sharma, K. S. Sharma, I. Tanihata, A. C. C. Villari, Y. Wang, Q Value of the Superallowed Decay of ^{46}V and Its Influence on V_{ud} and the Unitarity of the Cabibbo-Kobayashi-Maskawa Matrix, Phys. Rev. Lett. 95 (10) (2005) 102501, URL http://link.aps.org/abstract/PRL/v95/e102501.

[129] T. Eronen, V. Elomaa, U. Hager, J. Hakala, A. Jokinen, A. Kankainen, I. Moore, H. Penttilä, S. Rahaman, J. Rissanen, A. Saastamoinen, T. Sonoda, J. Äystö, J. C. Hardy, V. S. Kolhinen, Q Values of the Superallowed β Emitters ^{26}Al^m, ^{42}Sc, and ^{46}V and Their Impact on Vud and the Unitarity of the Cabibbo-Kobayashi-Maskawa Matrix, Phys. Rev. Lett. 97 (23) (2006) 232501, URL http://link.aps.org/abstract/PRL/v97/e232501.

[130] I. S. Towner, J. C. Hardy, Improved calculation of the isospin-symmetry-breaking corrections to superallowed Fermi beta decay, Phys. Rev. C 77 (2) (2008) 025501, URL http://link.aps.org/abstract/PRC/v77/e025501.

[131] A. Saastamoinen, T. Eronen, A. Jokinen, V. V. Elomaa, J. Hakala, A. Kankainen, I. D. Moore, S. Rahaman, J. Rissanen, C. Weber, J. Äystö, L. Trache, Mass of ^{23}Al for testing the isobaric multiplet mass equation, Phys. Rev. C 80 (2009) 044330, doi:10.1103/PhysRevC.80.044330, URL http://link.aps.org/doi/10.1103/PhysRevC.80.044330.

[132] A. Kankainen, T. Eronen, D. Gorelov, J. Hakala, A. Jokinen, V. S. Kolhinen, M. Reponen, J. Rissanen, A. Saastamoinen, V. Sonnenschein, J. Äystö, High-precision mass measurement of ^{31}S with the double Penning trap JYFLTRAP improves the mass value for ^{32}Cl, Phys. Rev. C 82 (2010) 052501, doi:10.1103/PhysRevC.82.052501, URL http://link.aps.org/doi/10.1103/PhysRevC.82.052501.

[133] A. Kankainen, V.-V. Elomaa, T. Eronen, D. Gorelov, J. Hakala, A. Jokinen, T. Kessler, V. S. Kolhinen, I. D. Moore, S. Rahaman, M. Reponen, J. Rissanen, A. Saastamoinen, C. Weber, J. Äystö, Mass measurements in the vicinity of the doubly magic waiting point ^{56}Ni, Phys. Rev. C 82 (2010) 034311, doi:10.1103/PhysRevC.82.034311, URL http://link.aps.org/doi/10.1103/PhysRevC.82.034311.

[134] M. MacCormick, G. Audi, Evaluated experimental isobaric analogue states from to and associated {IMME} coefficients, Nucl. Phys. A 925 (2014) 61 – 95, ISSN 0375-9474, doi:http://dx.doi.org/10.1016/j.nuclphysa.2014.01.007, URL http://www.sciencedirect.com/science/article/pii/S0375947414000

[135] M. MacCormick, G. Audi, Corrigendum to "Evaluated experimental isobaric analogue states from to and associated {IMME} coefficients" [Nucl. Phys. A 925 (2014) 61–95], Nucl. Phys. A 925 (2014) 296 – 297, ISSN 0375-9474, doi:http://dx.doi.org/10.1016/j.nuclphysa.2014.05.010, URL http://www.sciencedirect.com/science/article/pii/S0375947414001

[136] Y. H. Lam, B. Blank, N. A. Smirnova, J. B. Bueb, M. S. Antony, The isobaric multiplet mass equation for revisited, At. Data and Nucl. Data Tables 99 (6) (2013) 680 – 703, ISSN 0092-640X, doi:http://dx.doi.org/10.1016/j.adt.2012.11.002, URL http://www.sciencedirect.com/science/article/pii/S0092640X13000

[137] M. Brodeur, T. Brunner, C. Champagne, S. Ettenauer, M. J. Smith, A. Lapierre, R. Ringle, V. L. Ryjkov, S. Bacca, P. Delheij, G. W. F. Drake, D. Lunney, A. Schwenk, J. Dilling, First Direct Mass Measurement of the Two-Neutron Halo Nucleus ^{6}He and Improved Mass for the Four-Neutron Halo ^{8}He, Phys. Rev. Lett. 108 (2012) 052504, doi:10.1103/PhysRevLett.108.052504, URL http://link.aps.org/doi/10.1103/PhysRevLett.108.052504.

[138] R. J. Charity, J. M. Elson, J. Manfredi, R. Shane, L. G. Sobotka, Z. Chajecki, D. Coupland, H. Iwasaki, M. Kilburn, J. Lee, W. G. Lynch, A. Sanetullaev, M. B. Tsang, J. Winkelbauer, M. Youngs, S. T. Marley, D. V. Shetty, A. H. Wuosmaa, T. K. Ghosh, M. E. Howard, Isobaric

multiplet mass equation for $A = 7$ and 8, Phys. Rev. C 84 (2011) 051308, doi:10.1103/PhysRevC.84.051308, URL http://link.aps.org/doi/10.1103/PhysRevC.84.051308.

[139] A. A. Kwiatkowski, B. R. Barquest, G. Bollen, C. M. Campbell, D. L. Lincoln, D. J. Morrissey, G. K. Pang, A. M. Prinke, J. Savory, S. Schwarz, C. M. Folden, D. Melconian, S. K. L. Sjue, M. Block, Precision test of the isobaric multiplet mass equation for the $A = 32$, $T = 2$ quintet, Phys. Rev. C 80 (2009) 051302, doi:10.1103/PhysRevC.80.051302, URL http://link.aps.org/doi/10.1103/PhysRevC.80.051302.

[140] K. Blaum, G. Audi, D. Beck, G. Bollen, F. Herfurth, A. Kellerbauer, H.-J. Kluge, E. Sauvan, S. Schwarz, Masses of ^{32}Ar and ^{33}Ar for Fundamental Tests, Phys. Rev. Lett. 91 (2003) 260801, doi:10.1103/PhysRevLett.91.260801, URL http://link.aps.org/doi/10.1103/PhysRevLett.91.260801.

[141] C. Yazidjian, G. Audi, D. Beck, K. Blaum, S. George, C. Guénaut, F. Herfurth, A. Herlert, A. Kellerbauer, H.-J. Kluge, D. Lunney, L. Schweikhard, Evidence for a breakdown of the isobaric multiplet mass equation: A study of the $A = 35, T = 3/2$ isospin quartet, Phys. Rev. C 76 (2007) 024308, doi:10.1103/PhysRevC.76.024308, URL http://link.aps.org/doi/10.1103/PhysRevC.76.024308.

[142] A. Signoracci, B. A. Brown, Effects of isospin mixing in the $A = 32$ quintet, Phys. Rev. C 84 (2011) 031301, doi:10.1103/PhysRevC.84.031301, URL http://link.aps.org/doi/10.1103/PhysRevC.84.031301.

[143] F. Herfurth, J. Dilling, A. Kellerbauer, G. Audi, D. Beck, G. Bollen, H.-J. Kluge, D. Lunney, R. B. Moore, C. Scheidenberger, S. Schwarz, G. Sikler, J. Szerypo, I. Collaboration, Breakdown of the Isobaric Multiplet Mass Equation at $A = 33$, $T = 3/2$, Phys. Rev. Lett. 87 (2001) 142501, doi:10.1103/PhysRevLett.87.142501, URL http://link.aps.org/doi/10.1103/PhysRevLett.87.142501.

[144] Y. H. Zhang, H. S. Xu, Y. A. Litvinov, X. L. Tu, X. L. Yan, S. Typel, K. Blaum, M. Wang, X. H. Zhou, Y. Sun, B. A. Brown, Y. J. Yuan, J. W. Xia, J. C. Yang, G. Audi, X. C. Chen, G. B. Jia, Z. G. Hu, X. W. Ma, R. S. Mao, B. Mei, P. Shuai, Z. Y. Sun, S. T. Wang, G. Q. Xiao, X. Xu, T. Yamaguchi, Y. Yamaguchi, Y. D. Zang, H. W. Zhao, T. C. Zhao, W. Zhang, W. L. Zhan, Mass Measurements of the Neutron-Deficient ^{41}Ti, ^{45}Cr, ^{49}Fe, and ^{53}Ni Nuclides: First Test of the Isobaric Multiplet Mass Equation in fp-Shell Nuclei, Phys. Rev. Lett. 109 (2012) 102501, doi:10.1103/PhysRevLett.109.102501, URL http://link.aps.org/doi/10.1103/PhysRevLett.109.102501.

[145] M. C. Pyle, A. García, E. Tatar, J. Cox, B. K. Nayak, S. Triambak, B. Laughman, A. Komives, L. O. Lamm, J. E. Rolon, T. Finnessy, L. D. Knutson, P. A. Voytas, Revalidation of the Isobaric Multiplet Mass Equation, Phys. Rev. Lett. 88 (2002) 122501, doi:10.1103/PhysRevLett.88.122501, URL http://link.aps.org/doi/10.1103/PhysRevLett.88.122501.

[146] J. Su, W. Liu, N. Zhang, Y. Shen, Y. Lam, N. Smirnova, M. MacCormick, J. Wang, L. Jing, Z. Li, Y. Wang, B. Guo, S. Yan, Y. Li, S. Zeng, G. Lian, X. Du, L. Gan, X. Bai, Z. Gao, Y. Zhang, X. Zhou, X. Tang, J. He, Y. Yang, S. Jin, P. Ma, J. Ma, M. Huang, Z. Bai, Y. Zhou, W. Ma, J. Hu, S. Xu, S. Ma, S. Chen, L. Zhang, B. Ding, Z. Li, G. Audi, Revalidation of the isobaric multiplet mass equation at A = 53, T = 3/2, Phys. Lett. B 756 (2016) 323 – 327, ISSN 0370-2693, doi:http://dx.doi.org/10.1016/j.physletb.2016.03.024, URL http://www.sciencedirect.com/science/article/pii/S0370269316001957.

[147] T. Dickel, W. Plaß, S. A. S. Andres, J. Ebert, H. Geissel, E. Haettner, C. Hornung, I. Miskun, S. Pietri, S. Purushothaman, M. Reiter, A.-K. Rink, C. Scheidenberger, H. Weick, P. Dendooven, M. Diwisch, F. Greiner, F. Heiße, R. Knöbel, W. Lippert, I. Moore, I. Pohjalainen, A. Prochazka, M. Ranjan, M. Takechi, J. Winfield, X. Xu, First spatial separation of a heavy ion isomeric beam with a multiple-reflection time-of-flight mass spectrometer, Phys. Lett. B 744 (2015) 137–141, doi:10.1016/j.physletb.2015.03.047, URL http://dx.doi.org/10.1016/j.physletb.2015.03.047.

[148] J. Rissanen, V.-V. Elomaa, T. Eronen, J. Hakala, A. Jokinen, S. Rahaman, S. Rinta-Antila, J. Äystö, Conversion electron spectroscopy of isobarically purified trapped radioactive ions, Eur. Phys. J. A 34 (2) (2007) 113, URL http://dx.doi.org/10.1140/epja/i2007-10495-1.

[149] E. Liénard, G. Ban, C. Couratin, P. Delahaye, D. Durand, X. Fabian, B. Fabre, X. Fléchard, P. Finlay, F. Mauger, A. Méry, O. Naviliat-Cuncic, B. Pons, T. Porobic, G. Quéméner, N. Severijns, J. C. Thomas, P. Velten, Precision measurements with LPCTrap at GANIL , Hyperfine Interact. 236 (1-3) (2015) 1–7, doi:10.1007/s10751-015-1198-9, URL http://dx.doi.org/10.1007/s10751-015-1198-9.

[150] M. G. Sternberg, R. Segel, N. D. Scielzo, G. Savard, J. A. Clark, P. F. Bertone, F. Buchinger, M. Burkey, S. Caldwell, A. Chaudhuri, J. E. Crawford, C. M. Deibel, J. Greene, S. Gulick, D. Lascar, A. F. Levand, G. Li, A. P. Galván, K. S. Sharma, J. V. Schelt, R. M. Yee, B. J. Zabransky, Limit on Tensor Currents from ^{8}Li β Decay, Phys. Rev. Lett. 115 (18), doi:10.1103/physrevlett.115.182501, URL http://dx.doi.org/10.1103/PhysRevLett.115.182501.

[151] N. Scielzo, G. Li, M. Sternberg, G. Savard, P. Bertone, F. Buchinger, S. Caldwell, J. Clark, J. Crawford, C. Deibel, J. Fallis, J. Greene, S. Gulick, A. Hecht, D. Lascar, J. Lee, A. Levand, M. Pedretti, R. Segel, H. Sharma, K. Sharma, I. Tanihata, J. Van Schelt, R. Yee, B. Zabransky, The Paul trap: A radiofrequency-quadrupole ion trap for precision studies, Nucl. Instrum. Methods Phys. Res., Sect. A 681 (0) (2012) 94–100, ISSN 0168-9002, URL http://www.sciencedirect.com/science/article/pii/S0168900212003

[152] M. Beck, S. Coeck, V. Kozlov, M. Breitenfeldt, P. Delahaye, P. Friedag, F. Glück, M. Herbane, A. Herlert, I. Kraev, J. Mader, M. Tandecki, S. Van Gorp, F. Wauters, C. Weinheimer, F. Wenander, N. Severijns, First detection and energy measurement of recoil ions following beta decay in a Penning trap with the WITCH experiment, Eur. Phys. J. A 47 (3) (2011) 1–9, ISSN 1434-6001, doi:10.1140/epja/i2011-11045-0, URL http://dx.doi.org/10.1140/epja/i2011-11045-0.

[153] G. Savard, J. Clark, C. Boudreau, F. Buchinger, J. Crawford, H. Geissel, J. Greene, S. Gulick, A. Heinz, J. Lee, A. Levand, M. Maier, G. Munzenberg, C. Scheidenberger, D. Seweryniak, K. Sharma, G. Sprouse, J. Vaz, J. Wang, B. Zabransky, Z. Zhou, Development and operation of gas catchers to thermalize fusion–evaporation and fragmentation products, Nucl. Instrum. Methods Phys. Res., Sect. B 204 (2003) 582–586, doi:10.1016/s0168-583x(02)02134-1, URL http://dx.doi.org/10.1016/S0168-583X(02)02134-1.

[154] T. Brunner, A. Lapierre, C. Andreoiu, M. Brodeur, P. Delheji, S. Ettenauer, D. Frekers, A. T. Gallant, R. Gernhauser, A. Grossheim, R. Krücken, A. Lennarz, D. Lunney, D. Mücher, R. Ringle, M. C. Simon, V. V. Simon, S. K. L. Sjue, K. Zuber, J. Dilling, Trapped-ion decay spectroscopy towards the determination of ground-state components of double-beta decay matrix elements, Eur. Phys. J. A 49 (11), doi:10.1140/epja/i2013-13142-4, URL http://dx.doi.org/10.1140/epja/i2013-13142-4.

[155] A. Lennarz, A. Grossheim, K. G. Leach, M. Alanssari, T. Brunner, A. Chaudhuri, U. Chowdhury, J. R. C. López-Urrutia, A. T. Gallant, M. Holl, A. A. Kwiatkowski, J. Lassen, T. D. Macdonald, B. E. Schultz, S. Seeraji, M. C. Simon, C. Andreoiu, J. Dilling, D. Frekers, In-

Trap Spectroscopy of Charge-Bred Radioactive Ions, Phys. Rev. Lett. 113 (8), doi:10.1103/physrevlett.113.082502, URL http://dx.doi.org/10.1103/PhysRevLett.113.082502.

[156] M. Kowalska, S. Naimi, J. Agramunt, A. Algora, D. Beck, B. Blank, K. Blaum, C. Böhm, C. Borgmann, M. Breitenfeldt, L. Fraile, S. George, F. Herfurth, A. Herlert, S. Kreim, D. Lunney, E. Minaya-Ramirez, D. Neidherr, M. Rosenbusch, B. Rubio, L. Schweikhard, J. Stanja, K. Zuber, Trap-assisted decay spectroscopy with ISOLTRAP, Nucl. Instrum. Methods Phys. Res., Sect. A 689 (2012) 102–107, doi:10.1016/j.nima.2012.04.059, URL http://dx.doi.org/10.1016/j.nima.2012.04.059.

[157] J. Stanja, C. Borgmann, J. Agramunt, A. Algora, D. Beck, K. Blaum, C. Böhm, M. Breitenfeldt, T. E. Cocolios, L. M. Fraile, F. Herfurth, A. Herlert, M. Kowalska, S. Kreim, D. Lunney, V. Manea, E. Minaya Ramirez, S. Naimi, D. Neidherr, M. Rosenbusch, L. Schweikhard, G. Simpson, F. Wienholtz, R. N. Wolf, K. Zuber, Mass spectrometry and decay spectroscopy of isomers across the $Z = 82$ shell closure, Phys. Rev. C 88 (2013) 054304, doi:10.1103/PhysRevC.88.054304, URL http://link.aps.org/doi/10.1103/PhysRevC.88.054304.

[158] I. Matea, J. Souin, J. Äystö, B. Blank, P. Delahaye, V. V. Elomaa, T. Eronen, J. Giovinazzo, U. Hager, J. Hakala, J. Huikari, A. Jokinen, A. Kankainen, I. D. Moore, J. L. Pedroza, S. Rahaman, J. Rissanen, J. Ronkainen, A. Saastamoinen, T. Sonoda, C. Weber, Precise half-life measurement of the 26Si ground state, The European Physical Journal A 37 (2) (2008) 151–158, ISSN 1434-601X, doi:10.1140/epja/i2008-10623-5, URL http://dx.doi.org/10.1140/epja/i2008-10623-5.

[159] A. Bey, B. Blank, G. Canchel, C. Dossat, J. Giovinazzo, I. Matea, V. V. Elomaa, T. Eronen, U. Hager, J. Hakala, A. Jokinen, A. Kankainen, I. Moore, H. Penttilä, S. Rinta-Antila, A. Saastamoinen, T. Sonoda, J. Äystö, N. Adimi, G. de France, J. C. Thomas, G. Voltolini, T. Chaventré, Beta-decay branching ratios of 62Ga, The European Physical Journal A 36 (2) (2008) 121–126, ISSN 1434-601X, doi:10.1140/epja/i2008-10578-5, URL http://dx.doi.org/10.1140/epja/i2008-10578-5.

[160] J. Souin, T. Eronen, P. Ascher, L. Audirac, J. Äystö, B. Blank, V. V. Elomaa, J. Giovinazzo, J. Hakala, A. Jokinen, V. S. Kolhinen, P. Karvonen, I. D. Moore, S. Rahaman, J. Rissanen, A. Saastamoinen, J. C. Thomas, Precision half-life and Q -value measurement of the super-allowed beta emitter 30S, The European Physical Journal A 47 (3) (2011) 1–7, ISSN 1434-601X, doi:10.1140/epja/i2011-11040-5, URL http://dx.doi.org/10.1140/epja/i2011-11040-5.

[161] C. R. Triguero, A. M. Bruce, T. Eronen, I. D. Moore, M. Bowry, A. M. D. Bacelar, A. Y. Deo, V.-V. Elomaa, D. Gorelov, J. Hakala, A. Jokinen, A. Kankainen, P. Karvonen, V. S. Kolhinen, J. Kurpeta, T. Malkiewicz, P. J. R. Mason, H. Penttilä, M. Reponen, S. Rinta-Antila, J. Rissanen, A. Saastamoinen, G. S. Simpson, J. Äystö, Trap-assisted separation of nuclear states for gamma-ray spectroscopy: the example of 100Nb, Journal of Physics G: Nuclear and Particle Physics 39 (1) (2012) 015101, URL http://stacks.iop.org/0954-3899/39/i=1/a=015101.

[162] J. Kurpeta, W. Urban, A. Plochocki, J. Rissanen, J. A. Pinston, V. V. Elomaa, T. Eronen, J. Hakala, A. Jokinen, A. Kankainen, P. Karvonen, I. D. Moore, H. Penttila, A. Saastamoinen, C. Weber, J. Äystö, Signatures of oblate deformation in the ^{111}Tc nucleus, Phys. Rev. C 84 (4) (2011) 044304, doi:10.1103/PhysRevC.84.044304.

[163] D. Jordan, A. Algora, J. L. Tain, B. Rubio, J. Agramunt, A. B. Perez-Cerdan, F. Molina, L. Caballero, E. Nacher, A. Krasznahorkay, M. D. Hunyadi, J. Gulyas, A. Vitez, M. Csatlos, L. Csige, J. Äystö, H. Penttilä, I. D. Moore, T. Eronen, A. Jokinen, A. Nieminen, J. Hakala, P. Karvonen, A. Kankainen, A. Saastamoinen, J. Rissanen, T. Kessler, C. Weber, J. Ronkainen, S. Rahaman, V. Elomaa, U. Hager, S. Rinta-Antila, T. Sonoda, K. Burkard, W. Hüller, L. Batist, W. Gelletly, A. L. Nichols, T. Yoshida, A. A. Sonzogni, K. Peräjärvi, A. Petrovici, K. W. Schmid, A. Faessler, Total absorption study of the β decay of ^{102,104,105}Tc, Phys. Rev. C 87 (4) (2013) 044318, URL http://link.aps.org/doi/10.1103/PhysRevC.87.044318.

[164] A.-A. Zakari-Issoufou, M. Fallot, A. Porta, A. Algora, J. L. Tain, E. Valencia, S. Rice, V. M. Bui, S. Cormon, M. Estienne, J. Agramunt, J. Äystö, M. Bowry, J. A. Briz, R. Caballero-Folch, D. Cano-Ott, A. Cucoanes, V.-V. Elomaa, T. Eronen, E. Estévez, G. F. Farrelly, A. R. Garcia, W. Gelletly, M. B. Gomez-Hornillos, V. Gorlychev, J. Hakala, A. Jokinen, M. D. Jordan, A. Kankainen, P. Karvonen, V. S. Kolhinen, F. G. Kondev, T. Martinez, E. Mendoza, F. Molina, I. Moore, A. B. Perez-Cerdán, Z. Podolyák, H. Penttilä, P. H. Regan, M. Reponen, J. Rissanen, B. Rubio, T. Shiba, A. A. Sonzogni, C. Weber, Total Absorption Spectroscopy Study of ^{92}Rb Decay: A Major Contributor to Reactor Antineutrino Spectrum Shape, Phys. Rev. Lett. 115 (2015) 102503, doi:10.1103/PhysRevLett.115.102503, URL http://link.aps.org/doi/10.1103/PhysRevLett.115.102503.

[165] J. L. Tain, E. Valencia, A. Algora, J. Agramunt, B. Rubio, S. Rice, W. Gelletly, P. Regan, A.-A. Zakari-Issoufou, M. Fallot, A. Porta, J. Rissanen, T. Eronen, J. Äystö, L. Batist, M. Bowry, V. M. Bui, R. Caballero-Folch, D. Cano-Ott, V.-V. Elomaa, E. Estevez, G. F. Farrelly, A. R. Garcia, B. Gomez-Hornillos, V. Gorlychev, J. Hakala, M. D. Jordan, A. Jokinen, V. S. Kolhinen, F. G. Kondev, T. Martínez, E. Mendoza, I. Moore, H. Penttilä, Z. Podolyák, M. Reponen, V. Sonnenschein, A. A. Sonzogni, Enhanced γ -Ray Emission from Neutron Unbound States Populated in β Decay, Phys. Rev. Lett. 115 (6), doi:10.1103/physrevlett.115.062502, URL http://dx.doi.org/10.1103/PhysRevLett.115.062502.

[166] M. B. Gómez-Hornillos, J. Rissanen, J. L. Taín, A. Algora, K. L. Kratz, G. Lhersonneau, B. Pfeiffer, J. Agramunt, D. Cano-Ott, V. Gorlychev, R. Caballero-Folch, T. Martínez, L. Achouri, F. Calvino, G. Cortés, T. Eronen, A. García, M. Parlog, Z. Podolyak, C. Pretel, E. Valencia, β-delayed neutron emission studies, Hyperfine Interact 223 (1-3) (2014) 185–194, doi:10.1007/s10751-012-0617-4, URL http://dx.doi.org/10.1007/s10751-012-0617-4.

[167] M. B. Gomez-Hornillos, J. Rissanen, J. L. Tain, A. Algora, D. Cano-Ott, J. Agramunt, V. Gorlychev, R. Caballero, T. Martinez, L. Achouri, J. Äystö, G. Cortes, V. V. Elomaa, T. Eronen, A. Garcia, J. Hakala, A. Jokinen, P. Karvonen, V. S. Kolhinen, I. Moore, M. Parlog, H. Penttilä, Z. Podolyak, C. Pretel, M. Reponen, V. Sonnenschein, E. Valencia, First Measurements with the BEta deLayEd Neutron Detector (BELEN-20) at JYFLTRAP, J. Phys.: Conf. Ser. 312 (5) (2011) 052008, ISSN 1742-6596, URL http://stacks.iop.org/1742-6596/312/i=5/a=052008.

[168] P. Möller, J. Nix, K.-L. Kratz, NUCLEAR PROPERTIES FOR ASTROPHYSICAL AND RADIOACTIVE-ION-BEAM APPLICATIONS, At. Data Nucl. Data Tables 66 (2) (1997) 131–343, doi:10.1006/adnd.1997.0746, URL http://dx.doi.org/10.1006/adnd.1997.0746.

[169] J. Agramunt, A. Garcia, A. Algora, J. Äystö, R. Caballero-Folch, F. Calvino, D. Cano-Ott, G. Cortes, C. Domingo-Pardo, T. Eronen, W. Gelletly, M. Gomez-Hornillos, J. Hakala, A. Jokinen, D. Jordan, A. Kankainen, V. Kol-

hinen, T. Martinez, P. Mason, I. Moore, H. Penttilä, Z. Podolyak, M. Reponen, A. Riego, J. Rissanen, B. Rubio, A. Saastamoinen, J. Tain, E. Valencia, New Beta-delayed Neutron Measurements in the Light-mass Fission Group, Nuclear Data Sheets 120 (2014) 74 – 77, ISSN 0090-3752, doi:http://dx.doi.org/10.1016/j.nds.2014.07.010, URL http://www.sciencedirect.com/science/article/pii/S0090375214004621.

[170] S. K. L. Sjue, D. Melconian, A. Garcia, I. Ahmad, A. Algora, J. Äystö, V.-V. Elomaa, T. Eronen, J. Hakala, S. Hoedl, A. Kankainen, T. Kessler, I. D. Moore, F. Naab, H. Penttilä, S. Rahaman, A. Saastamoinen, H. E. Swanson, C. Weber, S. Triambak, K. Deryckx, Electron-capture branch of ^{100}Tc and tests of nuclear wave functions for double-beta decays, Phys. Rev. C 78 (6) (2008) 064317, URL http://link.aps.org/abstract/PRC/v78/e064317.

[171] C. Wrede, S. K. L. Sjue, A. Garcia, H. E. Swanson, I. Ahmad, A. Algora, V.-V. Elomaa, T. Eronen, J. Hakala, A. Jokinen, V. S. Kolhinen, I. D. Moore, H. Penttilä, M. Reponen, J. Rissanen, A. Saastamoinen, J. Äystö, Electron capture on ^{116}In and implications for nuclear structure related to double-β decay, Phys. Rev. C 87 (3) (2013) 031303, URL http://link.aps.org/doi/10.1103/PhysRevC.87.031303.

[172] S. Rahaman, V.-V. Elomaa, T. Eronen, J. Hakala, A. Jokinen, A. Kankainen, J. Rissanen, J. Suhonen, C. Weber, J. Äystö, Double-beta decay Q values of ^{116}Cd and ^{130}Te, Phys. Lett. B 703 (4) (2011) 412, ISSN 0370-2693, doi:10.1016/j.physletb.2011.07.078, URL http://www.sciencedirect.com/science/article/pii/S0370269311008975.

[173] H. Schatz, A. Aprahamian, J. Görres, M. Wiescher, T. Rauscher, J. Rembges, F.-K. Thielemann, B. Pfeiffer, P. Möller, K.-L. Kratz, H. Herndl, B. Brown, H. Rebel, rp-process nucleosynthesis at extreme temperature and density conditions, Physics Reports 294 (4) (1998) 167 – 263, ISSN 0370-1573, doi:http://dx.doi.org/10.1016/S0370-1573(97)00048-3, URL http://www.sciencedirect.com/science/article/pii/S0370157397000483.

[174] K. Peräjärvi, T. Eronen, V.-V. Elomaa, J. Hakala, A. Jokinen, H. Kettunen, V. Kolhinen, M. Laitinen, I. Moore, H. Penttilä, J. Rissanen, A. Saastamoinen, H. Toivonen, J. Turunen, J. Äystö, Ultra-high resolution mass separator–Application to detection of nuclear weapons tests, Appl. Radiat. Isot. 68 (3) (2010) 450, ISSN 0969-8043, URL http://www.sciencedirect.com/science/article/B6TJ0-4XY4JXT-5/2/26228003b371844001fb97e29b545174.